

RIGA TECHNICAL UNIVERSITY

Faculty of Power and Electrical Engineering

Institute of Power Engineering

Deniss Bezrukovs

Doctoral study program „Power and Electrical Engineering”

**THE STUDY OF WIND ENERGY RESOURCE AND
THE ASSESSMENT OF THE ECONOMIC
FEASIBILITY OF WIND ENERGY PROJECTS**

Doctoral Thesis

Scientific supervisor
Professor Dr. habil. sc. ing.
ANTANS SAULUS SAUHATS

RTU Press
Riga 2019

Abstract

The purpose of the work is to reduce the cost of wind energy production and increase the feasibility of wind power projects. The author considers methods for predicting operational efficiency of WT and revenue streams generated by wind energy projects using stochastic differential equation models. The study develops wind shear assessment methods based on the analysis of the results of long-term wind speed measurements. Furthermore, the study presents density maps of long-term average wind speed and wind energy distribution on the territory of Latvia at the height of 10 m based on the results of wind speed measurements obtained from LEGMC for the period 2015 – 2016. Along with wind shear estimation, the possibility of using the power law function to extrapolate the values of the parameters of the Weibull distribution to the height corresponding to the location of the wind turbine axis is investigated. In order to evaluate the possibility of using the network of communication masts for wind speed measurements, the effect of lattice mast structure on the results of wind speed measurements using CFD modelling and experimental results is performed. It is shown that the recommendations of IEC 61400-12-1 technical standard regarding the placement of sensors on the lattice mast do not allow conducting wind speed measurement with the required level of precision. A method for improving the accuracy of wind speed measurements using lattice masts is proposed by comparing the estimation results of two sensors installed at the same height and displaced by an angle of at least 120° . The density maps of Weibull distribution parameters for average values of wind speed at the height of 10 m for the territory of Latvia are provided. These maps serve as a reference tool for assessing wind energy resource potential at any location in Latvia at a height of 10 m and estimating operational efficiency of low-power wind generators for WTs with vertical and horizontal axes. In order to demonstrate the practical applicability of the approach, the model of the spatial distribution of relative capacity factor for horizontal axes WT with rated power 2.5 kW at the height of 10 m above the ground is developed. Finally, the study investigates variations in the operational efficiency of WT in the conditions of low winds depending on the height of the mast and generator type, as well as provides suggestions with respect to the optimal choice of wind generator type for Latvian weather conditions.

The Doctoral Thesis has been written in English. It consists of an Introduction; 5 Chapters; 93 Figures; 20 Tables; 1 Annexes; the total number of pages is 141; the Bibliography of 140 titles.

Anotācija

Darba mērķis ir samazināt vēja enerģijas ražošanas izmaksas un veicināt vēja enerģijas projektu īstenošanas iespējas. Autors izskata metodes vēja turbīnu darbības efektivitātes un vēja enerģijas projektu radīto ieņēmumu plūsmu prognozēšanai, izmantojot stohastiskos diferenciālvienādojuma modeļus. Pētījumā izstrādātas vēja nobīdes novērtēšanas metodes, kuru pamatā ir ilgtermiņa vēja ātruma mērījumu rezultātu analīze. Turklāt pētījumā sniegti ilgtermiņa vidējā vēja ātruma un vēja enerģijas sadales blīvuma kartes Latvijas teritorijā 10 m augstumā, balstoties uz vēja ātruma mērījumiem, kas iegūti no LEGMC laika posmā no 2015. līdz 2016. gadam. Līdz ar vēja nobīdes novērtējumu tiek pētīta iespēja izmantot pakāpes funkciju, lai ekstrapolētu Weibull sadalījuma parametru vērtības līdz vēja turbīnas ass atrašanās augstumam.

Lai novērtētu iespēju izmantot sakaru mastu tīklu vēja ātruma mērījumiem, tiek pētīta režģa masta struktūras ietekme uz vēja ātruma mērījumu rezultātiem, izmantojot CFD modelēšanu un eksperimentālos rezultātus. Ir pierādīts, ka IEC 61400-12-1 tehniskā standarta ieteikumi attiecībā uz sensoru izvietošanu uz režģa masts neļauj veikt vēja ātruma mērīšanu ar nepieciešamo precizitātes līmeni. Tiek piedāvāta metode vēja ātruma mērījumu precizitātes uzlabošanai, izmantojot režģa mastus, salīdzinot divu vienā augstumu uzstādīto sensoru novērtēšanas rezultātus, kas izvietoti ar vismaz 120° leņķī attiecībā viens pret otru. Tiek sniegti Weibull sadalījuma parametru blīvuma kartes vidējām vēja ātruma vērtībām 10 m augstumā Latvijas teritorijā. Blīvuma kartes domātas kalpošanai par atsauces instrumentu, kas ļauj novērtēt vēja enerģijas resursa potenciālu jebkurā vietā Latvijas teritorijā 10 m augstumā un aprēķināt mazjaudas vēja ģeneratoru darbības efektivitāti vēja turbīnām ar vertikālām un horizontālām asīm. Lai demonstrētu pieejas praktisko pielietojamību, tiek veidots relatīvās kapacitātes koeficienta telpiskās sadalījuma modelis vējā turbīnai ar nominālo 2,5 kW jaudu 10 m augstumā virs zemes. Noslēgumā, pētījums aplūko vēju turbīnu darbības efektivitātes izmaiņas zema vēja apstākļos atkarībā no masta un ģeneratora tipa augstuma, kā arī sniedz ieteikumi attiecībā uz vēja ģeneratoru optimālo izvēli Latvijas laika apstākļiem.

Promocijas darbs ir uzrakstīts angļu valodā. Tas sastāv no ievada; 5 nodaļām; 93 attēliem; 20 tabulām; 1 pielikumiem; Kopējais lappušu skaits ir 141. Bibliogrāfijā ir 140 atsauces.

Abbreviations

ADF	Augmented Dickey-Fuller
AEP	Annual energy production
ANN	Artificial neural networks
AR	Auto Regressive
BNEF	Bloomberg NEF
CAGR	Compound Annual Growth Rate
CCM	Cellular communication mast
CFD	Computational Fluid Dynamics
EES	Electrical Energy Storage
FiTs	Feed-in tariffs
HAWT	Horizontal axis wind turbines
HPC	High-performance computer
IEC	International Electrotechnical Commission
IRENA	International Renewable Energy Agency
LBNL	Lawrence Berkeley National Laboratory
LCOE	Levelised Cost of Electricity
LEGMC	Latvian Environment, Geology and Meteorology Centre
LES	Large Eddy Simulation
MAE	Mean Absolute Error
NDC	Nationally Determined Contributions
NREAP	National Renewable Energy Action Plans
NREL	National laboratory of the U.S. Department of Energy
NWP	Numerical Weather Prediction model
OLS	Ordinary Least Square
PDE	Partial differential equations
RES	Renewable Energy Sources
RMSE	Root Mean Squared Error
SCADA	Supervisory Control And Data Acquisition
SDE	Stochastic differential equations
SWTG	Small wind turbine generators
TFEC	Total Final Energy Consumption
(U)RANS	(Unsteady) Reynolds-Averaged Navier-Stokes
VAR	Vector Autoregressive Models
VAWT	Vertical axis wind turbines
WPP	Wind Power Park
WT	Wind turbine
WWEA	World Wind Energy Association

Table of figures

Figure 1.1 World energy consumption in the period 1630 – 2005 in British thermal units (Btu) [1].	14
Figure 1.2 Annual energy-related CO ₂ emissions and reductions, 2015-2050 (Gt/yr) [5].	16
Figure 1.3 Growth in global renewable energy compared to TFEC, 2005-2015 [6].	17
Figure 1.4 Estimated renewable share of total final energy consumption, end-2017 [6].	18
Figure 1.5 Estimated renewable energy share of global electricity production, end-2017 [6].	18
Figure 1.6 The share of renewable energy resources in electricity production in Europe [7].	19
Figure 1.7 Global wind power installed capacity (GW) [9].	20
Figure 1.8 Forecasted global wind power market installed capacity (GW), 2017-2025 [10].	20
Figure 1.9 Total power generation capacity in the European Union 2005-2017 [11].	21
Figure 1.10 The share of solar and wind energy in electricity production in Europe [7].	21
Figure 1.11 Percentage of the average annual electricity demand covered by wind in 2017 in Europe [11].	22
Figure 1.12 LCOE of major power generation technologies in Europe [14].	23
Figure 1.13 Wind power market, key countries, auction, 2017, bubble size represents overall capacity awarded [10].	24
Figure 1.14 Cumulative installations onshore and offshore in the EU [11].	25
Figure 1.15 Wind park construction project in shallow water in the North Sea [16].	26
Figure 1.16 The scheme of transformation and transmission of wind energy from a WT to the network [19].	27
Figure 1.17 The design of a three-phase AC 3x1200 mm ² high-voltage submarine cable for transmitting 220 kV power from offshore WT to a grid on the shore	28
Figure 1.18 The design of a high-voltage underground DC cable 1x2500 mm ² for the transfer of 320 kV power from a WT to a grid on the shore.	28
Figure 1.19 Power transmission scheme connecting an off-shore WPP with an existing high-voltage grid ashore [20].	29
Figure 1.20 Wind Turbine price dynamics in 2015 USD per kW of nominal power [22].	30
Figure 1.21 Global weighted average total installed costs, capacity factors and LCOE for onshore wind, 2010-2017 [26].	31
Figure 1.22 Global weighted average total installed costs, capacity factors and LCOE for offshore wind, 2010-2017 [26].	32
Figure 1.23 Classification of electrical energy storage systems according to energy form International Electrotechnical Commission [33].	35
Figure 1.24 Different uses of electrical energy storage in grids, depending on the frequency and duration of use [33].	36
Figure 1.25 OPS Prevento algorithm for wind power prediction [39].	37
Figure 1.26 Net generation of wind power plants for 18.06.2018 - 24.06.2018 in Germany and a day ahead forecast [40].	38
Figure 1.27 Electricity prices in the Latvian segment of Nord Pool in EUR/MWh [41].	39
Figure 1.28 Histogram of electricity prices in the Latvian segment of Nord Pool [41].	39
Figure 1.29 Hourly fluctuations of electricity prices in the Latvian segment of Nord Pool in the period of 1-6 May 2018 in EUR/MWh [41].	40
Figure 2.1 Installed wind power plant capacity in Latvia in MW.	47
Figure 2.2 Electricity prices in the Latvian segment of Nord Pool power market.	52
Figure 2.3 Wind speed in Irbene, Ventspils region, Latvia at the altitude of 50 m.	52

Figure 2.4 Power law fit of wind speed in relationship to observation height.	53
Figure 2.5 PDF of log wind speed vs standard normal PDF.	54
Figure 2.6 PDF of log energy prices vs standard normal PDF.	54
Figure 2.7 Autocorrelation Functions of extrapolated log wind speed at 100 m.	55
Figure 2.8 Autocorrelation Functions of log electricity prices time series.	55
Figure 2.9 Log electricity price and seasonality trend.	57
Figure 2.10 De-seasonalized log electricity prices.	57
Figure 2.11 Actual and simulated wind speed at 100 m altitude.	58
Figure 2.12 Actual and simulated electricity prices.	58
Figure 2.13 Histogram of operational efficiency based on 10000 Monte Carlo trials for Nordex 131 3000kW for different tower heights.	60
Figure 2.14 Histogram of revenues based on 10000 Monte Carlo trials for Nordex 131 3000kW for different tower heights.	60
Figure 3.1 Wind speed frequency distribution $F(V)$ calculated based on the results of wind speed measurements for heights 30, 50, 100, 140 and 180 m above the ground. Measurements carried out in Ireben, Venspils region in the period 01.02.2014-01.01.2015.	65
Figure 3.2 Horizontal cross-section of a triangular lattice CCM: K – cable lines; E – ladder structure; o – mast centre; F – mast frame; d – diameter of load-carrying tubes.	67
Figure 3.3 Distance R of wind speed sensor from the mast center to the point of observation depending on the mast structure solidity t for different mast side length.	67
Figure 3.4 Mesh around the triangular lattice mast structure, vertical cross-section.	69
Figure 3.5 CFD model of the wind flow interaction with a triangular lattice metrological mast, side width $L = 0.74$ m, at the wind speed $U = 10.0$ m/s and angle $\alpha = 0^\circ$ relative to the position of a boom with sensor S	70
Figure 3.6 CFD modelling results of the wind flow field around a triangular lattice CCM, side width $L = 0.74$ m, for wind speeds $U = 5$ and 10 m/s and angles $\alpha = 0$ and 180° relative to the position of a boom with sensor S	71
Figure 3.7 CFD modelling results of the wind flow field around a triangular lattice CCM, a) side width $L = 1.0$ m and b) side width $L = 1.2$ m, for wind speeds $U = 5.0$ and 10.0 m/s and the angle $\alpha = 0^\circ$ relative to the position of a boom with sensor S	72
Figure 3.8 Distance from the center of a triangular lattice CCM, R , m, to the boundaries of areas where the wind flow speed decreases by 1.0 - 1.5%, for masts with side widths $L = 0.74$ and 1.2 m, angle $\alpha = 0^\circ$, relative to the position of a boom with sensor S , depending on the wind flow speed U , m/s.	73
Figure 3.9 Distance from the center of a triangular lattice CCM, R , m, to the boundaries of areas where the wind flow speed decreases by 1.0 –1.5%, for wind speed $U = 5.0$ m/s, depending on the width L , m, of the mast side.	74
Figure 3.10 The map location of three tall triangular lattice CCM and LEGMC Met Stations on the shore of the Baltic Sea at sites Staļdzene, Tebra and Rozēni in Ventspils, Pāvilosta and Ainaži regions.	76
Figure 3.11 NRG Symphonie PLUS3 logger with battery, programming console and channels configuration diagram (left) and its side view with GSM module (iPACK), terminals for 15 analog or digital sensors and extremal power connection (right).	76
Figure 3.12 Wind measurement cup anemometer of WindSensor P2546A-OPR type placed at the end of the boom (bottom left), wind direction sensor NRG #200P (top right), hygrometer RH-5X: 4414 installed on the mast (bottom right) and thermometer NRG #110S (top left).	77

Figure 3.13 Guyed type lattice triangular CCM in the Site 3 – Rozēni, Ainaži, which has a height of about 100 m with the side length of 1.4 m.....	78
Figure 3.14 The vector diagram of the arrangement of a wind direction sensor S_{Dir} on a 1.6 m boom with an angle of offset β with respect to the northward vector N and anemometers S_A , S_B , S_C on 2.8 m long booms that are located at a 3.2 m distance from the centre O of the triangular CCM with a side length $L = 1.2$ m.	79
Figure 3.15 Placement of metrological sensors and the Symphonie PLUS3 measuring complex on the triangular lattice CCM with 100 m height located in Ventspils, Pāvilsta and Ainaži regions, where five levels correspond to reference heights of 2, 10, 40, 64 and 84.5 m.	80
Figure 3.16 The map of the terrain and the location of the CCM, indicating the angular position of the wind direction sensor S_{Dir} relative to the northward direction N , respectively, at the Stāldzene: -26° , Tebra: 51° , and Rozēni -54° sites.	80
Figure 3.17 Metrological sensors and a data logger mounted on a triangular lattice CCM. Level 2 (40 m) – anemometers S_A , S_B , S_C and wind direction sensor S_{Dir} (left), Level 4 (84.5 m) – anemometers S_A , S_B and wind direction sensor S_{Dir} (right).	81
Figure 3.18 Relative average wind speed V_{w_avg} from sensors S_A , S_B and S_C installed on the CCM with side length 1.2 m in Ventspils site at a Levels 1 – 4 in relationship to the angle of wind direction.....	83
Figure 3.19 Relative average wind speed V_{w_avg} of measured wind speeds from sensors S_A , S_B and S_C installed on the CCM with side length 1.4 m in Pāvilsta site at a Levels 1 – 4-in relationship to the angle of wind direction.....	84
Figure 3.20 Relative average wind speed V_{w_avg} of measured wind speeds from sensors S_A , S_B and S_C installed on the CCM with side length 1.4 m in Ainaži site at a Levels 1 – 4 in relationship to the angle of wind direction.....	85
Figure 3.21 Average wind speed data with 10 min increments from anemometers S_A , S_B , S_C and wind direction from sensor S_{Dir} . The grey area indicates the period when sensor S_B was in the shadow, which corresponds to the wind direction $75^\circ - 115^\circ$	86
Figure 3.22 The vector diagram of wind flows W_A , W_B , W_C and their shadows of sensors S_A , S_B , S_C	86
Figure 3.23 An example wind flow distortion V_{w_avg} calculated for each 10-minute simultaneous wind speed measurements from two anemometers S_A , S_B installed on the mast with side length 1.2 m in Ventspils site at Level 4, in relationship to the angle of wind direction.....	88
Figure 3.24 A snapshot of temperature, humidity and wind direction measurements on Site 1, Ventspils for a short time period when wind direction sensors were frozen.	89
Figure 3.25 Wind shear models for average wind speed V_{avg} for Ventspils, Pāvilsta and Ainaži sites, calculated using raw measurements (dashed lines) and corrected data (solid lines), for the period 01.2018 - 01.2019.	90
Figure 4.1 Map of Latvia with the locations of 22 meteorological stations and the mean elevation above sea level (m) with a 1x1 km resolution.	93
Figure 4.2 Frequency distribution functions of average wind speed V_{avg} over the period of observations from 01.01.2015 to 31.12.2016 for five meteorological observation stations at a height of 10 m above the ground.....	95
Figure 4.3 Model of the spatial distribution of average values of wind speed V_{avg} m/s at an altitude of 10 m above the ground on the territory of Latvia.	97
Figure 4.4 Models of spatial distribution of average wind speed at the heights for 10 m and 54 m, estimated using ERA5.....	98

Figure 4.5 Models of spatial distribution of average wind speed at the heights for 100 m and 136 m, estimated using ERA5.....	98
Figure 4.6 Monthly fluctuations of the average wind speed V_{avg} , m/s for the heights of 20, 40 and 60 m above ground in the measurement time interval T from 04.2009 to 02.2013.	101
Figure 4.7 Daily fluctuations of the average wind speed $V_{avg,d}$ (m/s) for the height of 60 m above ground in the measurement time interval T from 04.2009 to 02.2013.	101
Figure 4.8 Wind speed frequency distribution curves, FV , for the period 04.2009 - 04.2013.	102
Figure 4.9 Weibull probability density function curves, FV , for the period 04.2009 - 04.2013. .	102
Figure 4.10 Weibull parameters k (shape factor) and c (scale factor) for the measurement heights of 40, 50 and 60 m (points) and their extrapolations up to 150 m using power law. Dashed blue line is the assumed constant parameter k above 60 m height.....	105
Figure 4.11 Model of the spatial distribution of the scale parameter c of Weibull wind speed probability density at the height of 10 m above the ground.....	106
Figure 4.12 Model of the spatial distribution of the shape parameter k of Weibull wind speed probability density at the height of 10 m above the ground.....	106
Figure 4.13 Model of the spatial distribution of the average wind energy density in relative units $P * avg$ at the height of 10 m above the ground in the territory of Latvia.	108
Figure 4.14 Horizontal Axis Wind Turbine 0.75 kW.	110
Figure 4.15 Vertical Axis Wind Turbine Darrieus H-type 0.75 kW.....	110
Figure 4.16 Power curves $P(V)$ of HAWT 0.75, 2.5 kW and VAWT 0.75, 2.5 kW Darrieus H-type.	111
Figure 4.17 Weibull wind speed frequency distribution function $F(V)$, the power curve $P(V)$ for HAWT 2.5 kW and the value of AEP $W = 4.6 MWh$, corresponding to wind type at Ventspils meteorological observation station.....	113
Figure 4.18 Forecasted capacity factor C_e and AEP for HAWT converters with rated power 0.75, 2.5, 5.0, 20.0 kW and VAWT Darrieus H-type 0.75, 2.5, 6.0 kW for Ventspils.	114
Figure 4.19 Model of the spatial distribution of relative capacity factor $C_e *$ for HAWT type generator with rated power 2.5 kW at the height of 10 m above the ground.....	115
Figure 4.20 Power curve $P(V)$ for generator of Nordex N131/3000 type 3000 kW and Weibull probability density function FV curves for wind speeds V , m/s at heights 114 and 131 m..	118
Figure 4.21 Power curve $P(V)$ for generator of Enercon E101 type 3050 kW and Weibull probability density function FV curves for wind speeds V , m/s at heights 124 and 135 m..	119
Figure 4.22 Power curve $P(V)$ for generator of Vestas V136-3.45 type 3450 kW and Weibull probability density function FV curves for wind speeds V , m/s at heights 112 and 132 m..	119
Figure 4.23 Power curve $P(V)$ for generator of Siemens SWT-3.2-113 type 3.5 MW and Weibull probability density function $F(V)$ curves for wind speeds V , m/s at heights 122 and 142 m.	120
Figure 4.24 Power curve $P(V)$ for generator of Siemens SWT-2.3-108 type 2 MW and Weibull probability density function FV curves for wind speeds V , m/s at heights 90 and 100 m. ..	120
Figure 4.25 Forecasted efficiency C_e , %, for Nordex N131/3000, Enercon E101, Vestas V136-3.45 and Siemens SWT-3.2-113, SWT-2.3-108 WTs for different heights of rotor hubs (height in meters) performing under the low-wind conditions in Latvia.	121

Table of contents

Introduction	11
1. Alternative energy sources in modern energetics	13
1.1. Problems and solutions	13
1.1.1. Challenges of the contemporary world energetics	13
1.1.2. The roadmap to the global environmental safety and energy security	14
1.2. The use of renewable energy resources	16
1.2.1. Modern renewable energy sources	16
1.2.2. Wind power development trends	19
1.2.3. Wind energy transfer from WTs to the grid	27
1.3. Economical risks of wind energy projects	29
1.3.1. Cost of onshore and offshore WPP	29
1.3.2. Risk management in renewable energy projects	33
1.4. Modern methods of increasing wind turbine efficiency	34
1.4.1. Electrical energy storage systems	34
1.4.2. Methods of forecasting wind power generation and consumption	36
1.4.3. Unresolved problems	41
1.5. Conclusions	41
2. Economic and operational risks in wind energy projects in Latvia	43
2.1. Risks and uncertainty factors in the design of wind power projects	43
2.1.1. The problem of operational and economic uncertainty	43
2.1.2. The analysis of Latvian electricity market	44
2.2. The use of stochastic models in wind energy projects	48
2.2.1. An overview of forecasting models	48
2.2.2. The analysis of statistical data	51
2.3. The assessment of economic efficiency of wind energy projects	53
2.3.1. Data preparation for pre-testing procedures	53
2.3.2. The description of modelling methods	56
2.3.3. Model calibration and results	58
2.3. Conclusions	61
3. Reducing the costs and uncertainty of wind speed measurements	62

3.1. The modelling of wind flow interaction with a triangular lattice mast	62
3.1.1. The need for high quality wind speed measurements	62
3.1.2. Wind speed measurements and types of lattice masts	64
3.1.3. The results of mathematical modelling.....	67
3.2. The use of lattice CCM for wind shear assessment.....	74
3.2.1. The description of experimental site and wind measurement equipment.....	74
3.2.2. The installation of measuring sensors on CCM.....	77
3.3. The analysis of measurement results	81
3.1.1. Lattice mast structure impact on measurement results	81
3.1.2. The method of wind speed measurement uncertainty reduction	85
3.4. Conclusions	90
4. The assessment of wind energy potential in Latvia	92
4.1. Wind energy resource spatial distribution modelling.....	92
4.1.1. The landscape of the territory of Latvia.....	92
4.1.2. The network of meteorological stations.....	92
4.1.3. Wind types in the territory of Latvia.....	94
4.1.4. The model of wind speed spatial distribution	96
4.2. Wind energy assessment methods	100
4.2.1. Long-term wind speed measurements and wind shear assessment	100
4.2.2. Weibull distribution parameters' approximation	103
4.3. Wind energy potential assessment models	105
4.3.1. Modelling of the spatial distribution of Weibull parameters	105
4.3.2. The spatial distribution of wind energy resource.....	107
4.4. Forecasting the efficiency of SWTG	109
4.4.1. Types and power curves of the SWTG	109
4.4.2. The modelling of power production of HAWT and VAWT	112
4.5. The assessment of WT efficiency in Latvia under low-wind conditions	116
4.6. Conclusions	121
5. Implications and proposals	123
References	126
Annex 1	139

Introduction

Modern solutions to the problems of contemporary energetics are inseparable from the increased protection of the environment from pollution and reduction in carbon dioxide emissions caused by fossil fuel combustion. It is therefore not a coincidence that technologies based on the efficient utilization of Renewable Energy Sources (RES) are rapidly developing. For instance, wind energy installed capacity alone in the last 20 years grew more than fiftyfold.

The growing interest in the commercial use of wind energy can be attributed to a significant progress in improving the technological design of turbine manufacturing and increasing the height of hubs, that made it possible to significantly increase the nominal capacity of installed generators. At the same time, energy storage technologies are being developed and methods for planning Wind Power Park (WPP) energy generation output based on short-term wind turbine operational efficiency forecasting are being improved. The advancements made in these fields lead to the fact that alternative energy is becoming more profitable every year.

In the process of designing a new WPP, one of the main criteria for choosing the construction site is the existence of a technical report analysing the distribution of wind energy potential at the height of up to 200m. The modern methods of wind power modelling such as Global wind atlas and ERA5, developed based on climatological models, provide information on the global distribution of long-term wind speed averages with resolution 10x10 km. These results allow selecting primary locations with relatively high wind energy potential in a particular country that could be promising for the construction of a WPP.

However, in order to assess future efficiency of wind turbines and predict the commercial viability of a project for a specific location, it is necessary to calibrate the obtained wind speed values taking into consideration site specificities, because the results obtained by modelling, depending on the height above the ground level, can differ significantly from the actual values.

In order to calibrate the simulation results, physical measurements are made using sensors installed on high masts in the area selected for the construction of the WPP. The results of calibration can be used to estimate the effectiveness of wind turbines and make it possible to assess the commercial viability of pursuing the intended project with higher level of reliability.

Prospective studies in the field of improving wind energy efficiency are concerned with the possibility of short-term modelling of wind energy for up to 48 hours ahead at the height of

10 m to 500 m. This enables electricity producers to participate in the commercial sale of energy at market prices on the Nord Pool power market. The price of energy on this market depends on concurrent supply and demand, resulting in the fact that in certain periods of time price can significantly deviate from a daily or monthly average.

Against this background, the study of wind energy resource is fundamental in addressing the issues of improving the economic efficiency of WPPs. On the forefront of developing theoretical basis and conducting applied studies in the field of wind energy in Europe are such major research centers as DTU (Denmark), CENER (Spain), UPORTO (Portugal) and Fraunhofer IWES (Germany). In Latvia the topic is pursued by FEI, RTU, LU, VeA IZIVSRC and LEGMC. Among others, a great contribution to the study of wind energy in Latvia was made by the works of prominent Latvian scientists R. Vinogradovs, N. Levins, J. Greivulis, A. Grundulis, A. Sauhats, V. Bezrukovs, J. Ekmanis, P. Shipkovs, V. Pugačevs, D. Blumberga, J. Roliks.

The thesis presents the results of applications and further developments of methods aimed at improving the quality of wind measurements, estimating wind energy resource and predicting the efficiency of wind turbines in the conditions of low wind speed typical for Latvia. In order to achieve the proposed goals in the study of the distribution of wind energy potential in Latvia, a series of physical and modelling experiments were carried out using laser measuring complexes and measuring sensors installed on tall masts, in combination with theoretical Computational Fluid Dynamics (CFD) estimations.

The results obtained in the course of ENER/FP7/618122/NEWA ERA-NET PLUS project, enabled the development of a wind energy resource distribution map based on long-term wind speed measurements using the technical capabilities of the Latvian National Hydrometeorological and Climatological Service of the Latvian Environment, Geology and Meteorology Centre (LEGMC), which operate a network of 10 m high meteorological masts. In combination with the study of wind speed distribution over height a wind shear measurement method has been developed using lattice cellular communication masts. The approach makes it possible to predict the effectiveness of wind turbine operation depending on the chosen hub height at lower costs.

1. Alternative energy sources in modern energetics

1.1. Problems and solutions

1.1.1. Challenges of the contemporary world energetics

Nowadays, the human civilization can exist only by producing and consuming an enormous, ever-increasing amount of energy. At the same time, prior to the industrial revolution at the turn of the 18th–19th centuries humanity was relying practically exclusively on renewable energy sources – energy of water, wind and bio fuel.

Industrial technology development and the associated growth in energy needs led to a rapid increase in the use of, predominantly, non-renewable energy resources — first coal, and then oil and gas; therefore, the global energy industry of the 20th and early 21st centuries was, and remains, largely hydrocarbon-based that makes the cornerstone of the energy problem that world nations try to tackle.

The global energy problem can be viewed as a task of ensuring a reliable supply of fuel and energy for the humanity, while limiting associated environmental costs. The main reason for the emergence of the energy problem could be attributed to a rapid increase in the consumption of mineral fuels and the volumes of greenhouse gasses emitted in the process of their consumption.

As can be seen from Figure 1.1, in the course of the last 150 years the rate of energy consumption has increased dramatically. It is notable that the period when the volumes have skyrocketed includes only the last 70 years [1]. Therefore, already in the middle of the 20th century academics and politicians were contemplating how the economies of the leading industrial countries would be developing in the period of the shortage of energy sources [2].

It is unarguable that Earth's crust contains all types of hydrocarbons in huge quantities, but it should be noted that their overall volume is still limited and can be exhausted. Therefore, initially the emergence of a global energy shortage problem was associated with the depletion of the world's explored oil reserves. However, it turned out that the volumes of proven oil reserves grew in parallel with the growth in its consumption and production.

According to 1989 data, such proven reserves should have been excused in the next 40 years. However, in 2007, when oil production was reaching record high levels, according to expert estimates, proven reserves should have lasted for another 40 years.

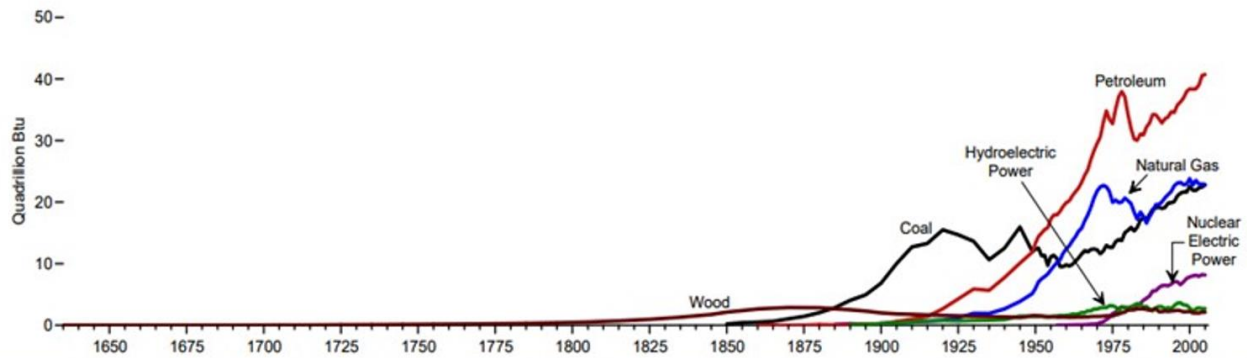


Figure 1.1 World energy consumption in the period 1630 – 2005 in British thermal units (Btu) [1].

This fact can be explained by advancements in the methods and technologies of oil exploration, as well as to the development of new oil-bearing areas. Nowadays, the so-called "cheap oil" occurring in layers accessible to modern technology is still being extracted and consumed. This oil is called "conventional" as opposed to "non-conventional", which lies at great depths, contained in oil sands and asphalt shale.

In the beginning of the 21st century, the concept of "global energy security" has come into wide use. The strategy of such security rests on the principles of a long-term, reliable, environmentally friendly energy supply at reasonable prices that suits both exporting countries and consumers.

It is therefore indicative, that in a number of European countries such as Germany, Denmark and Belgium, there is a trend of abdicating from the use of nuclear fuel and gas in the production of electrical energy. The main focus of these countries is on the development of technologies exploiting wind and solar energy.

At the same time, global energy security largely depends on practical measures of further ensuring the world economies primarily with traditional types of energy resources that are more stable and predictable. Therefore, the search for sustainable solutions to energy problem remains relevant also nowadays.

1.1.2. The roadmap to the global environmental safety and energy security

The most traditional and extensive way to tackle the global energy problem is to further increase the stock of explored mineral fuels. As a result of this approach, the global resources of

coal and natural gas have not only increased significantly in the last three decades, but have also grown at a faster rate than their production.

The path of increasing the stock of fuel reserves has always been the main one, but nowadays, an alternative approach has come to the forefront, which is to use energy resources more rationally and economically, that is to implement energy conservation policies.

In recent years, many technical and technological innovations have been carried out to improve the situation. Energy saving is increasing due to the improvement of industrial and municipal equipment, the production of more efficient cars, thermal isolation of buildings and etc. The range of macroeconomic measures should in the first place include a gradual change in the structure of consumption of energy resources with an emphasis on increasing the share of renewable and non-traditional primary energy resources.

The sharp increase in energy consumption in the world over the past decades has led to the problem of an anthropogenic influence on climate change. In this regard, on 12 December 2015 in Paris, parties to the UNFCCC reached a landmark agreement to combat climate change and to accelerate and intensify the actions and investments needed for a sustainable low carbon future [3, 4].

Thanks to the efforts of the states that signed the Paris Agreement, outlining the measures to combat CO₂ emissions into the atmosphere, there is a gradual decrease in the share of fossil energy sources and their replacement with renewable resources. According to the assessment of International Renewable Energy Agency (IRENA) the energy system, consequently, requires rapid, immediate and sustainable change. However, in order to achieve these goals, the deployment of renewables must increase at least six-fold compared to the levels set out in current plans [3].

The share of electricity in total energy use must double, with substantial electrification of transport and heating. Renewables would then make up two-thirds of energy consumption and 85% of power generation. Together with energy efficiency, this could deliver over 90% of the climate mitigation needed to maintain a 2°C limit.

According to the Reference Case (which reflects current and planned policies including Nationally Determined Contributions (NDCs)), energy-related CO₂ emissions will increase slightly year on year to 2040, before dipping slightly by 2050 to remain roughly at today's level (Figure 1.2). The assessment suggests that renewable energy and energy efficiency can provide over 90% of the reduction in energy related CO₂ emissions [5].

This is an improvement in comparison to the previous analysis conducted in 2017, which found annual CO₂ emissions would be higher in 2050 and shows that NDCs and the rapidly decreasing cost and improving performance of renewable energies are having an effect on long-term energy planning and scenarios [5]. Nevertheless, significant additional reductions of greenhouse gas emissions are needed. To meet a climate target of limiting warming by 2°C, annual energy-related CO₂ emissions still need to decline by 2050 from 35 Gt (in the Reference Case) to 9.7 Gt, a fall of more than 70%.

Overall, actions undertaken by global participants at the current stage will be crucial for the creation of a sustainable energy system in the future. Ultimately, the path to secure a better future depends on pursuing a positive, inclusive, economically, socially and environmentally beneficial energy transformation.

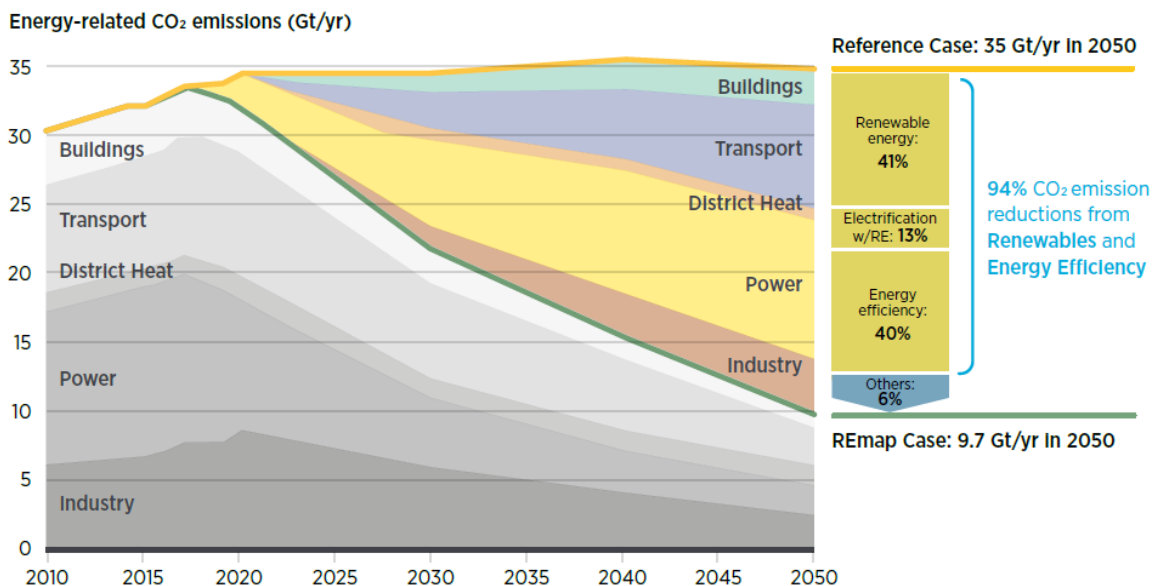


Figure 1.2 Annual energy-related CO₂ emissions and reductions, 2015-2050 (Gt/yr) [5].

1.2. The use of renewable energy resources

1.2.1. Modern renewable energy sources

Almost 40 years ago, the UN General Assembly, in accordance with resolution 33/148 (1978), introduced the concept of "new and renewable energy sources" (RES), which includes the following forms of energy: solar, geothermal, wind, sea waves, ocean tides, biomass energy of wood, charcoal, peat, cattle, shale, tar sands, hydropower.

However, it is more common to include in RES the energy of solar radiation, wind, water flows, biomass, thermal energy of the upper layers of the earth's crust and ocean.

Typically distinguish the following classes of RES:

- mechanical energy (wind energy and water flows);
- thermal and radiant energy (the energy of solar radiation and heat of the Earth);
- chemical energy (energy contained in biomass).

In order to access the progress in the development of power sector it is necessary to see how the importance of renewable sources changes over the last decade. The overall share of renewable energy in the Total Final Energy Consumption (TFEC) has increased only modestly in recent years, but it has to be noted that total demand for energy has also increased during that time (see Figure 1.3) [6].

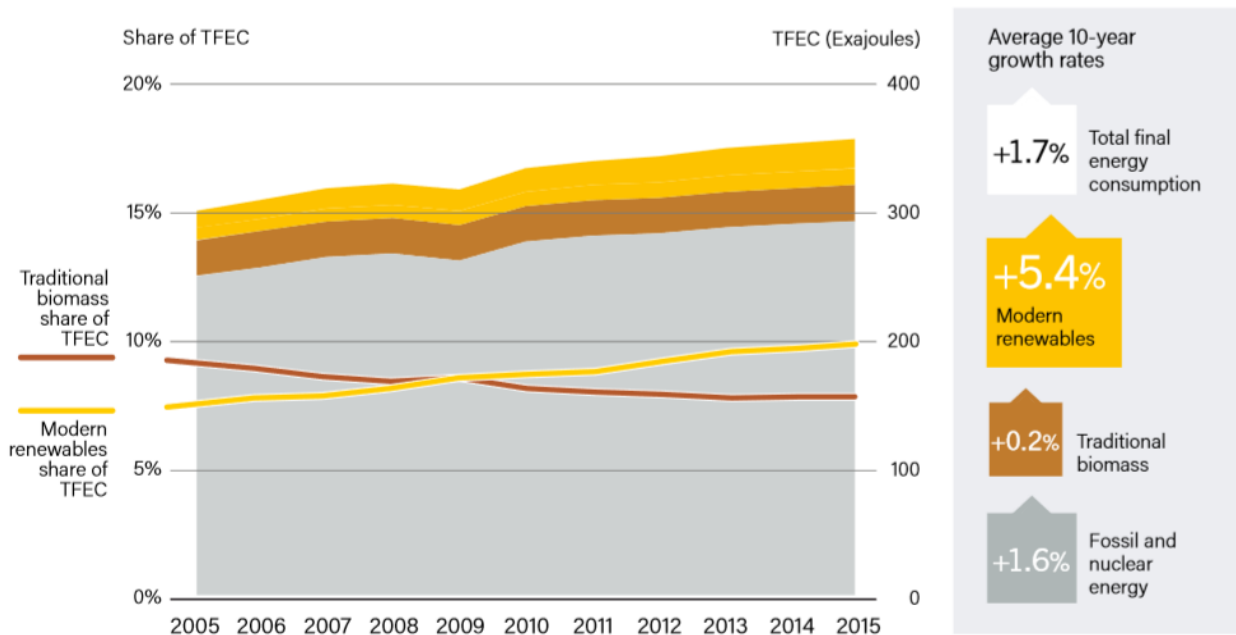


Figure 1.3 Growth in global renewable energy compared to TFEC, 2005-2015 [6].

Overall trends in the power production suggest that the transition to renewable energy is feasible, as in 2016 renewables accounted for 18.2% of final energy consumption, while modern renewables, not including traditional use of biomass, contributed approximately 10.4% (see Figure 1.4) [6].

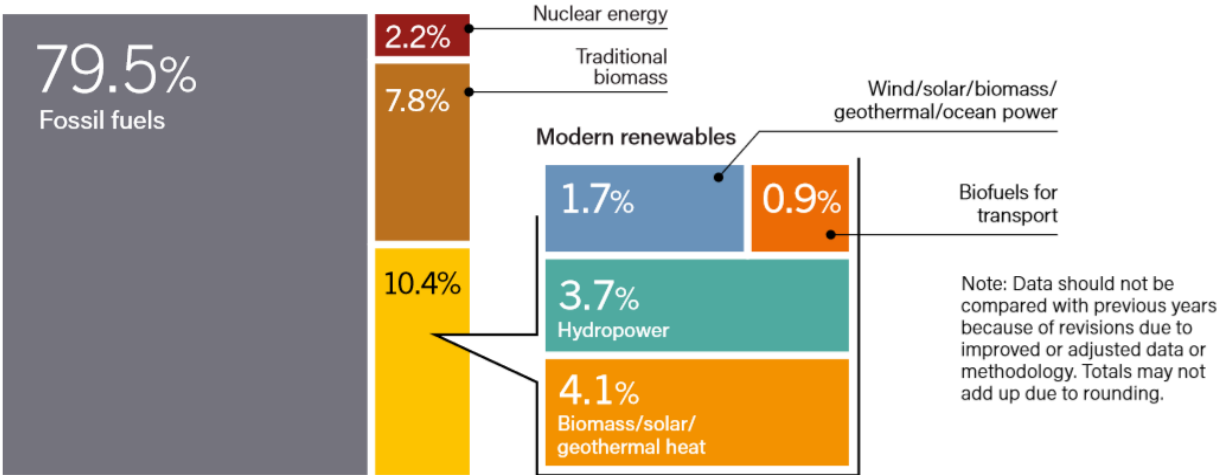


Figure 1.4 Estimated renewable share of total final energy consumption, end-2017 [6].

Renewable energy sources are mainly used to produce electrical energy (see Figure 1.5), as they provided 26% of global electricity demand at the end of 2017 [6].

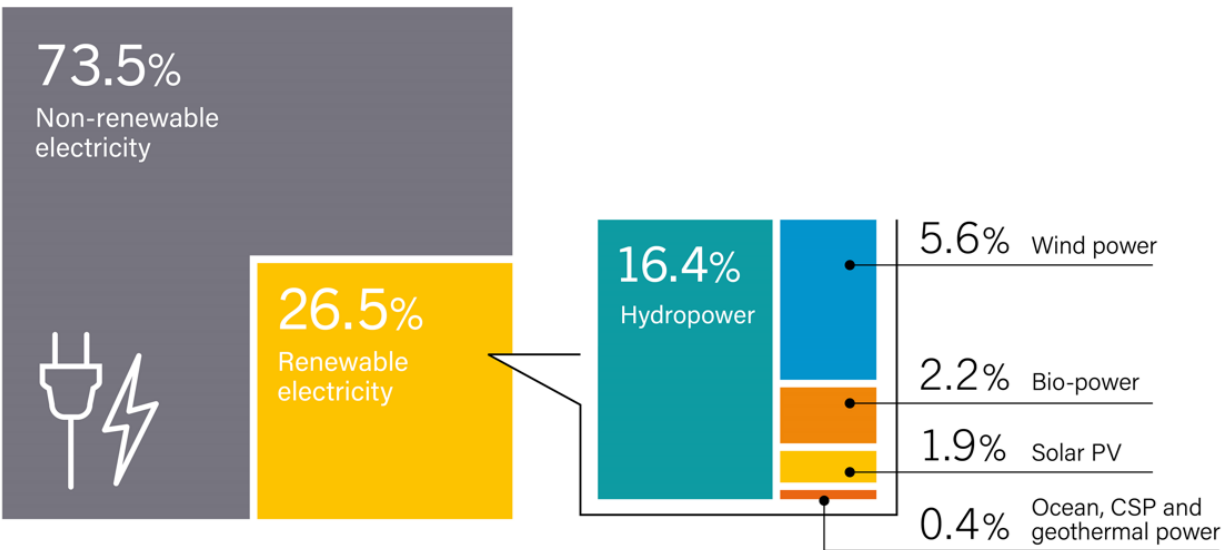


Figure 1.5 Estimated renewable energy share of global electricity production, end-2017 [6].

The growth in the use of renewable energy resources in the production of electrical energy in Europe is shown on Figure 1.6. It can be seen that the use of renewable resources has practically doubled in the last 25 years [7].

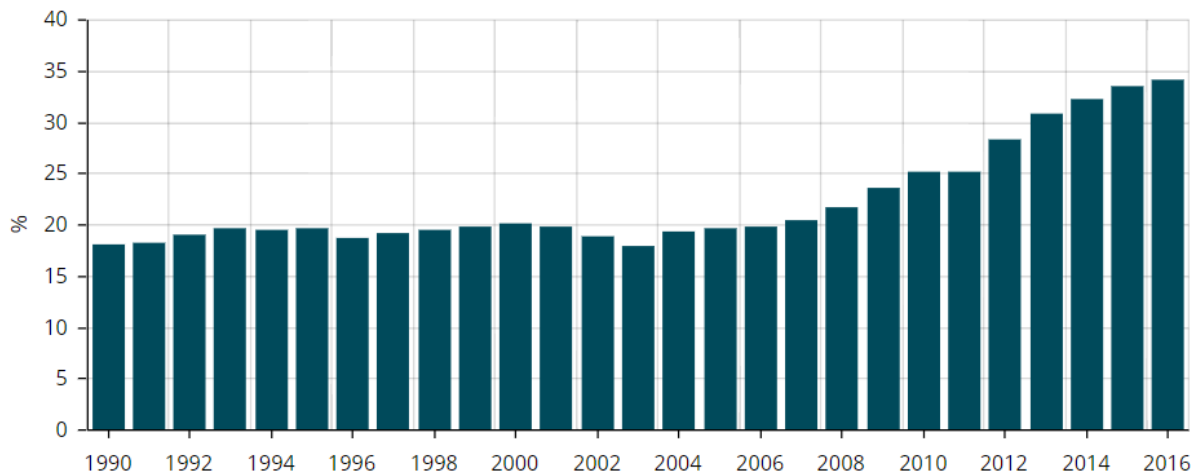


Figure 1.6 The share of renewable energy resources in electricity production in Europe [7].

Referring to the concept of energy quality that is closely linked to the efficiency, which determines the proportion of the source energy turned into mechanical work, it can be noted that the quality of hydropower is characterized by the ratio of 0.6-0.7; wind - 0.3-0.4. The quality of thermal renewable energy sources does not exceed 0.3-0.35. The quality indicator of solar radiation used for photoelectric conversion is even lower – 0.15-0.3. Power quality of biofuels is also relatively low and usually does not exceed 0.3 [8].

It should be pointed out that the main factor stimulating the development of renewable energy in the world is still decarbonization, fostering the need to take measures to reduce greenhouse gas emissions to combat global warming. This is the main aim of Paris Climate Change Agreement adopted on December 12, 2015 and entered into force on November 4, 2016.

1.2.2. Wind power development trends

The speed and magnitude of the structural changes in wind energy sector can be seen from long-term statistics on the penetration of wind energy globally and in Europe. As reported by Global Wind Energy Council [9], in the last 20 years wind energy power globally grew more than fiftyfold (see Figure 1.7).

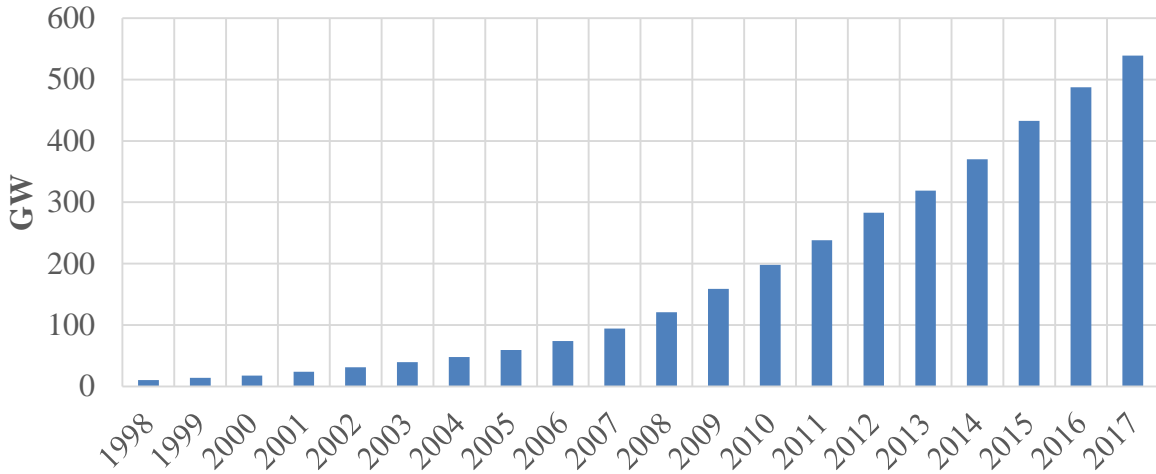


Figure 1.7 Global wind power installed capacity (GW) [9].

Market forecasts taking into considerations latest development trends indicate that globally installed wind power capacities will reach 1 TW by the end 2025 (see Figure 1.8) [10].

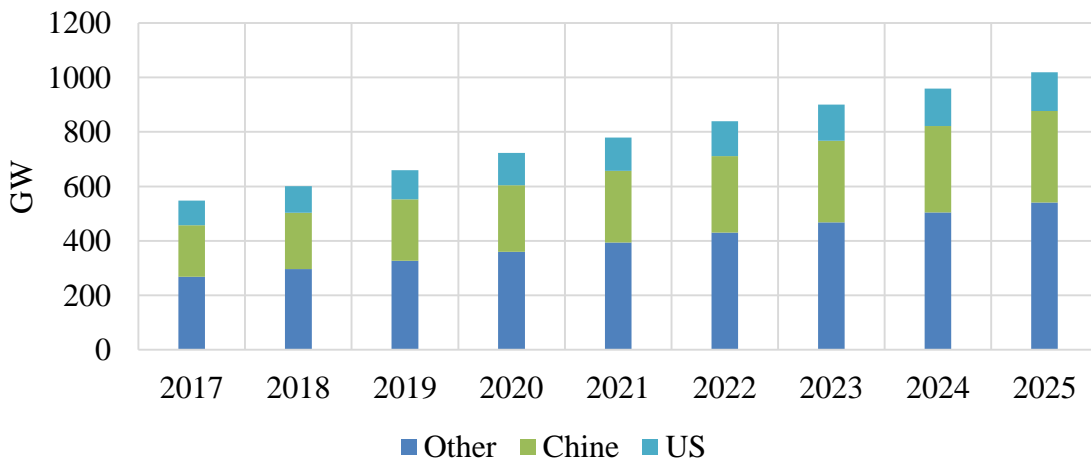


Figure 1.8 Forecasted global wind power market installed capacity (GW), 2017-2025 [10].

European trends are even more distinct, as in terms of the speed of development and relevancy wind power has become the second most important energy source in Europe in terms of installed capacity overtaking traditional gas power plants (see Figure 1.9) [11].

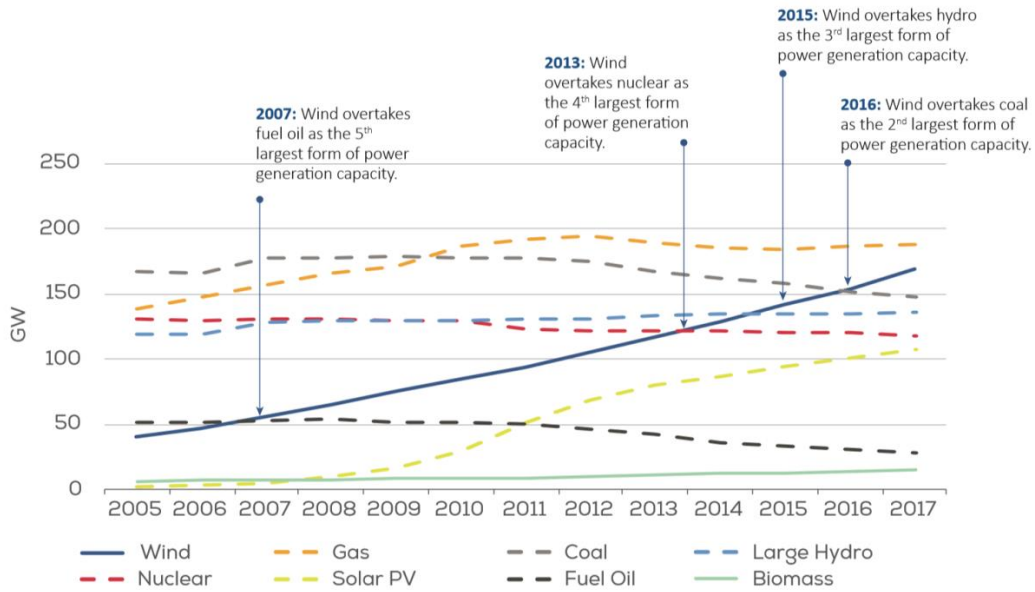


Figure 1.9 Total power generation capacity in the European Union 2005-2017 [11].

The growth in the production of electrical energy using wind and solar energy are presented in Figure 1.10, which shows the change in the structure of energy over the past 25 years [7]. The manifold increase in the generation of electric energy from renewable sources is associated with several main factors: it is driven by an increase in the installed capacity of wind parks; it is the result of improved manufacturing technology of WT design and an increase in the height of masts of up to 200 m that is a consequence of the emergence of new materials and construction equipment.

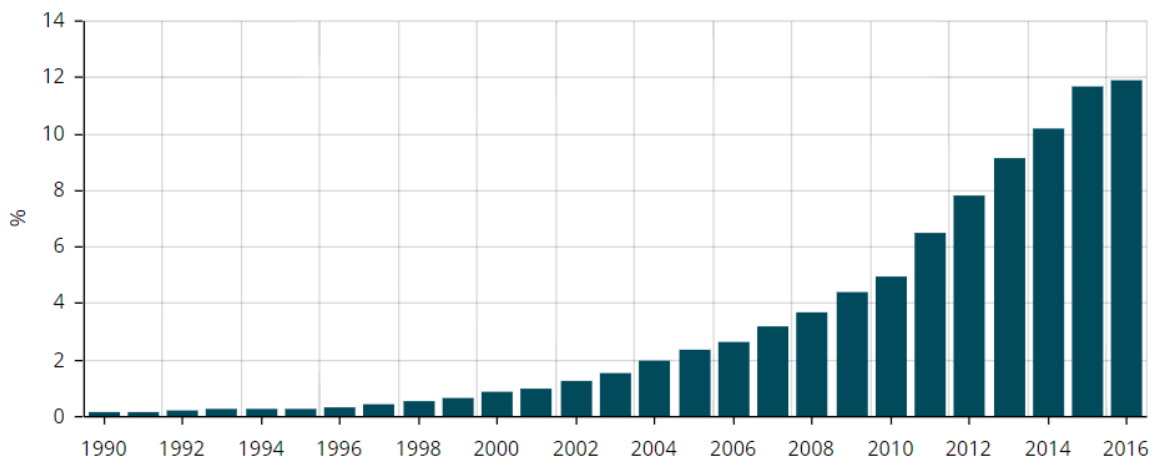


Figure 1.10 The share of solar and wind energy in electricity production in Europe [7].

According to the World Wind Energy Association (WWEA) in 2017 installed wind power capacity could cover more than 5% of global electricity demand [12]. For many countries, wind power has become a cornerstone in their strategies to phase out fossil and nuclear energy. For instance, Denmark sourced 44% of its power from wind in 2017, while in Portugal, Ireland and Germany wind energy accounted for more than a fifth of the average annual electricity demand (Figure 1.11).

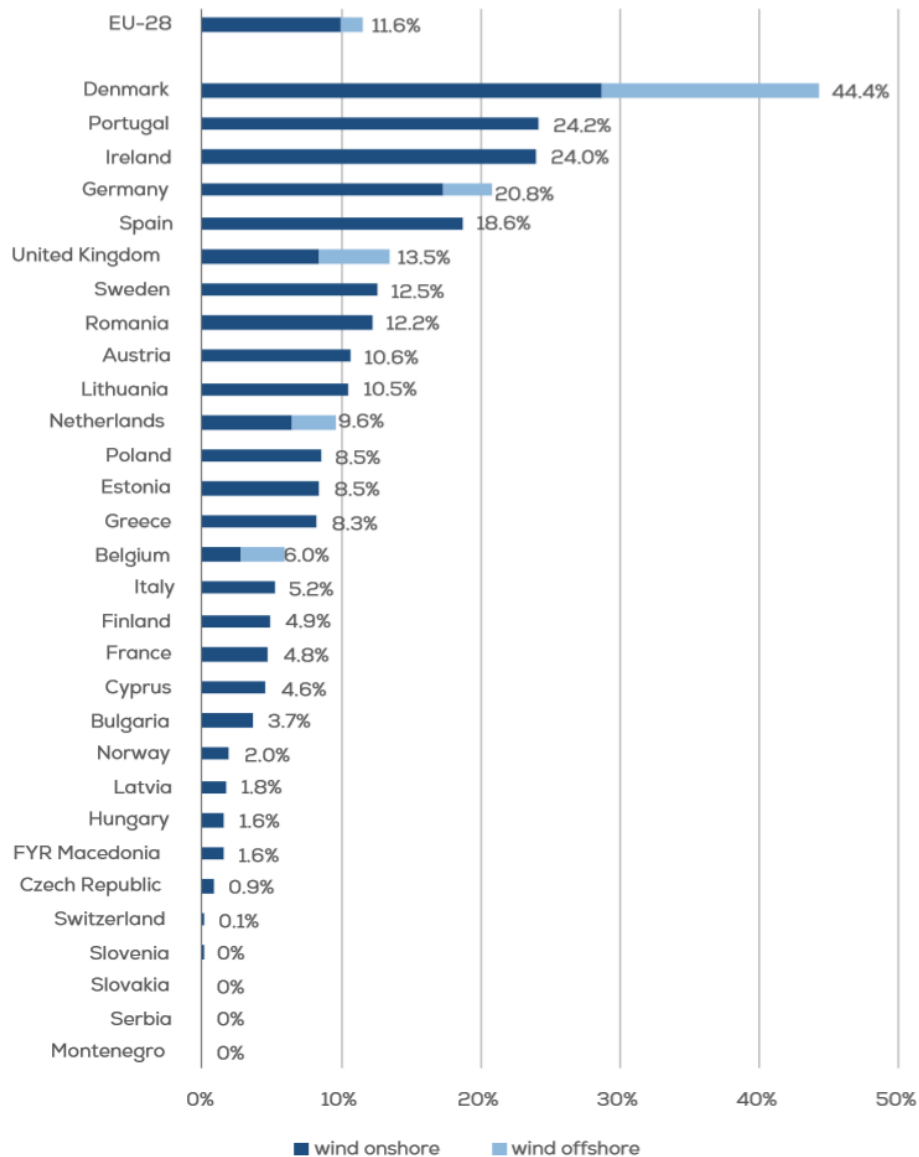


Figure 1.11 Percentage of the average annual electricity demand covered by wind in 2017 in Europe [11].

It is acknowledged that the cost of "green" energy is higher in comparison to the traditional power, derived from the combustion of hydrocarbons or the splitting of atomic nuclei.

However, at present, alternative energy is becoming more profitable every year [13]. This is facilitated by the active construction of wind parks in the mountains and offshore. According to the European Commission, the levelised cost of electricity (LCOE) of onshore wind ranges from €52 EUR/MWh to €110 EUR/MWh. (see Figure 1.12).

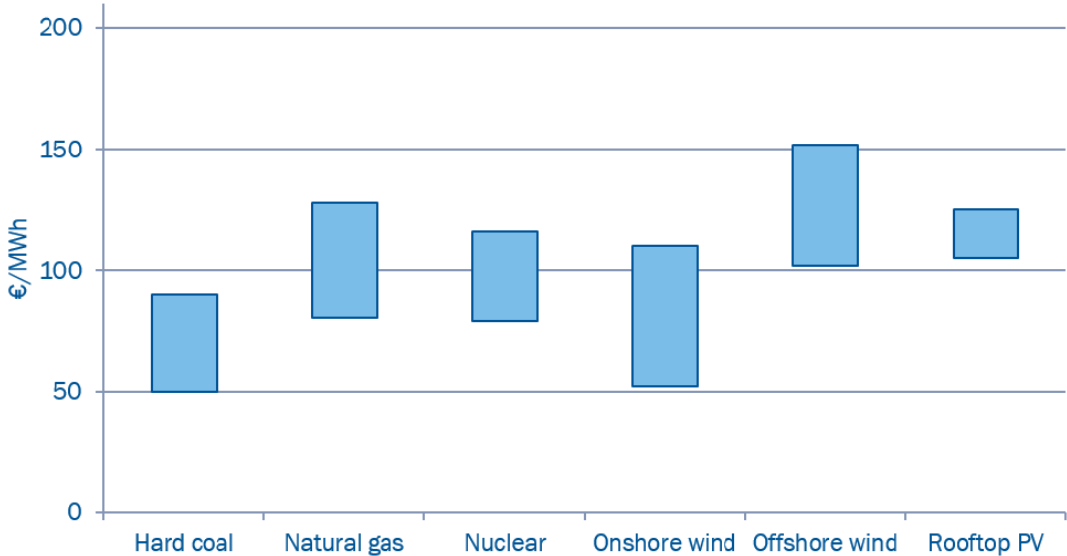


Figure 1.12 LCOE of major power generation technologies in Europe [14].

A report prepared by GlobalData [10] finds that auction-based competitive bidding has become a popular mechanism to develop wind energy in several countries. Countries including Mexico, Brazil, Argentina, Canada, Germany and India have adopted the auction mechanism for various renewable energy technologies including wind. Globally, in 2017, around 18 GW of wind capacity was awarded with an average price of 49.4 \$/MWh. The average awarded price in 2016 auctions for 8 GW of wind capacity was 52.6 \$/MWh (see Figure 1.13).

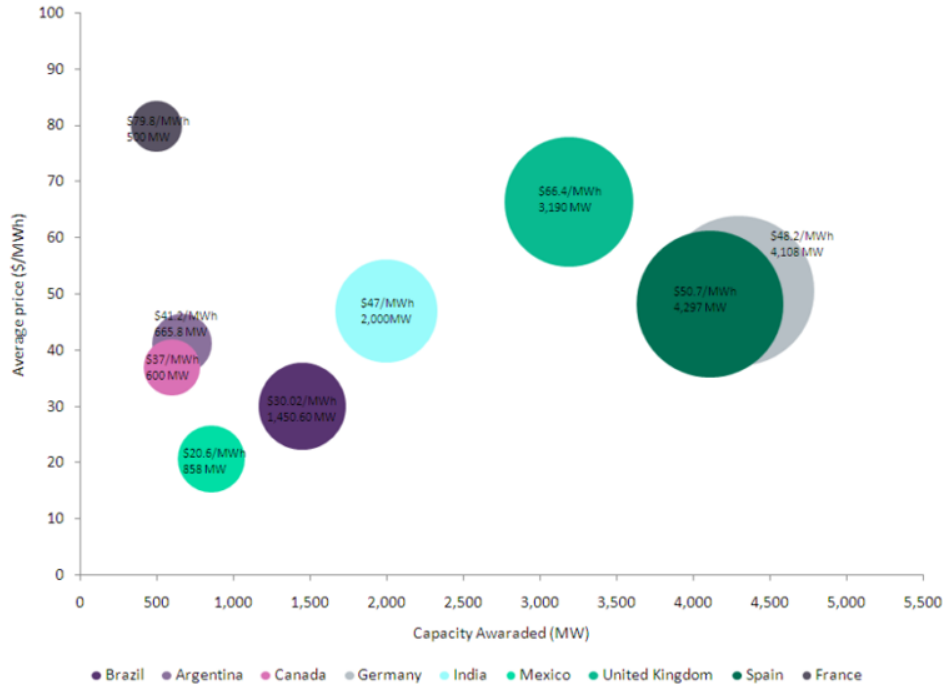


Figure 1.13 Wind power market, key countries, auction, 2017, bubble size represents overall capacity awarded [10].

The report also concludes that feed-in tariffs (FiTs) were the key incentive mechanism to drive the growth of wind energy up to 2016. However, due to the continuous reduction in the cost of wind power generation, auction-based competitive bidding has replaced FiTs as the most prominent mechanism to drive wind power installations in some of the key wind power markets in 2017. The authors expect the trend to continue in the near-term with more and more countries adopting competitive auction mechanism for wind power development.

Offshore wind farms are, by definition, more expensive than land installations, because for the transfer of energy to the mainland, it is necessary to lay underwater cables that tend to be tens of kilometres long. On top of this, higher towers and massive foundations are required for the placement of generators, taking into consideration the complications that can be caused by salt-water corrosion of metal structures.

In all respects, sea windmills are much more expensive compared to land-based analogues. Along with much higher installation costs, off-shore turbines are more demanding in terms of maintenance and more likely to be exposed to extreme weather conditions. However, they have an important advantage – they have greater efficiency due to regular sea winds. On Figure 1.14, it can be seen that over the past 5 years, interest in building offshore WPPs in the EU

has increased significantly. The main driver of off-shore installations in Europe are UK and Germany, that together account for more than 70% of the installed capacities [11].

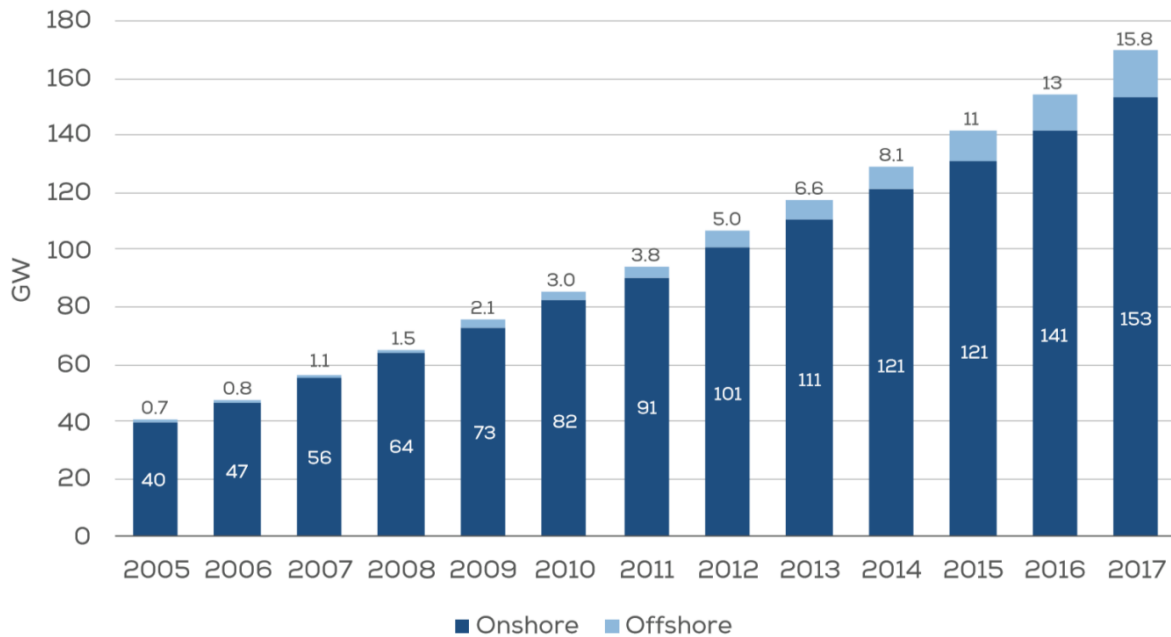


Figure 1.14 Cumulative installations onshore and offshore in the EU [11].

According to the forecasts, offshore wind parks without government subsidies will be profitable only after 2024-2025, when construction of WT's with a capacity of 13 and 15 MW will be mastered. So far, the largest manufactured turbines have a capacity of only 8-12 MW. Indicatively, a 12 MW ocean WT would be able to generate 67 GWh annually.

For instance, one Haliade-X 12 MW would generate enough power to supply 16000 European households according to wind conditions on a typical German North Sea site. Based on a 750 MW windfarm and an estimated annual energy production (AEP), such power plant could produce enough electricity for up to 1 million households [15].

Currently, European wind energy is approaching an important milestone. As shown on the map Figure 1.15, three new WPPs are planned to be built on the coastal shelf in the North Sea, which will be built for the first time without government subsidies [16]. In 2013, new WPP projects delivered electricity at about 160 euros per megawatt-hour, while manufacturers set a “realistic long-term goal” to reduce energy costs to 100 Eur/MWh by 2020.

Several ongoing projects promise to further reduce the cost of electricity. For example, the Danish company Dong Energy aims at an unprecedented price of 62 Eur/MWh. This

company has already begun to build the Hornsea Project One offshore power station near the North Sea, which is positioned as the largest off-shore power station in the world.

It is foreseen that 174 Siemens 7 MW WT's as high as 190 meters will be located on an area of 407 km² in the sea. By 2020, they should reach a maximum capacity of 1.2 GW, so this giant power facility 120 km from the coast will be the first gigawatt wind power plant in the world.

Another power plant in the North Sea is being planned by the German company Energie Baden-Württemberg, which also expects prices below 75 Eur/MWh. According to experts, such a rapid fall in prices is caused by strong competition on all fronts - from the production of wind generators to installation and cabling services.

The map on Figure 1.15 also shows the North Sea Dogger Bank Power Hub, which will gather energy from several power plants - and deliver it to different countries. It is planned to lay power cables from the hub to the UK, the Netherlands, Germany, Denmark and Norway. The energy hub is supposed to be constructed on one or several artificial islands in the North Sea where the HVDC converters will be located, which will reduce the losses for the conversion and transmission of electricity. Consequently, the station operators would be able to sell electricity to the customers that are willing to pay the highest price.



Figure 1.15 Wind park construction project in shallow water in the North Sea [16].

In Latvia, the first WTs TAKE TW600 with rated power of 600 kW, hub height of 50 m and a rotor diameter of 43 m were installed in 1994 in Ainaži [17]. Later, wind power parks Winergy, Vēja parks, Vides enerģija, Baltnorvent, Lenkas Energo and others with total installed capacity of 70 MW were built. It is noteworthy that the total amount of permits issued for the construction of wind parks in Latvia was 203 MW that greatly exceeds the size of implemented projects [18].

1.2.3. Wind energy transfer from WTs to the grid

A schematic presentation on Figure 1.16 shows a standard scheme for converting the energy of the wind flow into rotational motion of the generator rotor due to WT [19]. Because of the rotation of the rotor, alternating voltage occurs at the terminals of the generator phase windings and the mechanical energy is converted into electrical energy.

From the output terminals of the generator, alternating voltage is supplied to the power interface, consisting of a semiconductor frequency converter and a transformer, which serve to match the output voltage of the generator to the frequency and voltage of the power line.

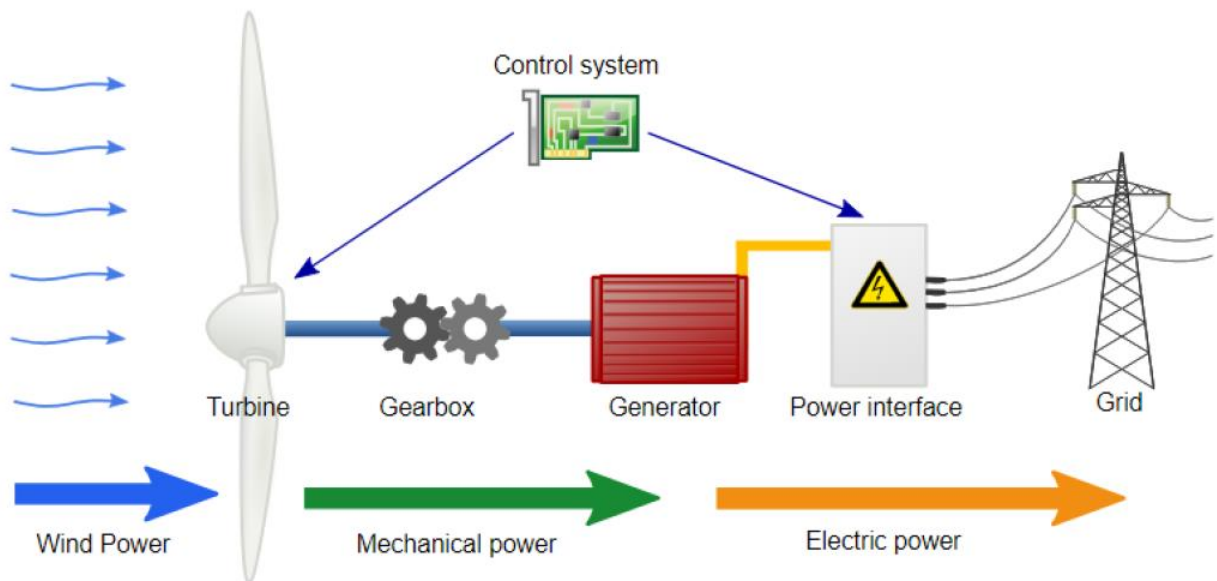


Figure 1.16 The scheme of transformation and transmission of wind energy from a WT to the network [19].

In the case of off-shore WTs, energy is transferred from a generator located in the cabin on the top of wind generator hub to the consumer over a cable, which has a high degree of protection. An armoured high-voltage three-phase AC cable for a voltage of 220 kV was presented at WindEurope 2018 exhibition in Hamburg.

In Figure 1.17, one can see the location of three copper conductors with a section of $3 \times 1200 \text{ mm}^2$ in isolation, as well as thin optical cables of communication lines. From the outside, a metal braid made of steel rods protects the cable. The design of a $1 \times 2500 \text{ mm}^2$ high-voltage DC cable for 320 kV, presented at Windindustry 2015 exhibition in Parise, is shown in Figure 1.18.



Figure 1.17 The design of a three-phase AC $3 \times 1200 \text{ mm}^2$ high-voltage submarine cable for transmitting 220 kV power from offshore WT to a grid on the shore



Figure 1.18 The design of a high-voltage underground DC cable $1 \times 2500 \text{ mm}^2$ for the transfer of 320 kV power from a WT to a grid on the shore.

A typical power transfer scheme from an offshore WPP to an onshore grid for one of Tennet projects in Europe is shown in Figure 1.19 [20]. As can be seen, along with WTs located offshore, the project includes an offshore AC substation that integrates power from several individual power stations located in direct proximity to the substation.

The project foresees that the AC substation will be connected with a high-voltage on-shore substation via submarine 220 kV cables, where the voltage level is converted from 220 kV

to 380 kV. Finally, the national 380 kV high-voltage grid is used to distribute the wind energy to households across the country.

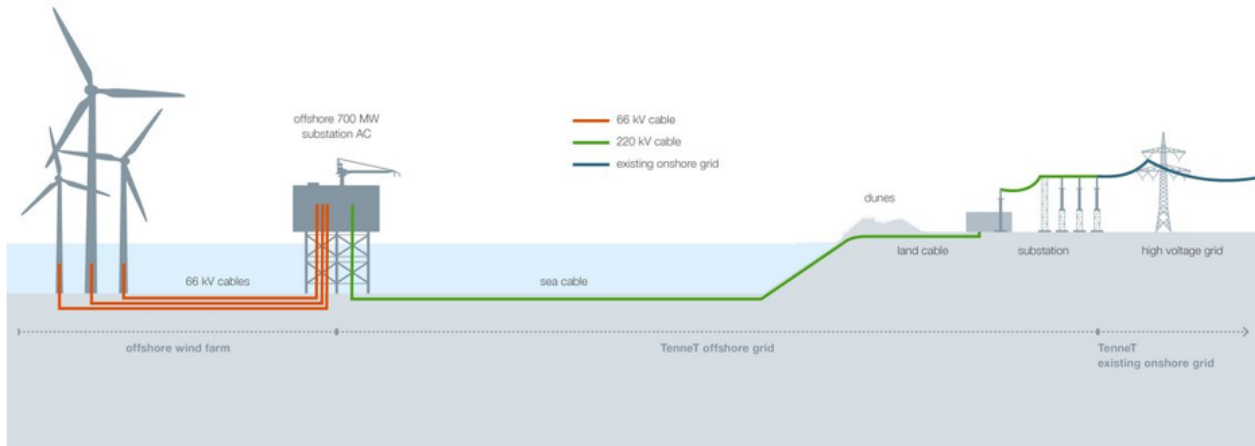


Figure 1.19 Power transmission scheme connecting an off-shore WPP with an existing high-voltage grid ashore [20].

1.3. Economical risks of wind energy projects

1.3.1. Cost of onshore and offshore WPP

The total project costs depend on many factors, including the cost of the turbine itself, the extent and scope of supporting environmental work for the planning application, the cost of any electrical distribution network upgrades and the cost of site works including access roads, foundation and cabling costs.

The cost structure of a typical 2 MW WTs installed in Europe calculated based on selected data for European WT installations presented in Table 1.1 [21].

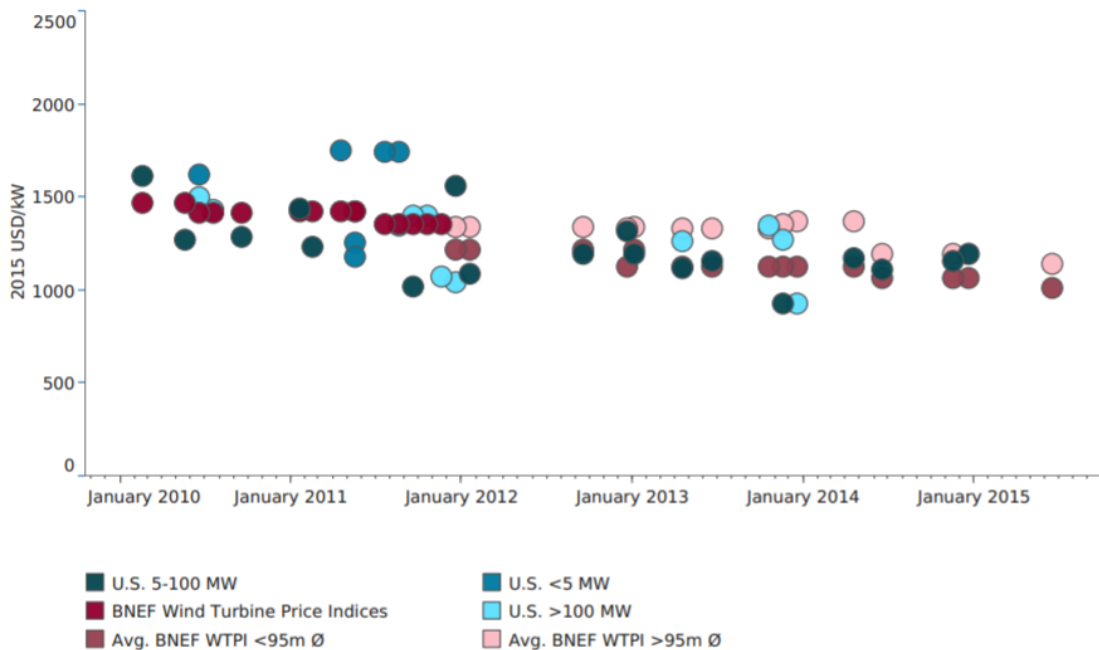
According to the statistics gathered by IRENA from several data sources, including Lawrence Berkeley National Laboratory (LBNL) and Bloomberg NEF (BNEF), the prices of WTs in the US decreased by 29% to 45% in the period between 2010 and 2015 as presented on Figure 1.20 [22]. Another comparative analysis and summary of total investment costs per kW in different regions of the world is also presented in [23].

Table 1.1

Cost structure of a typical 2 MW WT installed in Europe [21]

	Investment (€1,000/MW)	Share of total cost %
Turbine	928	75.6
Grid connection	109	8.9
Foundation	80	6.5
Land rent	48	3.9
Electric installation	18	1.5
Consultancy	15	1.2
Financial costs	15	1.2
Road construction	11	0.9
Control systems	4	0.3
TOTAL	1 227	100

Due to the economies of scale, larger turbines cost less per kW installed than smaller ones. Typically, the actual wind turbine costs around 69% of the total project cost. In that respect, a reasonable conservative budget price, for a standard WT is presented in Table 1.2 [24].



Source: LBNL and BNEF

Figure 1.20 Wind Turbine price dynamics in 2015 USD per kW of nominal power [22].

As shown in Figure 1.21 and Figure 1.22, construction costs, the values of capacity factor and levelised cost of electricity for onshore and offshore wind power parks have markedly changed in the period from 2010 to 2017 [26]. It should be noted that there is a gradual increase in the efficiency of operation of WTs, which leads to a decrease in the cost of energy produced. At the same time, the construction cost of per kW depends on the installed capacity of WPP and in recent years, the costs have a downward trend.

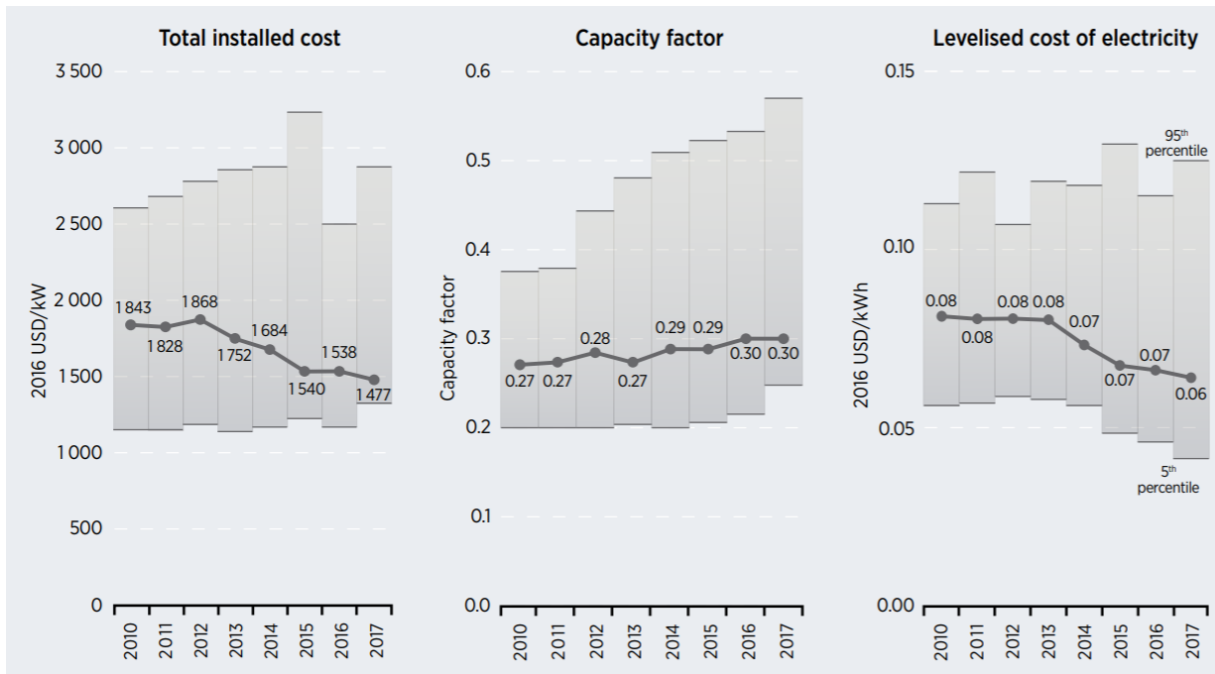


Figure 1.21 Global weighted average total installed costs, capacity factors and LCOE for onshore wind, 2010-2017 [26].

Table 1.2

Estimated costs for a sample project [24]

Power Output, kW	Typical WT Type	Project Cost £'000
55	Endurance E-3120	320
800	Enercon E53/48/44	1 400
900	EWT DW61	1 400
1500	GE 1.5sle	2 700
2000 – 3000	Enercon E82	3 100

According to a research conducted by the National laboratory of the U.S. Department of Energy (NREL) costs for installing a WT of the Land-Based Reference Project using the 2.0-MW

turbines and the Fixed-Bottom Reference Project using the 4.14-MW WT are the values shown in Table 1.3 and 1.4 [25].

Table 1.3

Summary of the Land-Based Reference Project using 2.0-MW WT [25]

Component	Costs \$/kW
Turbine capital cost	1 210
Balance of system 330 kV	330
Financial costs	150
Total	1 690

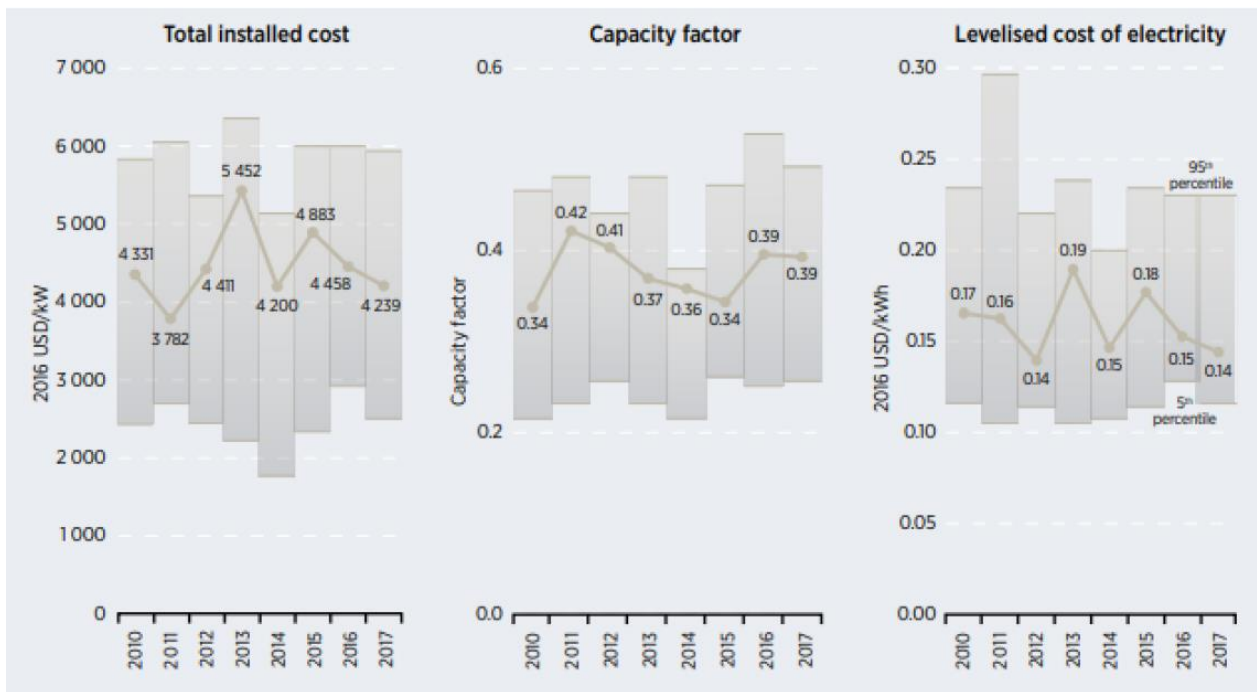


Figure 1.22 Global weighted average total installed costs, capacity factors and LCOE for offshore wind, 2010-2017 [26].

As can be inferred from the above tables and graphs, the total cost of offshore projects is more than 2.5 times higher than the capital expenditures for the land-based reference wind plant project.

Table 1.4.

Summary of the Fixed-Bottom Offshore Reference Project using 4.14 - MW WT [25]

Component	Costs \$/kW
Turbine capital cost	1 466
Balance of system 330 kV	2 167
Financial costs	983
Total	4 616

Note: In 2015-nominal dollars.

1.3.2. Risk management in renewable energy projects

The planning of wind farm projects is usually complex, because the multitude of economic and operational risks have to be considered. After the completion of a wind park, various risks may arise during the lifetime, such as general operational and maintenance risks, business interruption due to damages or grid availability risks, natural disasters and many other factors.

Moreover, the intermittency of the flow of wind energy introduces significant uncertainty in the calculations of the predicted WPP profitability. The questions of assessing these risks and the degree of their influence on the payback period and profitability of projects have been studied by many authors [27]–[31].

The analysis of these studies allows to systematize and present the main risks in the form of Table 1.5, where risk categories are divided in two groups depending on whether they refer to technical and structural factors or economic problems.

The risks related to the first category are associated with technical problems that are addressed at the stage of preparation of project documentation and manufacture of WT. Essentially the burden of addressing these risks rests on manufacturers that leverage on their accumulated experience by introducing new construction technologies, developing more advanced structural materials and optimising maintenance operations.

A technical failure or damage of the WT construction usually leads to a temporary shutdown of operations until the issue is addressed. Such events decrease the amount of electrical energy produced and eventually result in the deterioration of WPP economic performance.

Table 1.5

Risk factors in the commercial use of wind energy

Typical Wind Power Plant (WPP) project risks	
I. Technical and structural factors	II. Economic factors
<ol style="list-style-type: none"> 1. Turbine power curve correspondence to the prevailing wind type 2. The choice of mast height 3. Choice of wind the turbine type 4. Reliability of the gearbox, generator and control unit 5. Reliability of power transmission lines 6. Reliability of the foundation and mast 7. Impact of the environmental on Wind Turbine 8. Possibility to use energy storage 9. Ease of maintenance 	<ol style="list-style-type: none"> 1. Possibility to take a loan 2. Insurance terms 3. Land lease 4. Obtaining a license 5. Changes in the price of electric energy 6. Estimation of wind energy resource 7. Availability of support schemes 8. Fluctuations in the demand on the consumption market 9. The impact of Wind turbines on the environment

The risks assigned to the second category are related to the management issues, site selection, park design and wind energy potential estimation, which can be directly expressed in monetary terms. However, estimating the magnitude of losses from these risk factors is not straightforward. This is due to the constant change in electricity prices and fluctuations in the flow of wind energy, which introduces uncertainty in the calculation of the economic efficiency of WPP in the short- and long-term period of operation.

In order to reduce the impact of risks attributable to the second group on the performance of WPP, analysts apply forecasting methods that aim at determining the patterns of change and relationships between the main risk drivers.

1.4. Modern methods of increasing wind turbine efficiency

1.4.1. Electrical energy storage systems

The development of renewable energy sources should not be viewed in isolation, but as part of a wider energy transition process of a long-term change in the structure of energy systems. This process is characterized by the emergence of new technologies, equipment and other important changes, many of which enhance the "green" energy, increasing its chances of success.

One of such changes is the development of energy storage technologies. The emergence of commercially attractive technologies in this field will create conditions for more intensive use of renewable energy resources that are highly dependent on weather conditions and the time of day.

Electric energy storages are the most important element of future active adaptive networks [32], [34]. Electrical energy storage (EES) is one of the key technologies in the areas covered by the IEC. EES techniques have shown unique capabilities in coping with some critical characteristics of electricity, for example hourly variations in demand and price. In the near future reliable, high capacity and efficient EES will become indispensable in emerging IEC-relevant markets in the use of more renewable energy, to achieve CO₂ reduction and for Smart Grids. Nowadays already exist installations with a capacity of up to 1 GW and more.

A widely-used approach for classifying EES systems is the determination according to the form of energy used. In Figure 1.23 EES systems are classified into mechanical, electrochemical, chemical, electrical and thermal energy storage systems [33].

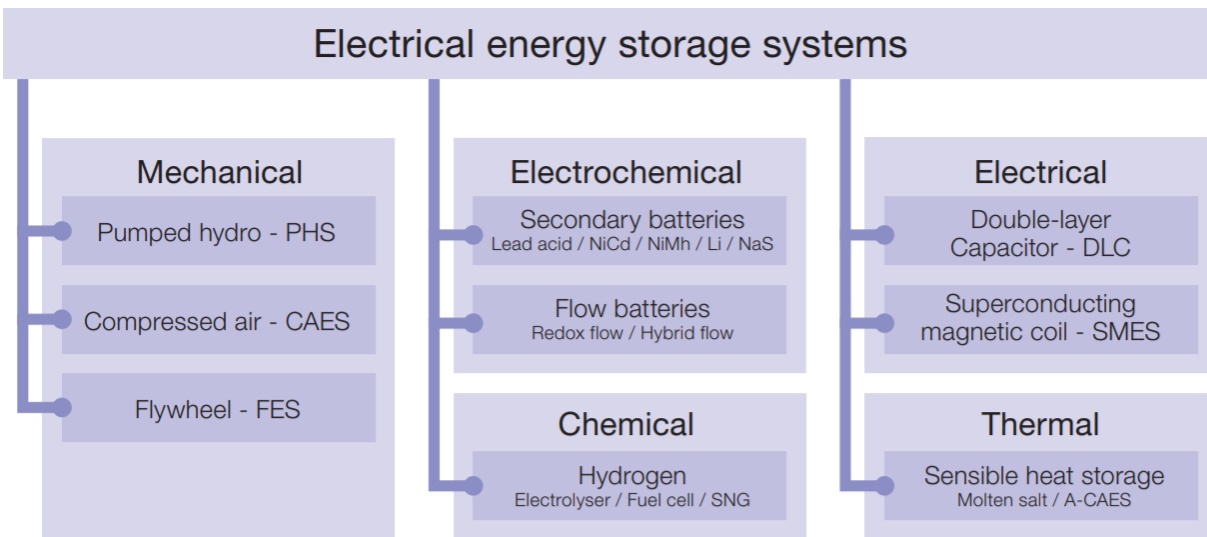


Figure 1.23 Classification of electrical energy storage systems according to energy form International Electrotechnical Commission [33].

Generally, the roles for on-grid EES systems can be described by the number of uses (cycles) and the duration of the operation, as shown in Figure 1.24. For the maintenance of voltage quality (e.g. compensation of reactive power), EES with high cycle stability and short duration at high power output is required; for time shifting on the other hand longer storage duration and fewer cycles are needed.

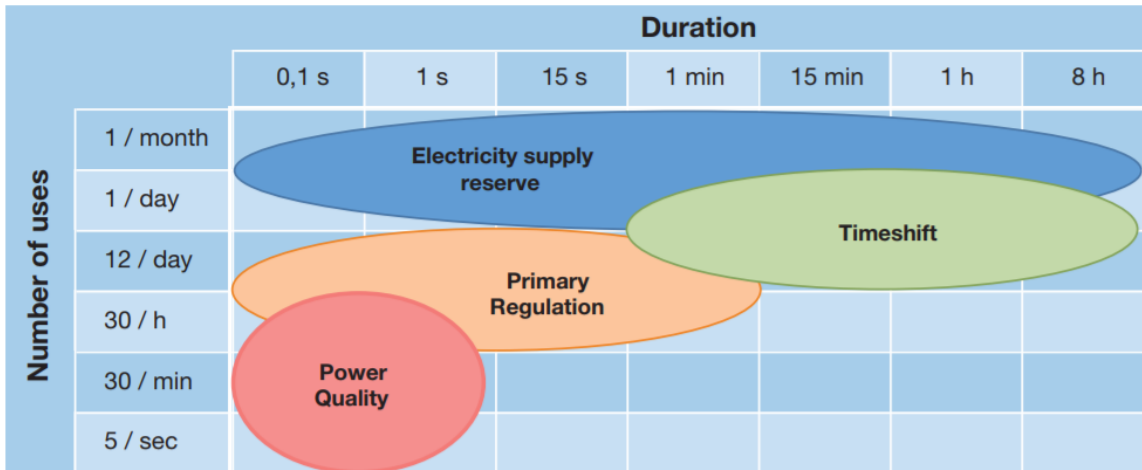


Figure 1.24 Different uses of electrical energy storage in grids, depending on the frequency and duration of use [33].

1.4.2. Methods of forecasting wind power generation and consumption

The main specifics of the wind energy resource is related to the fluctuation of its flow in time. This circumstance leads to the uncertainty in the amount of power production, which reduces the market value of the product. Market price discount for such volatile product is justified by the fact that the power grid balance between electricity consumption and generation should be maintained at any time – otherwise, reduction in the quality of electric power or interruptions of supply can occur. The wind power generation is a direct function of wind speed and, unlike conventional generation systems, is not easily predictable.

The prediction of wind energy generation in terms of time frames can be considered from different perspectives, depending on the intended use. Forecasts from milliseconds to several minutes ahead can be used for turbine-active monitoring. This type of forecast is usually referred to as very short-term forecasts.

Forecasts for 24-72 hours ahead are needed for power system management and energy trading. They can serve to determine the use of plant's standard capacity (unit commitment) and to optimize the planning of these plants (economic dispatch). The energy proposals that will be delivered per day are usually required during the morning of the previous day. These forecasts are called short-term forecasts. The numerical weather prediction model (NWP) model results can be obtained for a geographical point of the wind farm or for a grid of surrounding points. In

the first case the models could be characterized as “advanced power curve models”, in the second case as a “statistical downscaling” model. LocalPred for example uses principal component analysis and artificial intelligence techniques from the surrounding NWP grid points [35, 36].

The next step is the so-called downscaling procedure. The wind speed and direction from the relevant NWP level is scaled to the hub height of the turbine. This involves a few steps, first finding the best-performing NWP level - often the wind speed at 10 m above ground level or at one of the lowest model or pressure levels [37], [38].

For example, the algorithm of Operational Prediction System (OPS) Prevento, which is shown in Figure 1.25 [39] can be considered. The basis of a precise wind power prediction is typically a good weather forecast. The algorithm uses weather data from all leading weather services and utilizes their proprietary algorithm for wind power prediction. A complex calculation model gives the ability to make forecasts with a high degree of accuracy.

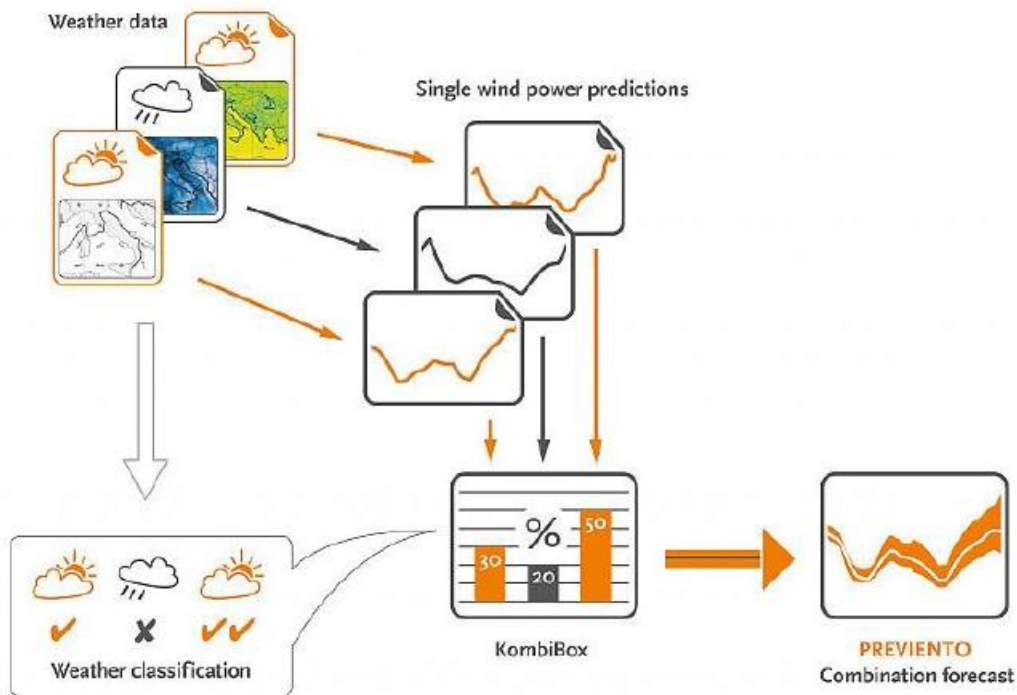


Figure 1.25 OPS Prevento algorithm for wind power prediction [39].

The basis of the calculation is numerical weather data from various weather services. In the first step an initial wind power prediction based on the available weather data. In a second step, the predictions are optimized by the so-called KombiBox. The KombiBox procedure puts

more weight on those predictions, which show the least prediction error in the corresponding weather situation. The result provides an improved wind power prediction.

A diagram on Figure 1.26 shows net generation of power for wind plants for a sample period from 06.18.2018 to 06.24.2018 and a day ahead forecast performed by Fraunhofer ISE that provides graphs displaying electricity production and spot market prices in Germany [40].

The ability to forecast wind power production volumes allows manufacturers to participate in the process of selling energy on the exchange, where the price is formed based on supply and demand considerations. At the market of commodities, participants offer quantities of energy to be provided during the next day at a given price. This allows market participants to settle the trade of electricity for various periods, depending on the various offers.

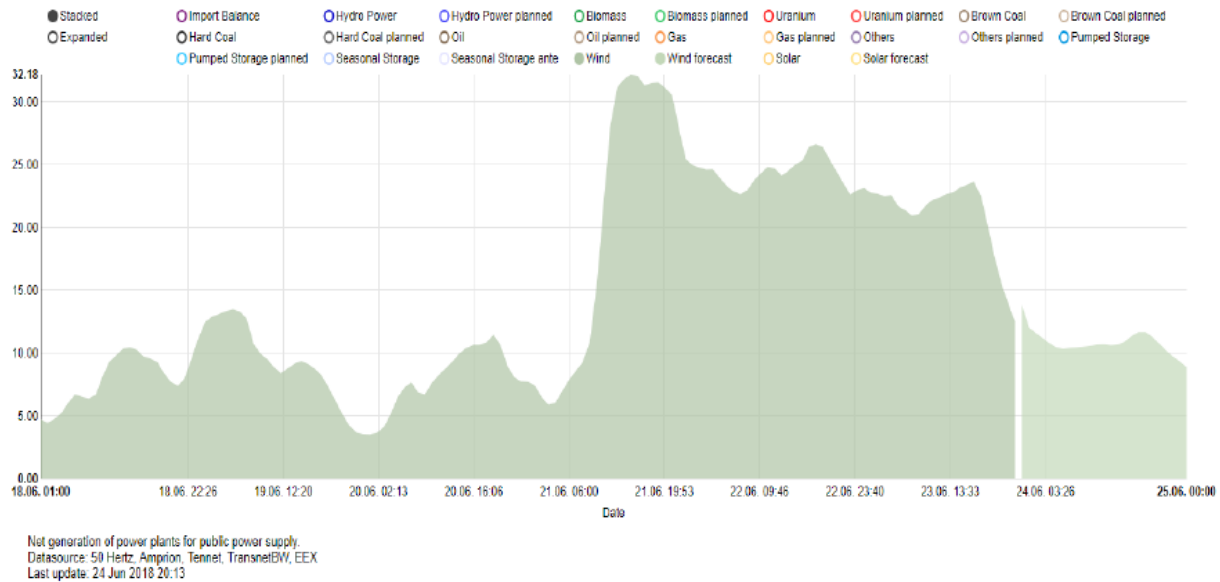


Figure 1.26 Net generation of wind power plants for 18.06.2018 - 24.06.2018 in Germany and a day ahead forecast [40].

The dynamics of changes in the price of electricity on the Nord Pool exchange can be seen in Figure 1.27 Figure 1.28, where data on the magnitude of fluctuations and frequency distribution of prices for the period from 2013 to 2018 are given [41]. As can be seen, depending on the magnitude of demand and supply in the market, price for electric energy can change manifold.

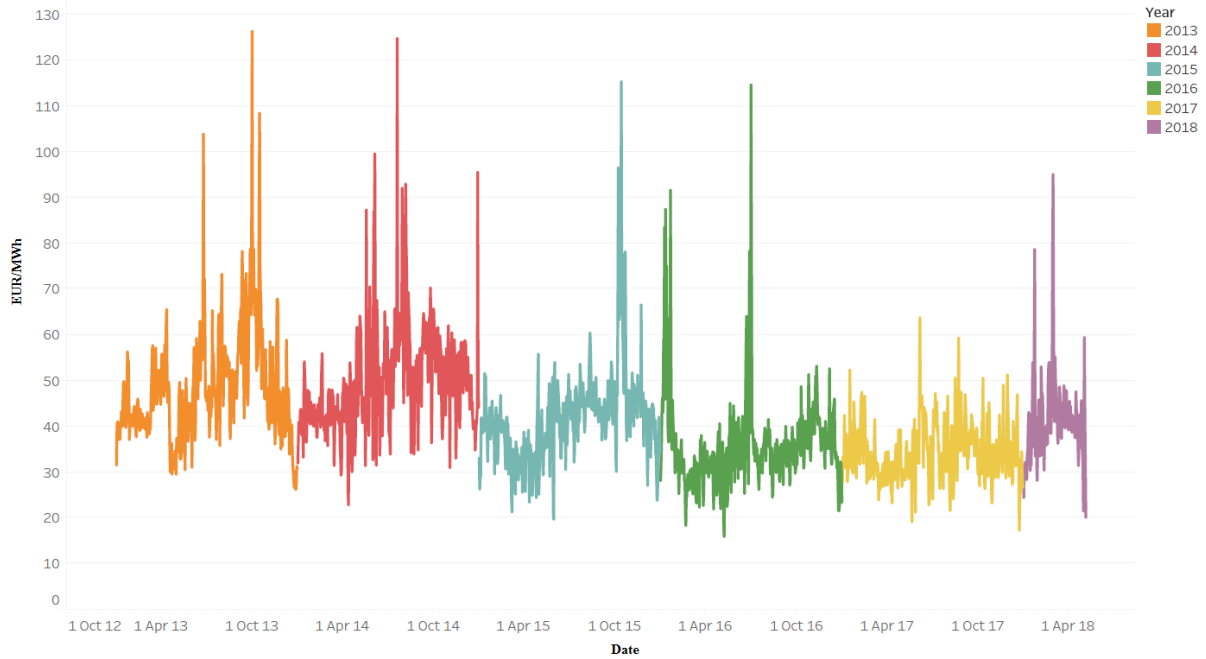


Figure 1.27 Electricity prices in the Latvian segment of Nord Pool in EUR/MWh [41].

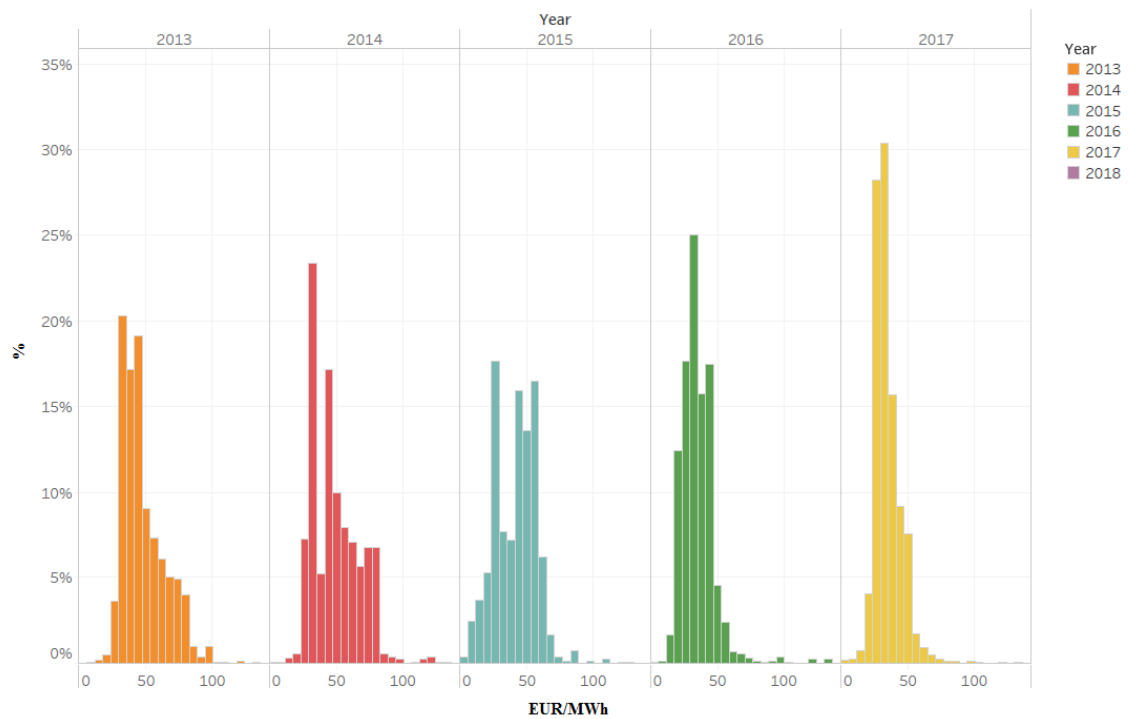


Figure 1.28 Histogram of electricity prices in the Latvian segment of Nord Pool [41].

Along with the seasonal fluctuations that occur each year, the periodic price fluctuations due to the daily consumption schedule also affect the value of the price of electrical energy. In Figure 1.29, it can be seen how the price of electricity varies depending on the hour of the day during the week [41].

Getting a favourable price for the energy produced is a prerequisite for improving the economic efficiency of WTs. Therefore, forecasting of power production as well as the use of EES devices are promising areas for improving competitiveness enhancing methods for wind power production.

Against this background, a conclusion can be made that nowadays it is important to address the issues of improving the technical and economic efficiency of wind parks. At the same time, it can be noted that the results of solving these tasks can be achieved by increasing the installed WT power (up to 13-15 MW), increasing the mast height (up to 180-200 m), using storage devices and energy storage (up to 10 GW), developing offshore and shallow water zones, using wind power production forecasting methods and searching for other solutions.

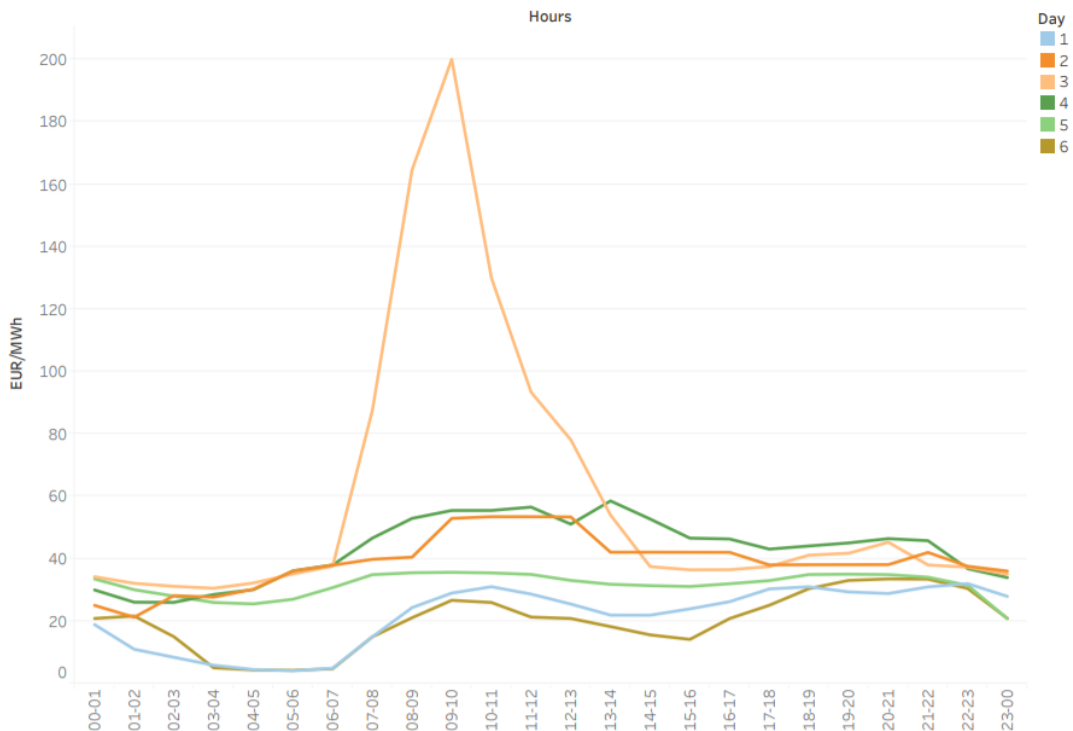


Figure 1.29 Hourly fluctuations of electricity prices in the Latvian segment of Nord Pool in the period of 1-6 May 2018 in EUR/MWh [41].

1.4.3. Unresolved problems

If we look back on the period over the past 30 years, we can see that operating experience, the development of new technologies in generator and hub manufacturing industry, along with the emergence of unique materials made it possible to make a leap in improving the efficiency of WTs. However, wind energy is volatile, and this non-stationary nature brings uncertainty in wind power generation as compared to conventional power generating systems. Wind powered grid stability and safety are affected by severe fluctuations in wind speed resulting in the generation of fluctuating wind power generation.

Accurate and reliable prediction of wind speed and wind power plays an important role in solving various problems which, among others, include the design of electricity markets, planning and development of wind power system, power generation scheduling and dispatch at the main grid to fulfil the power demand, power system stability and reliability, transmission capacity upgrades, etc. [42].

Thus, the results of research in the field of improving methods for predicting the production of wind energy can serve to further improve the efficiency of WTs and promote the use of this type of RES. At the same time, work on the assessment of wind energy resources should include the study of average long-term wind speed distribution covering relevant territories at an altitude of up to 200 m.

A significant number of publications in this area indicates that an active search is being conducted to find solutions to existing problems in this field [35], [38].

1.5. Conclusions

Modern development of renewable energy sources should not be considered in isolation, but as part of a broader process of “energy transition” taking the form of a long-term change in the structure of energy systems.

At the moment, the cost of "green" energy is higher than that of traditional, derived from the combustion of hydrocarbons and the splitting of atomic nuclei; however, alternative energy is becoming more profitable every year. This is facilitated by the improvement of technology, declining costs of WT production and the rapid construction of WPP in mountains and offshore regions. Based on the above, it can be concluded that the task of increasing the technical and economic efficiency of WPP is especially relevant nowadays.

Improving technical and economic efficiency can be achieved by increasing the installed power of WTs, increasing the height of the hub, using storage devices and energy storage, developing offshore and shallow water zones, the use of advanced wind power production forecasting methods and search for other solutions.

The results of research in the field of improving wind power forecasting methods can serve to further improve the efficiency of WTs and promote the use of this type of RES. At the same time, work on the assessment of wind energy resources should include physical experiments and studies of the average long-term wind speeds distributed throughout the relevant areas at an altitude of 10 to 200 m, along with efforts in improving the quality of wind speed measurements.

2. Economic and operational risks in wind energy projects in Latvia

2.1. Risks and uncertainty factors in the design of wind power projects

2.1.1. The problem of operational and economic uncertainty

The study considers the problem of operational and economic uncertainty in wind energy projects in the absence of state subsidies and the conditions of a liquid, integrated and free electricity market. The author highlights the problem of uncertainty in wind energy projects associated with the volatility of wind speed, concurrent electricity market prices and technical characteristics of wind turbines.

The goal of the research is to create a practical basis for decision-making under uncertainty in wind energy projects based on publicly available electricity price data, producer provided technical characteristics of wind generator power curves and experimental wind speed measurements. The study is based on proprietary wind measurements data gathered in the north-western coastal part of Latvia at the range of altitudes of up to 50 m and daily electricity market prices from the Latvian segment of Nord Pool power market.

This analysis starts with a brief overview of the Latvian electricity generation market with an emphasis on wind energy. As the basis for the analysis, the study also presents an overview of existing modelling options currently used in forecasting. Following designated pre-testing procedures and model calibration on historical data, the study uses stochastic differential equations (SDE) for the out-of-sample forecasting of wind speed and electricity prices.

Pre-testing procedures suggest that mean reverting Vasicek model can be used for wind speed modelling, while electricity price development is better described by a mean reverting model with jump diffusion. Time series modelling is combined with Monte Carlo simulation technique in order to come-up with the distribution of revenue projections and efficiency estimates for a hypothetical wind park.

Subsequently, the author performs a sensitivity analysis of wind generator efficiency and revenue generation potential across a range of technical factors. A broad range of project development scenarios involving several wind generator types and multiple mast height options is considered.

The author proposes a comprehensive approach towards the feasibility evaluation of wind energy projects in the conditions of limited wind speed data availability at high altitudes and

deregulated electricity market in Latvia. The results of the study provide quantitative basis for optimal decision-making process at the planning stage of wind energy projects and highlight the importance of the initial choice of wind generator models. The analysis also suggests that in the absence of state support, a prudent approach towards the selection of wind generator types should be chosen.

2.1.2. The analysis of Latvian electricity market

Latvian electricity market is characterized by large balance deficit. The installed power plant capacity is sufficient to satisfy only two thirds of the gross electricity consumption in the country. Latvian energy sector has historically been relying heavily on imported energy resources in terms of electricity via Russia – Baltic – Belarus energy grid and a direct gas pipeline that ensures electric power generation within the country.

The development of the Latvian electricity market has been affected by several major factors over the last ten years – tighter integration into the European energy network, market deregulation and increased state support of energy production from renewable energy sources (RES) following the EU directives. Each of the factors had a paramount effect on wind energy projects in the country.

In comparison with the Nordic countries, that deregulated their power markets in the early 1990s and brought their individual markets together into a common Nordic market, Latvia deregulated its power market and joined the Nord Pool market only in 2013. The deregulation of electricity market implies that prices are determined by free competition rather than by the state.

Altogether, the electricity grid connecting the Nordic countries, the European continent and the Baltics is open for power from many different sources – hydro, thermal, nuclear, wind and solar. It creates a liquid market on which large volumes of electricity and associated financial instruments, such as options and futures, can be traded.

The demand for electricity produced by wind power plants has been stimulated by the 2009/28/EC Directive promoting the use of energy from renewable sources. The directive sets the objective of reaching at least 20% of the EU's final energy consumption through renewable energy sources by 2020. National Renewable Energy Action Plans (NREAP) have been developed by each member state detailing the implementation strategy covering electricity, transport, heating and cooling sectors.

According to an overview of RES development in the Baltic countries carried out by the national independent Transmission System Operators, renewables will continue to be a key instrument helping the EU to meet its energy needs also beyond 2020. Specifically, Clean Energy Package proposals approved by the European Commission in December 2018 introduces a new renewable energy target of at least 27% of final energy consumption in the EU by 2030 [42].

According to WindEurope's central scenario, 323 GW of cumulative wind energy capacity would be installed in the EU by 2030, 253 GW onshore and 70 GW offshore. That would be more than double the capacity installed at the end of 2016 (160 GW). In terms of electricity production, that would imply 888 TWh of wind generated electricity in 2030, corresponding to 30% of the EU's projected electricity demand in that period [44]. Overall, it means that RES are bound to play a central role in achieving energy efficiency and greenhouse gas emission reduction goals.

According to the Latvian Bureau of Statistics in 2017, Latvia had the third highest share of RES in the final energy consumption among the EU countries with 37.2%, following only Sweden and Finland [45]. The role of RES in Latvia has historically been exceptionally high due to the contribution of hydro power stations to the overall electricity production. In 2015, hydro power stations accounted for one third of the installed electrical capacity and for 30% of the electricity production in the country.

Overall installed capacity of RES power stations in Latvia reached 1.8 GW in 2015 that favourably compares to other Baltic countries; however, the level of installed capacities of wind power plants is small even compared to the two neighbouring countries, where capacities are at least fourfold higher than in Latvia (see Table 2.1) [46]. Because of the large existing installed capacities of RES the economy was lacking stimulus for the development of wind energy power plants.

Although the overall level of installed wind power plant capacity in Latvia is unsatisfactorily low, this type of RES has been persistently gaining importance in the overall mix of energy generation sources. Apart from the overwhelming dominance of cost-efficient hydropower in the mix of RES in Latvia, the reason for the unsatisfactorily low level of installed wind energy capacities can be traced to the high level of operational and economic uncertainty associated with the projects.

Table 2.1

Installed RES generating capacities in the Baltic States, as of 31st December 2014

Source	Lithuania		Latvia		Estonia		Total
	Total	Connected to transmission network	Total	Connected to transmission network	Total	Connected to transmission network	
	MW						
Biofuel	97		118	24	131	97	346
Hydro	128	101	1593	1562	8		1729
Solar	72		0.68		3		76
Wind	287	222	67	21	303	274	657
Total	584	323	1779	1607	445	371	2808

Recent political initiatives are directed towards mitigating dependency on imports by the means of renewable energy sources – biomass, biogas and wind power. From the perspective of the government, sub-optimal level of investments in renewable energy projects requires subsidies that address the problem of high economic uncertainty. Consequently, in order to promote energy production from RES, Latvian government introduced subsidies in the form of long-term contracts and higher feed-in tariffs.

According to the latest legislative initiative of the Cabinet of Ministers Regulation of Latvia Nr.262 “Regulation of electrical energy production using renewable energy sources and procedure for energy price calculation” from 2010 March 16, wind power electricity producers could get a right to sell electricity to the grid under the “compulsory purchase“ scheme for the price of around 120 EUR/MWh during the first 10 years of operation and for 72 EUR/MWh during the subsequent 10 years. Subsidized electricity tariffs for renewable energy made the operations of wind generator farms more profitable, making this field attractive for international investors.

Such approach is in line with the EU Directive promoting the use of energy from renewable sources; however, it is in stark contradiction with the power market deregulation efforts ongoing in Latvia since 2013, when it joined the Nord Pool. In the given situation, RES

producers are not incentivized to participate in the free electricity market in Latvia, because the subsidized tariff substantially exceeds market price.

The aforementioned factors drastically changed the landscape of the Latvian electrical energy generation market. The amount of installed capacities of wind power plants grew from negligible 2 MW in year 2000 to almost 80 MW by the end of 2017 [47]. Over the last ten years, in the period from 2007 to 2017, the installed capacity of wind power parks has been growing with the Compound Annual Growth Rate (CAGR) of 11% that compares to only 1.3% growth rate in the installed capacity of RES power plants of all types in the country over the same period (see Figure 2.1). That led to the increase of wind power energy share in the overall electricity production in Latvia, which now stands close to 3%.

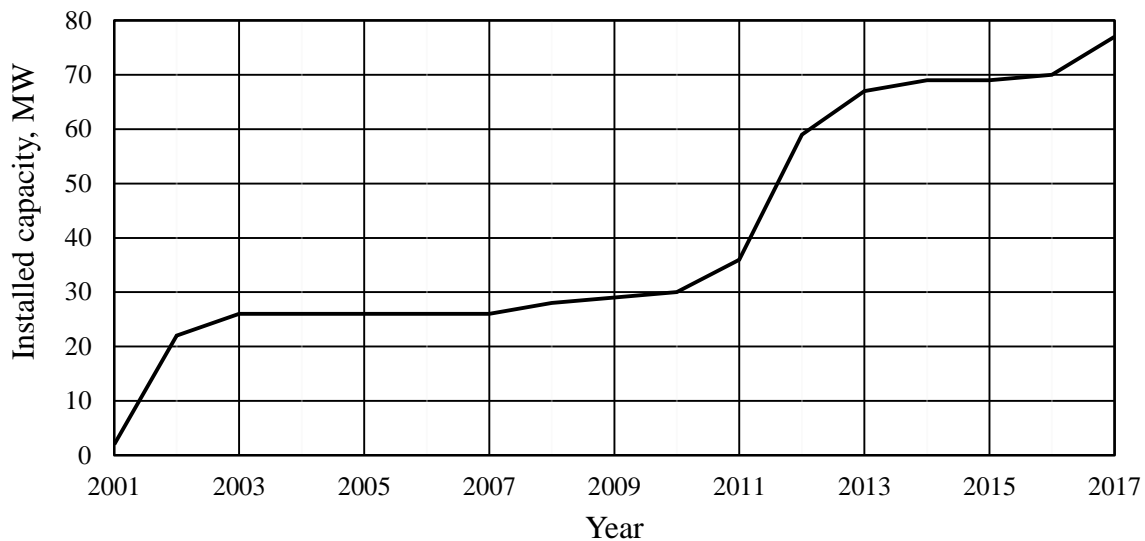


Figure 2.1. Installed wind power plant capacity in Latvia in MW.

It can be concluded, that the achievement of the strategic goal of higher penetration of wind power energy comes at the cost of deviations from the principals of market economy. That is justified only if it results in at least equally valuable positive externality to the society.

Moreover, subsidies that are not meant to support technologies at the early stages of their development cycle can be wasteful in the long run. Therefore, it is important to address the problem of high project risks without eliminating the aspect of the free market discipline. Operational uncertainty, on the other hand, can be reduced through modelling efforts, more transparent technical data availability and access to long-term wind speed measurements at high altitudes.

2.2. The use of stochastic models in wind energy projects

2.2.1. An overview of forecasting models

As widely acknowledged by many practitioners and academics, the penetration of wind energy will be limited without advancements in forecasting methods applicable to wind speed, due to electricity network balancing difficulties associated with the volatility of this source of energy [48 - 51]. The advancement can be viewed from the perspective of “forecast reliability”, usually measured by the ex post Root Mean Squared Error (RMSE) and “forecast efficiency”, under which a forecast minimizes the expected squared error conditional on information about all current and past forecasts, the notion introduced by Nordhaus [52].

In order to progress in terms of wind power management it is essential to move away from point estimations in the direction of probabilistic forecasting. Moreover, as pointed out by Iversen et al. [53] in the dominion of probabilistic forecasting distinguish between parametric and nonparametric methods. The former assumes a certain standard distribution for the forecast error, and as a result, the modelling boils down to estimating the parameters that characterize such a distribution [54]. In contrast, nonparametric methods do not assume any pre-specified forecast error distribution and work directly with the empirical distribution instead [55].

Furthermore, a growing number of authors stress that, in order to analyse the impact of wind power generation on power system operation and planning, stochastic wind power models should be able to capture both the probability distribution and temporal correlation of the wind power generation [56]. To this end, the most popular approach is to fit a marginal predictive density for each univariate output variable and then combine these marginals into a multivariate cumulative density using copula theory [57].

Against this background, a comprehensive review of more than 380 papers on the topic of short-term forecasting of power generated by wind turbines conducted in the course of ANEMOS.plus and SafeWind projects co-funded by the EU was timely and essential [37], [58]. In the course of the review, the authors covered approaches that were widely spread already at the time of the study, namely persistence method (naïve predictor), physical approach and a range of statistical methods such as time series analysis and artificial neural networks (ANN).

Naïve predictor method is the model most frequently used as a benchmark for the performance evaluation of other forecasting models [59], [60]. In this model, the forecast for all times ahead is set to the value it has now. Therefore, the error for zero-time steps ahead by definition is zero. Physical approach refers primarily to NWP models and is based on the use of meteorological data such as wind speed and direction, pressure, temperature, humidity, terrain structure etc. Statistical approaches include a wide range of ARMA models [61]–[63] and machine learning techniques involving neural networks [64]–[66] and support vector machines [67], [68].

Among others, comprehensive reviews of existing state-of-the-art modelling approaches were conducted by Foley et al. [69], Costa et al. [70], and Monteiro et al. [71]. In the reviews conducted by Soman et al. [72] and Chang [73] the authors paid particular attention to the classification and systematization of different models.

In a brief review conducted by Chen et al. [74], the authors explicitly differentiate between the studies that employ wind speed approach, that is project wind speed and subsequently transform the projections into wind power through wind farm model, and those that use wind power approach, by directly projecting wind power. The authors point out that both approaches are based on wind speed measurements.

Papers that are more recent made further advancements in forecasting applications based on Vector Autoregressive Models (VAR), stochastic differential equations (SDE) and copulas. For instance, Ekström et al. [75] performed statistical modelling of wind power park locations with a VAR model, which takes into account both the temporal correlations in individual plants and the spatial correlations between the plants.

An alternative way to account for interdependence of marginal distributions is to use copulas. Pioneered by Sklar in 1959 [76], copula theory gained appreciation and put into framework only in the beginning of the following century [77]. Currently, models based on the copula theory are widely applied in financial market analyses, portfolio investments, and risk assessments [78], [79], but are also applicable for wind power forecasting errors modelling [80], power system uncertainty analysis [81], [82], power and wind dependence structures modelling [83], [84].

Another strain of literature relies on SDE models to forecast wind speed. For instance, Iversen et al. [85] showed that by using one single SDE model that is characterized by a few

parameters it is possible to capture the time dependence structure of wind speed prediction errors, derive point and quantile forecasts, predictive distributions, and time-path trajectories that is analogous to the ensemble forecasts obtained from a NWP system.

The input sources of data for the forecast models typically include various historical physical observation data, factory characteristics of generators, operating characteristics obtained through Supervisory Control And Data Acquisition (SCADA) systems installed on modern wind turbines, specifics of the surrounding terrain and the results of numerical weather prediction NWP models. On top of that, in order to improve the precision of models and quantify the uncertainty of forecasts an ensemble approach is used.

If the forecasting horizon is not too long, speed and power can be forecast just using time series analysis methods, without resorting to actual weather forecasts; however, state-of-the-art systems for short-term forecasting have both a NWP based component and an autoregressive part based on time-series analysis techniques [86].

Apart from identifying and categorizing relevant papers in the field, the authors in [58] proposed a common set of performance measures with which to compare forecasts across systems and locations. These common error measures, formally presented by Madsen et al. [87], are the bias, Mean Absolute Error (MAE), RMSE, the coefficient of determination R^2 , the skill score for comparison with other models, and the error distribution as a histogram.

A good practice for the modelling analysis is to split the data set into separate training and validation sets, and normalised mean errors with the installed capacity for a comparison across different wind farms. In order to investigate the sources of error, Tambke et al. [88] proposed to further decompose RMSE into the three components: bias in mean wind speed, bias in standard deviation and dispersion. This approach is useful to determine whether the main contribution to the errors of the NWP model come from level errors, or rather from phase errors.

The authors in Giebel et al. [37], admit that the verification and assessment of forecast models is not trivial, as it depends on the cost function involved and the performance often depends on the measure itself, as models can be good at one dimension and bad at another. Moreover, the performance of short-term forecasting can be unstable – it is not always the same model which is best across horizons and across geographical sites.

Overall, wind power output projection is an intricate task that many researchers have concerned themselves with, proposing a wide set of approaches to address it. However, the

choice of forecasting methods is greatly data, aim and location specific. The benefit of reducing uncertainty in power generation is relevant not only for the owners of RES installation, but also for transmission and distribution system operators charged with maintaining system stability.

2.2.2. The analysis of statistical data

This study is based on the daily average time series of electricity prices for the period of 01.01.2013 – 12.05.2015 from the Latvian segment of Nord Pool power market and a set of high frequency observations of wind speed at the heights of up to 50 m, carried out in the north-western part of Latvia – Irbene, Ventspils region. The wind speed measurements were performed continuously over 698 days during the period of 14.06.2013 – 12.05.2015. The summary statistic of the time series is presented in Table 2-2.

As it is shown on Figure 2.2, daily electricity prices can be highly volatile and exhibit seasonality patterns, which implies that the time series should be de-seasonalized prior to the analysis. On Figure 2.3 the results of daily averaging of wind measurements performed using NRG LOGGER Symphonie 9200 mounted on a 50 m mast are presented [89].

Table 2.2

Summary statistics of the time series of electricity price and wind speed, m/s data

Time series		Period	Interval	Sample	Min.	Avg.	Max.	SD	Source
Electricity prices, Eur/MWh		01/01/2013 - 12/05/2015	Daily average	862	21.3	47.3	126.3	12.2	Nord Pool
Wind speed, m/s at height	20 m	14/06/2013 - 12/05/2015	10 min average	100211	0.4	2.8	12.9	1.6	Latvia, Ventspils region, Irbene
	30 m				0.4	3.5	15.5	1.7	
	40 m				0.4	4.3	16.1	1.9	
	50 m				0.4	4.6	18.7	2.0	

In real life wind energy projects, it is common that long-term data on wind measurements is scarce. In the cases when historical measurements data are available, the maximum height of observation towers is limited to 50–60 m, as the construction of higher masts is usually not practical for small-scale projects. It is also the case for the current study, which is based on wind speed measurements conducted at the altitudes 20, 30, 40 and 50 m.

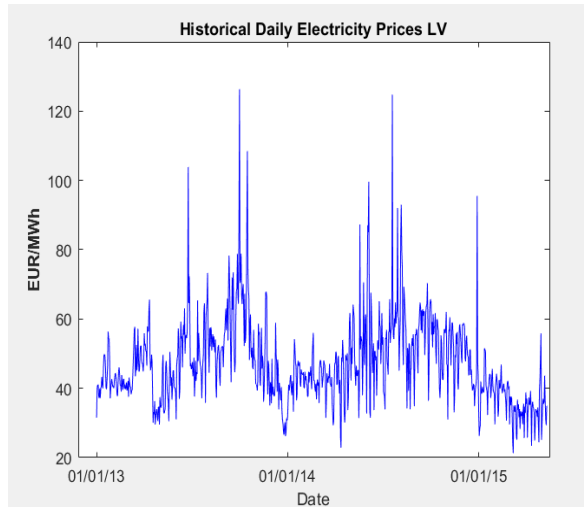


Figure 2.2 Electricity prices in the Latvian segment of Nord Pool power market

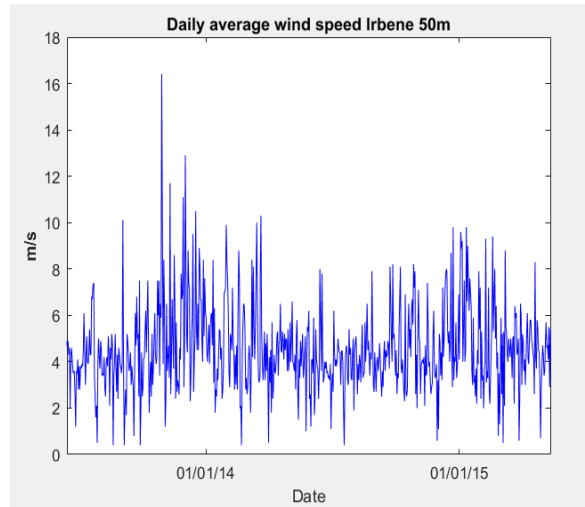


Figure 2.3 Wind speed in Irbene, Ventspils region, Latvia at the altitude of 50 m.

However, in order to assess future revenue potential of a certain geographical location, coupled with wind turbine efficiency estimates, it is necessary to possess data on wind speed at the altitudes of up to 140 m. For that reason, the usual first step in the assessment of wind energy project feasibility consists of estimating wind speed at the altitudes significantly above which physical measurements were made. For the purpose of the current study power law relationship between contemporary wind speed measurements and their height was used in accordance with Eq. 2-1 (Figure 2.4)

$$\ln(S_i) = \ln(\beta_0) + \beta_1 \ln(H_i), \quad (2.1)$$

where S_i – is wind speed (m/s); and

H_i – is height (m)

Parameters β_0 and β_1 were estimated for the set of actual wind measures every 10 min and used to contemporaneously extrapolate wind speed values to altitudes 80, 90, 100 and 110 m. The results of the extrapolation and daily averaging are summarized in Table 2.3.

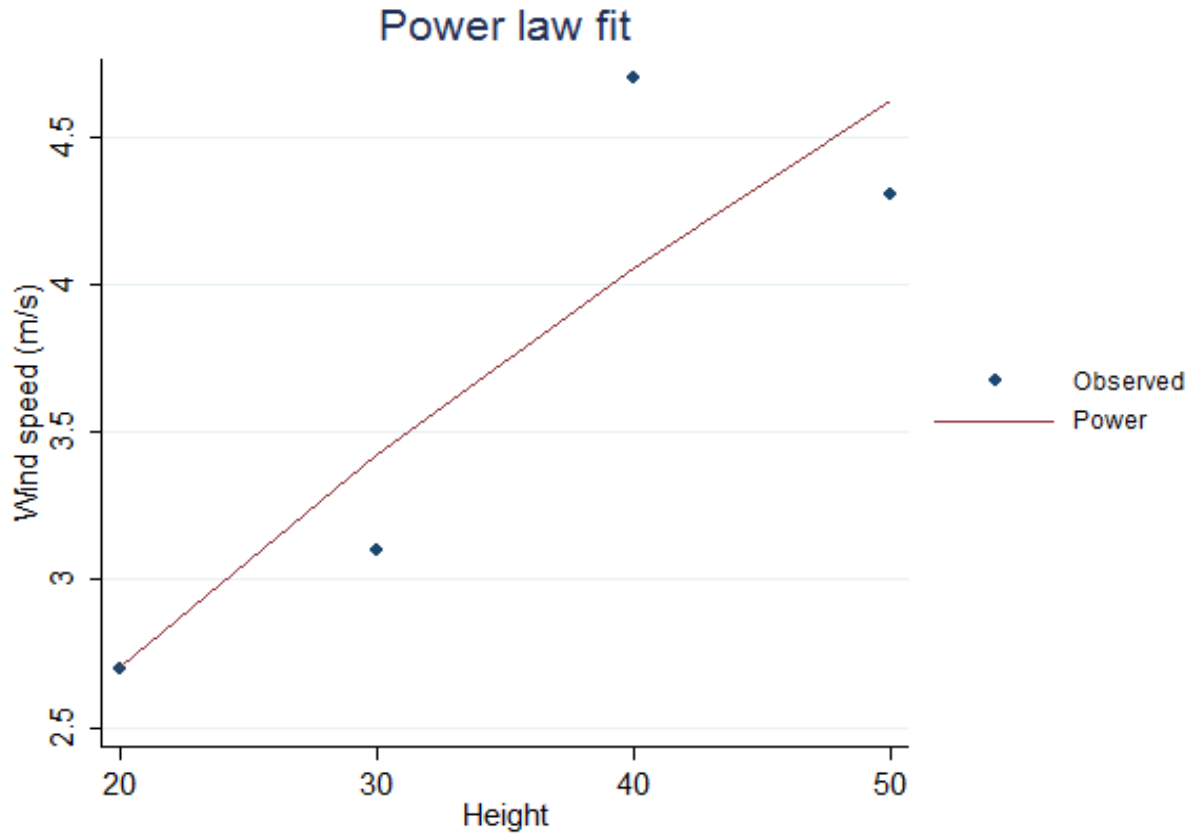


Figure 2.4 Power low fit of wind speed in relationship to observation height.

Table 2.3

Summary statistics of power law extrapolated wind speed, m/s data

Wind speed at height (m)	Period	Frequency	Sample	Min.	Avg.	Max.	SD
80	14/06/2013	Daily average	698	3.2	6.2	11.1	1.3
90				3.6	6.7	11.6	1.4
100	12/05/2015			3.8	7.2	12.3	1.5
110				4.0	7.7	14.4	1.6

2.3. The assessment of economic efficiency of wind energy projects

2.3.1. Data preparation for pre-testing procedures

This section covers the approach used for the pre-testing procedure and outlines the implications of the time series analysis results for SDE modelling. Prior to modelling historical time series, it is necessary to determine their general statistical properties. Time series pre-testing

procedures involve checking for fat tails of the probability density function (PDF), checking for mean reversion and checking for seasonal patterns.

The presence of autoregressives (AR) properties can be tested in the data typically on the returns of a series or on the series itself. In linear processes with normal shocks, this amounts to checking for stationarity [90]. The stationarity of time series can be an indication for mean reversion.

If time series are stationary, it can be assumed that the underlying data generating process is mean reverting. Another pre-requisite for making fitting distributional assumptions about the model parameters is the examination of the actual distribution of the time series.

In order to test the data for normality, first we transform the data by taking natural logarithm, and then apply standard tests for normality – Kolmogorov-Smirnov test, as well as Jarque-Bera test. The results of testing log wind speed data suggest that the null hypothesis of normality for extrapolated wind speed data at 100 m altitude cannot be rejected at 5% significance level for the log wind speed data, while for log electricity prices the null hypothesis is rejected at 5% by Jarque-Bera test. On Figure 2.5 and Figure 2.6 compare the PDF of log wind speed and log electricity prices to the standard normal PDF.

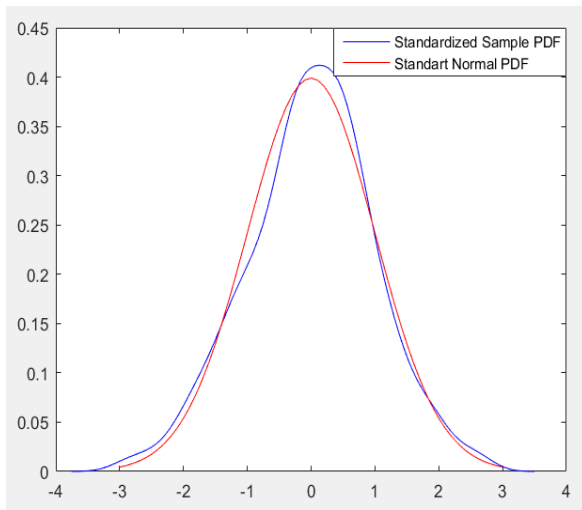


Figure 2.5 PDF of log wind speed vs standard normal PDF.

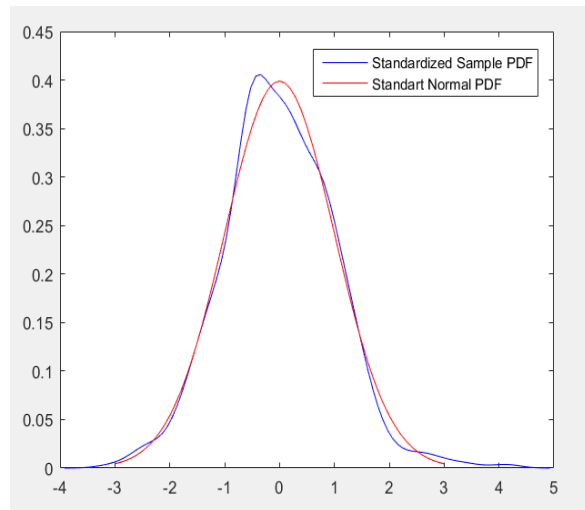


Figure 2.6 PDF of log energy prices vs standard normal PDF.

Apart from testing the distributional characteristics of the data it necessary to test whether mean reversion properties are present in the times series. Figure 2.7 visualizes the autoregressive properties of log wind speed, while Figure 2.8 serves the same purpose for log energy prices time series.

The results of formal tests for stationarity, such as Augmented Dickey-Fuller (ADF) and Kwiatkowski, Phillips, Schmidt, and Shin (KPSS) [91] confirm that the hypothesis of stationarity of the time series cannot be rejected for both time series. The results of the pre-testing procedures for the entire set of time series are summarized in Table 2.4.

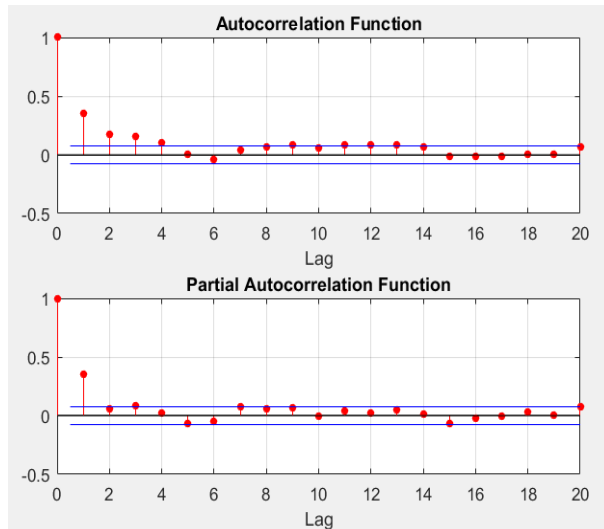


Figure 2.7 Autocorrelation Functions of extrapolated log wind speed at 100 m.

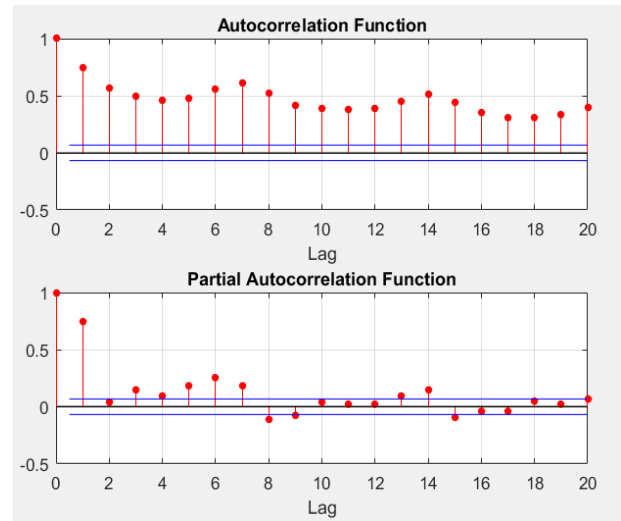


Figure 2.8 Autocorrelation Functions of log electricity prices time series.

Table 2.4

The results of pre-testing procedure for log wind speed, m/s and log energy prices

Type of test	Log Wind speed, at height				Log electricity prices
	80 m	90 m	100 m	110 m	
For normality (p-values)					
Kolmagorov-Smirnov	0.24	0.16	0.23	0.31	0.50
Jarque-Bera	0.36	0.32	0.30	0.42	0.00
For stationarity (p-values)					
Augmented Dickey-Fuller (ADF)*	0.00	0.00	0.00	0.00	0.13
Kwiatkowski, Phillips, Schmidt, and Shin (KPSS)**	0.10	0.10	0.10	0.10	0.10
For Random Walk (p-values)					
Variance ratio test	0.00	0.00	0.00	0.00	0.00

Note: * Autoregressive model with drift variant; ** Optimal number of lags according to [91].

Overall conclusion from the pre-testing procedures with respect to log wind speed and log energy prices data is that the time series can be modelled as a stochastic mean reverting process

with Gaussian diffusion using an Ornstein–Uhlenbeck type process [92], [93] such as Vasicek model [94].

However, given that the electricity price data cannot be assumed to be normally distributed, the model of this time series also has to include jump diffusion elements [95]. On top of this, electricity price time series exhibit seasonal patterns that have to be removed prior to modelling.

2.3.2. The description of modelling methods

As suggested by the pre-testing procedures, log wind speed time series can be modelled by an Ornstein-Uhlenbeck stochastic processes with mean reverting drift and Gaussian diffusions. The process is stationary, Gaussian, and Markovian. Over time, the process tends to drift towards its long-term mean.

The Ornstein–Uhlenbeck process can be considered as the continuous-time analogue of the discrete-time AR(1) process. It can be calibrated to historical data by performing a linear regression between the state variables and their first difference.

Wind speed data can be modelled using a standard Vasicek model:

$$\log(S_t) = x_t, \quad (2.2)$$

$$dx_t = \alpha(\theta - x_t)dt + \sigma dW_t, \quad (2.3)$$

where S_t – wind speed;

α – mean reversion speed (the rate of mean reversion $\alpha > 0$);

θ – mean reversion level (long-run mean or level);

σ – instantaneous volatility rate ($\sigma > 0$);

t – time period; and

dW_t – standard Wiener process (standard Brownian motion).

In comparison to the wind speed data, electricity prices have a prominent seasonal component that has to be considered prior to modelling. As suggested by Lucia and Schwartz [96], the deterministic seasonal trend of the electricity prices is modelled using a combination of trigonometric functions (see Figure 2.9 and Eq. (2.6)). First, the deterministic seasonality part is calibrated using the least squares method. Second, after the calibration, the seasonality is removed from the logarithm of the prices (see Figure 2.10).

$$\log(P_t) = f(t) + x_t, \quad (2.4)$$

$$dx_t = \alpha(\theta - x_t)dt + \sigma dW_t + J(\mu_J, \sigma_J)d\Pi(\lambda), \quad (2.5)$$

$$f(t) = s_1 \sin(2\pi t) + s_2 \cos(2\pi t) + s_3 \sin(4\pi t) + s_4 \cos(4\pi t), \quad (2.6)$$

where P_t – is spot electricity price;

s_i – is constant parameters $i=1,2,3,4$;

$d\Pi(\lambda)$ – is Poisson process with jump intensity λ ; and

J_t – is jump size with normally distributed mean μ_J and variance σ_J .

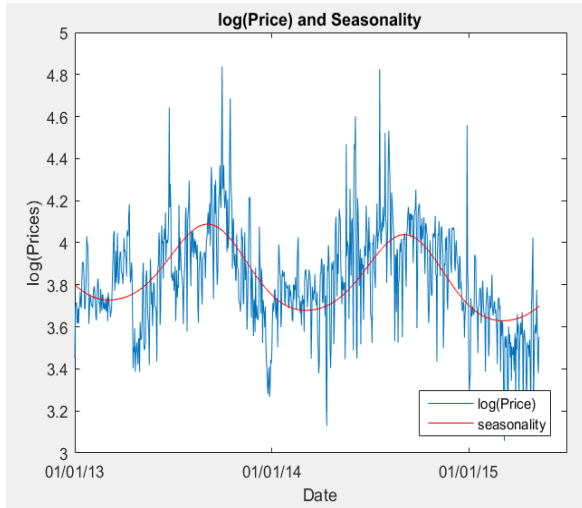


Figure 2.9 Log electricity price and seasonality trend.

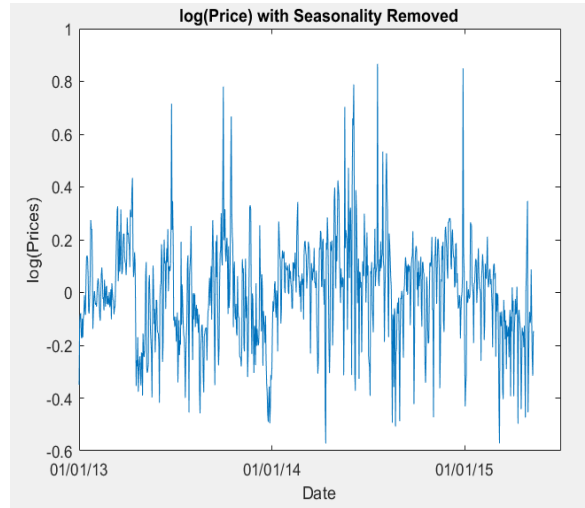


Figure 2.10 De-seasonalized log electricity prices.

The model addresses the features of electricity prices time series: fat tails, mean reversion and seasonality. The logarithm of electricity price is modelled with two components:

- deterministic seasonal part $f(t)$ is modeled by trigonometric functions,
- stochastic part x_t is modelled by mean reverting diffusion process with jumps.

Electricity price model adds jumps to a mean reverting process, assuming Poisson jumps (at most one jump per day). Overall, the process in short time instants features extreme movements beyond the Gaussian statistics, and in the long run features mean reversion.

Once the time series modelling process has been chosen and necessary seasonality adjustments are considered, the model parameters have to be calibrated to historical data, typically through OLS regression or maximum likelihood estimation.

2.3.3. Model calibration and results

Vasicek model of log wind speed data can be calibrated to historical data by performing a linear OLS regression between log wind speed and the first difference (see Eq. 2.7).

$$\frac{\Delta x_t}{\Delta t} = \alpha\theta - \alpha x_t + \frac{\sigma}{\Delta t} dW_t. \quad (2.7)$$

In order to calibrate the SDE model with jump diffusion part, it is necessary to discretize it (see Eq. (2.8) and (2.9)). To discretize, we assume a Bernoulli process for the jump events with probability $\lambda\Delta t$:

$$\Delta x_t = \alpha\theta\Delta t - \alpha x_{t-1}\Delta t + \sigma\Delta w_t^A + \mu_j + \sigma_j\Delta W_t^B \quad (2.8)$$

and with no jump event probability $(1-\lambda\Delta t)$:

$$\Delta x_t = \alpha\theta\Delta t - \alpha x_{t-1}\Delta t + \sigma\Delta W_t^A, \quad (2.9)$$

where W_t^A and W_t^B are independent standard Wiener processes.

The calibration of the model is performed using Maximum Likelihood approach [97]. The result of the model calibration is presented in Figure 2.11 for wind speed and in Figure 2.12 for electricity prices.

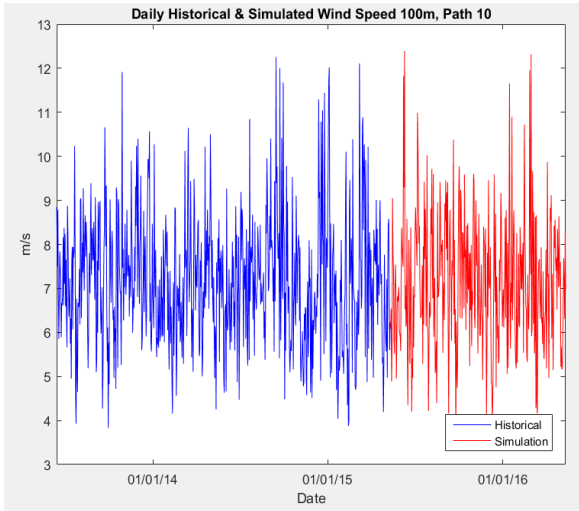


Figure 2.11 Actual and simulated wind speed at 100 m altitude.

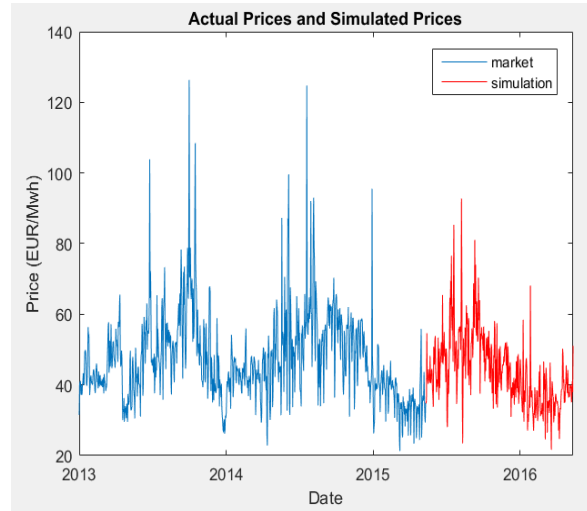


Figure 2.12 Actual and simulated electricity prices.

The resulting model parameter values are summarized in Table 2.5.

Table 2.5

Model parameter calibration results

Parameter of the model	Electricity price model	Wind speed at height			
		80 m	90 m	100 m	110 m
α	247.35	235.05	237.39	236.22	232.59
θ	0.01	1.81	1.88	1.95	2.01
σ	1.71	3.70	3.65	3.66	3.72
σ_j	0.21	-	-	-	-
μ_j	-0.02	-	-	-	-
λ	135.62	-	-	-	-
Δt	1/365				

Wind project development decision-making process has to answer several questions that are going to define the next ten to twenty years of its operations, locking in the success or failure of the project. Apart from the choice of the initial geographical location, the strategic decisions include the model of wind generators to be used on the pre-selected location and the height of support towers.

In order to address these two questions, it is necessary to assess the revenue potential and future efficiency of the considered wind generator power plant. The quantitative assessment should take into consideration a range of technical and economic factors. In contrast to the historical data on wind speed and electricity prices that can be objectively measured, the choice of a wind power generator model can be subjective.

The current study helps to address the uncertainty arising from volatile weather and market conditions, incorporating modelling of stochastic processes into technical limitations of operational efficiency associated with wind generator power curves. In order to map wind speed into power, it is straightforward to use manufacturer's power curve for each wind turbine as in Brown et al. [98].

In that respect, the author chose to consider three different generator models Nordex N54/1000, Siemens SWT-2.3-101 and Nordex N131/3000 in order to compare their hypothetical performance at the chosen location. The first two generator models are actively used in the Latvian conditions with more than ten units installed in the north-western part of the country, while the third generator is not yet represented in Latvia.

The join-up of the manufacturer's power curve specification of Nordex N131/3000 with one year-ahead wind speed forecast at different altitudes is present in the form of the distribution

of operational efficiency measure in Figure 2.13. The wind speed forecast implies that the wind turbine, if installed on a 100 m tower, would be operating approximately 44.3% of the time of the full capacity equivalent. Full capacity equivalent is assumed to the amount of energy produced during non-interrupted operations at 100% of the nominal power.

Figure 2.14 brings together the results of the one year ahead electricity price and operational efficiency forecast in order to provide an estimate of revenues obtained from selling generated electricity at the projected market prices. The results of the modelling exercise and Monte Carlo simulation show that the operational efficiency is highly dependent on the type of generators chosen for the project and very sensitive to the height at which the generator is going to operate. The summary of the results for all three generator types is presented in Table 2.6.

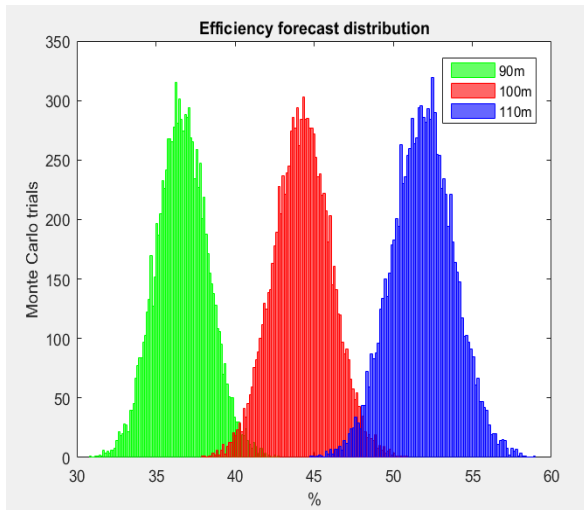


Figure 2.13 Histogram of operational efficiency based on 10000 Monte Carlo trials for Nordex 131 3000kW for different tower heights.

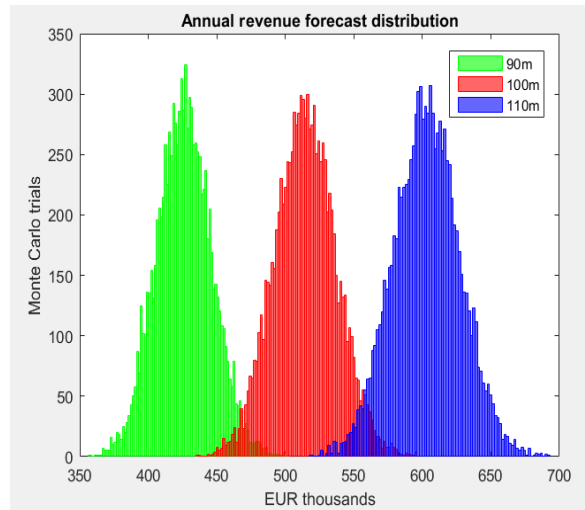


Figure 2.14 Histogram of revenues based on 10000 Monte Carlo trials for Nordex 131 3000kW for different tower heights.

Table 2.6

Out of sample forecasting results for three types of wind generators

Height (m)	Type of WT	Revenue (mean)	Revenue (SD)	Efficiency, %
80 m	Nordex N54/1000	47 445	3 085	12.5
90 m	Nordex N54/1000	62 050	3 727	16.0
	Siemens SWT-2.3-101	264 680	13 535	29.7
	Nordex N131/3000	432 010	21 071	37.2
100 m	Nordex N54/1000	78 868	4 486	20.4
	Siemens SWT-2.3-101	324 610	15 504	36.4
	Nordex N131/3000	514 580	22 547	44.3
110 m	Siemens SWT-2.3-101	387 210	17 456	43.5
	Nordex N131/3000	603 020	24 536	51.9

2.3. Conclusions

The study used historical daily data on electricity prices in the Latvian segment of the Nord Pool power market for the period of 2013-2015 in combination with long term wind speed measurements performed in Irbene, Latvia at the altitude of up to 50 m. Extrapolation approach based on power law functional relationship between the wind speed and altitude was used to obtain the estimates of wind speed at higher altitudes.

In the course of the study, several SDE models were calibrated to historical data and used to forecast operational efficiency of three wind generator types, along with the resulting revenue distribution. The revenue forecast takes into consideration seasonal patterns and stochastic jumps in electricity prices.

Overall, the results of the study show that forecasted efficiency and revenue potential are highly dependent on the initial choices of the generator model and can range from 12% for old, but still operational in Latvia, wind generators Nordex N54/1000 to 52% for new Nordex N131/3000 model at high altitudes of operation.

The study showed that 2.3 MW Siemens generators SWT-2.3-101 installed at the largest Latvian wind farm, accounting for one third of wind energy capacity installed in Latvia, might not be optimal generator type for the Latvian conditions. The study suggests that a rigid and multifaceted sensitivity analysis based on physical wind measures and historical electricity market data should be conducted prior to project implementation.

3. Reducing the costs and uncertainty of wind speed measurements

3.1. The modelling of wind flow interaction with a triangular lattice mast

3.1.1. The need for high quality wind speed measurements

The starting point of any decision regarding the construction of a wind power generator is the evaluation of wind energy potential at the selected construction site. Therefore, at the start of any WPP project, a set of estimations is carried out in order to assess its future efficiency. The analysis is primarily based on the technical characteristics of wind turbines and average annual measurements of wind speed collected at the foreseen construction location of the WPP. The main tools for evaluating the potential performance of a future WPP are wind measurement complexes.

The stage of project planning plays an important role in ensuring that the construction site, height of the hub and turbine type are chosen correctly. Altogether, the precision of wind speed measurements is the main factor determining the reliability of the economic feasibility studies and the precision of the break-even period estimation.

An important aspect of wind speed measurement implementation in wind projects is that the obtained results should refer to the height of WT axis. In order to satisfy this requirement it is necessary to place anemometers at the corresponding height and take measurements for the period of at least a year. In order to save time and resources in the deployment of new wind speed measurement masts it would be justified to use the existing network of cellular communication masts, as it minimizes the installation and assembly costs of the measurement equipment.

A standard wind measurement equipment set consist of a cup sensor and a recording unit, which are installed on a mast at the site of the future WPP. In order to avoid the measurement distorting effect of the surface, mast height should exceed 30 m [98]. At the same time, wind speed measurements have to be carried out in compliance with the requirements set by an international standard IEC [100].

This standard has been introduced to provide uniform methodology ensuring consistency, accuracy and replicability of wind measurements results used in the analysis of wind turbine power performance. The standard provides recommendations for determining the distance from the mast, depending on its design, at which measurement sensors should be placed [100].

However, the IEC standard does not take into account the effect of wind speed magnitude on the sizes of the area where the wind speed measurement error, caused by the turbulence, exceeds the acceptable limit. Moreover, the results reported in [101], [102] suggest that the boom length calculated in compliance with the recommendations of the standard is overestimated. This causes problems with the reliability of the boom mount rigidity in the process of installing sensor on the mast [103], [104].

In the data collection process it is important to ensure that the mast structure does not introduce distortions in the airflow that would cause $>1\%$ error in the measurements of wind speed. In practice, efforts and costs associated with the task of wind speed measurement can be greatly reduced if existing communication masts are used to place the measuring sensors instead of erecting new masts dedicated solely to the purpose of wind measurements [105].

However, in that case it is necessary to consider the impact of the mast design elements on the distribution of airflow and confirm the possibility of using the existing mast for obtaining reliable wind speed data [106], [107].

This study investigates the relationship between the speed of wind flow and the size of the area in which the deviation of wind speed measurements from the actual values is greater than 1.0%. Specifically, the author investigates how wind flow distribution around a cellular communication mast (CCM) depends on its sizes and design, taking into account communication cables placed inside the mast structure.

At the first stage of the analysis, the extent of the influence exerted by the structural elements of CCM on the turbulent airflow is analysed theoretically using CFD modelling of wind flow distribution.

At the next stage of the analysis, the estimation of the degree of influence of the CCM structure on the results of wind speed measurement was carried out by experimental studies using three lattice masts on which measurement sensors were placed. On each mast, 9 measurement sensors at four different height levels were installed. Two anemometers were installed at each of the three levels and at one level three sensors were installed displaced by 120° from each other. The temperature and direction of the wind were measured at two different levels.

Finally, using the results of simultaneous measurements from two anemometers taking into account the direction of the wind flow allows estimating the distribution of wind speed around the mast and presenting them in the form of relative velocity curves. Using these curves to correct the raw values of wind speed makes it possible to improve the accuracy of measurements.

3.1.2. Wind speed measurements and types of lattice masts

Wind speed can change in a wide range of values, for example, Figure 3.1 shows wind speed frequency distributions at different altitudes obtained using a laser wind speed measurement complex Pentalum SpiDAR. Measurements were performed in the period of 01.02.2014-01.01.2015 on the Baltic Sea shore in Latvia, Ventspils region, at different heights – 30, 50, 100, 140 and 180 m above the ground [108].

Moreover, previous research has shown that there is a cubical relationship between wind speed and energy that it can generate [109]. Therefore, the reliability of wind measurement results largely determines the precision with which wind energy potential and of the future efficiency of WPP can be determined.

Tower and guyed masts are the main types of masts used for the purpose of CCM. Tower type masts have wide base and are limited in height, therefore it is not practical to use them as load-carrying structures for installing wind measurement equipment [110]. Stranded wires that are fastened to the mast at several levels ensure the stability of guyed type masts. Masts of this type usually have the shape of an equilateral triangle, with rigidity enhancing elements in the form of lattices on each side.

Most commonly used masts have side width 0.74–1.4 m. CCM of the “Wibe” series typically have side width 1.0 and 1.2 m [111]. The height of masts belonging to this construction series can be up to 100 m, which makes them suitable for wind shear measurement applications. Based on measurement results obtained using this type of masts, wind energy potential can be estimated for the heights of up to 150–200 m.

According to the recommendations given by the IEC standard [100], measurement sensors should be placed at a pre-defined distance from the mast. The purpose of the regulation is to keep the level of wind speed deviation below $\pm 1\%$ of the airflow value. The standard prescribes that wind speed sensor should be offset from the mast centre to a distance determined by the following relationship:

$$R = \frac{L}{\frac{1-U_d}{(0.062C_T^2+0.076C_T)}+0.082}, \quad (3.1)$$

where: U_d – relative value of wind speed deviation (0.99);

R – distance of a wind speed sensor from the mast centre to the point of observation, m ;

L – width of the mast side, m;

C_T – the trust coefficient.

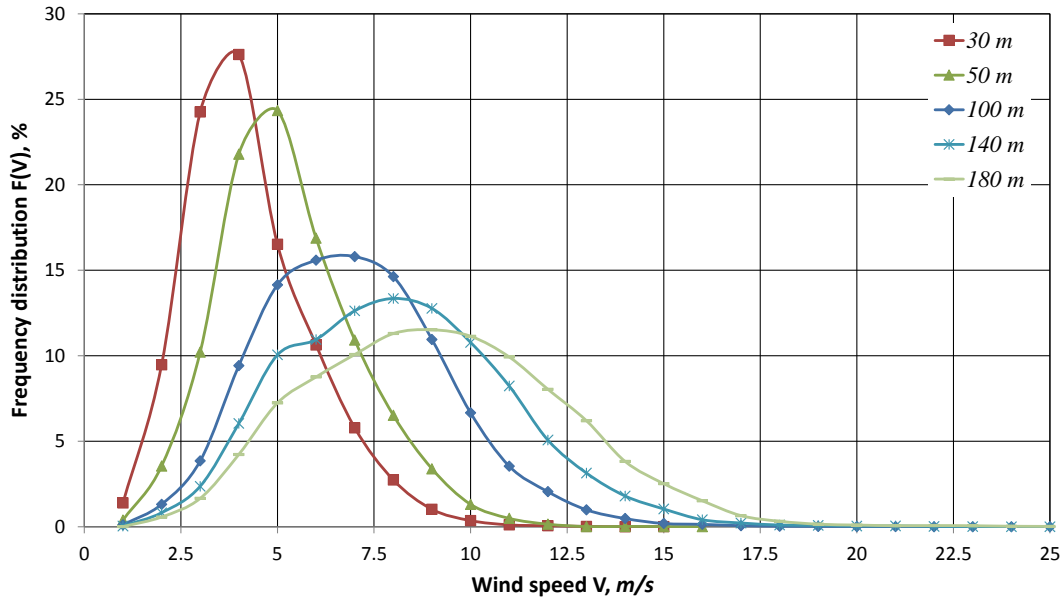


Figure 3.1 Wind speed frequency distribution $F(V)$ calculated based on the results of wind speed measurements for heights 30, 50, 100, 140 and 180 m above the ground. Measurements carried out in Ireben, Venspils region in the period 01.02.2014-01.01.2015.

The value of empirical coefficient C_T , that is used in the IEC standard [100] for estimating the distortion field, is determined according to the following equation:

$$C_T = 2.1 (1 - t)t, \quad (3.2)$$

where t is mast solidity coefficient defined as the ratio of the projected area of all structural elements on the side of the mast to the total exposure area. Therefore, it is possible to estimate the solidity of the mast based on the assumed geometry of its section. It is important to note, that the solidity parameter is affected by the cables of communication antennas laid inside the mast. Figure 3.2 shows a horizontal cross-section of a triangular CCM with side width L of the load-carrying tubes A , B , C . The mast consists of three vertical tubes with diameters $d = 0.06$ or 0.076 m and a connecting cross-arm frame with diameter 0.03 m.

Using Eqs. (3.1) and (3.2) it is possible to calculate the distance from the mast centre to the boundary of the area where the distortion of wind flow value does not exceed $\pm 1\%$. The distance to the observation point depending on the mast structure solidity t is shown on Figure 3.3. The

curves are calculated according to the IEC standard recommendations for masts with side width $L = 0.74, 1.0; 1.2; 1.4$ and 2.0 m.

For the masts of “Wibe” series [111] with the side width 1.0 and 1.2 m the solidity of the mast structure without considering cable lines is $t = (0.17 - 0.22)$. These values are in line with the calculations given in previously conducted research [102]. Taking into account cable lines and ladder design, the solidity coefficient can be $t = (0.3 - 0.4)$. For instance, for a mast with the side width $L = 0.74$ m and solidity $t = 0.35$ the distance of a sensor from the centre of the mast should be $R = 3$ m. However, the results obtained in a related study [102] suggest that the calculations of distance R using ICE standard methodology [99] give only an approximate value. Therefore, for a mast with the side width $L = 2.0$ m and solidity $t = 0.17$ the corresponding curve in Figure 3.3 gives the value of $R = 4.7$ m.

The results of the analysis obtained using CFD simulations and reported in [102], suggest that the boundary of the domain where the distortion of airflow speed does not exceed $\pm 1.0\%$ is at a distance of 3.5 m, covering 320° area around the mast. At the same time, in the 40° sector the boundary of this domain is at a distance of up to 9.0 m. Overall, it means that in cases when CCMs are used for placing measurement sensors, compliance with the recommendations of the IEC standard for determining distance R does not guarantee that the measurements are performed with required precision.

Against this background, let us consider a visual representation of wind flow distribution around a triangular lattice mast. A CCM of guyed type has been chosen as the main object of investigation because of its versatility. In order to analyse the influence exerted by mast structures on the results of wind speed measurements a set of contour maps showing CFD simulated distribution of airflow around the masts obtained by mathematical modelling is considered.

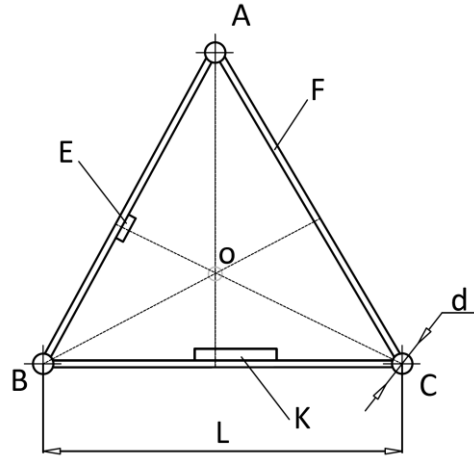


Figure 3.2 Horizontal cross-section of a triangular lattice CCM: K – cable lines; E – ladder structure; o – mast centre; F – mast frame; d – diameter of load-carrying tubes.

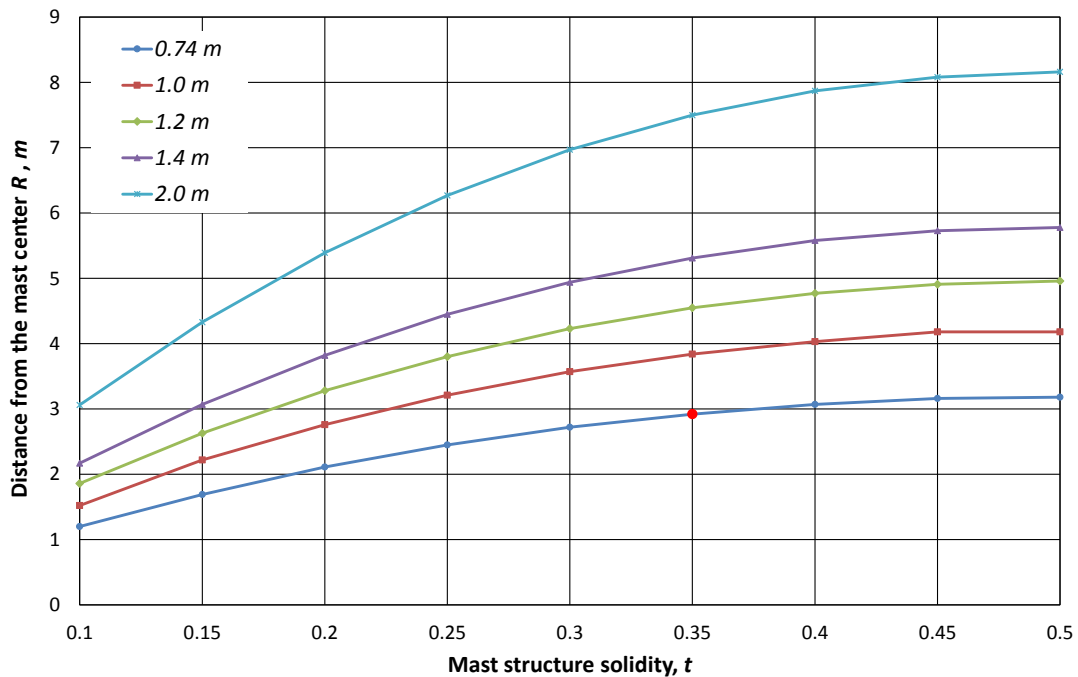


Figure 3.3 Distance R of wind speed sensor from the mast center to the point of observation depending on the mast structure solidity t for different mast side length.

3.1.3. The results of mathematical modelling

Nowadays CFD techniques are widely applied in numerical evaluations of interaction between turbulent flows and various types of solid structures. For this purpose such methods as (Unsteady) Reynolds Averaged Navier-Stokes ((U)RANS) and Large Eddy Simulation (LES) are used.

This study performs a computational estimation of an airflow around a 3D triangular lattice CCM using an open source CFD toolkit OpenFOAM. In this study, the construction of a mast is modelled as a rigid object. The flow is assumed to be turbulent, incompressible and isothermal.

In order to perform the calculations, a high-performance computer (HPC) cluster of Ventspils University College was used [110]. The cluster consists of 28 nodes with two x86 architecture 8 cores processors. The minimum RAM is 32 GB 3-10600R DDR3 and 300 GB 6 Gbps 10000 rpm SAS HDD for the node. On average, one estimation case needs two weeks of computations to converge given the stated accuracy level. Due to numerical complexity, a number of simplifications, such as the first-order accurate numerical schemes, were made for preliminary calculations. Solutions are assumed to be converged when the residuals are less than 10^{-5} .

The fluid flow is governed by Navier-Stokes equations and conservation of mass. The effects of the turbulence in the flow are represented by models of turbulence. The finite volume method is used to calculate partial differential equations (PDE). The flow field is described by the conservation of mass Eq. (3.3) and conservation of momentum Eq. (3.4) equations. A time-average approximation has been applied using RANS equations:

$$\frac{\partial \bar{u}_i}{\partial x_j} = 0, \quad (3.3)$$

$$\frac{\partial \bar{u}_i \bar{u}_j}{\partial x_j} = -\frac{\partial \bar{P}}{\partial x_i} + \frac{\partial}{\partial x_j} \left\{ \mu_i \left(\frac{\partial \bar{u}_i}{\partial x_j} + \frac{\partial \bar{u}_j}{\partial x_i} \right) - \rho \overline{u'_i u'_j} \right\}, \quad (3.4)$$

where \bar{u} is the Reynolds-averaged velocity, \bar{P} is the averaged pressure, μ is the eddy viscosity, $\overline{u'_i u'_j}$ is the Reynolds stress tensor. This introduces more variables than the number of equations. In order to deal with the system closure problem, two turbulence models are applied: one-equation Spalart–Allmaras turbulence model and the two-equation standard k – ε turbulence model [112]. In order to couple the pressure and the velocity fields SIMPLE technique has been applied using OpenFOAM solver SimpleFoam. Standard OpenFOAM wall functions were applied for turbulent viscosity, ν_t , turbulent kinetic energy, k , and turbulent dissipation, ε .

The three-dimensional computational domain is defined as a rectangular area and has the following dimensions: 30 m in the streamwise direction, 9 m in the spanwise direction, and 5 m in the vertical direction. The computational mesh was generated using the built-in OpenFOAM mesh

utilities: blockMesh and snappyHexMesh. Around the mast surfaces an unstructured mesh is generated, while for the remaining domain part the structured mesh is applied (see Figure 3.4). On average, the computational domain contains approximately $11 \cdot 10^6$ cells.

As a boundary condition of inflow, the constant inlet wind speed, U_∞ is used. The outflow is defined by constant pressure, $p = 0$. The velocity on the surface walls is equal to zero. At the bottom and top of the domain mirror symmetry conditions are applied. The inlet turbulent kinetic energy, k , and turbulent dissipation, ε , have constant values. The turbulence intensity is assumed to be 15%. For the mentioned parameters (v_t , k , ε) standard OpenFOAM wall functions have been applied. The wall function parameter y^+ on average is less than 400 for $U_\infty = 10.0$ m/s, and approximately 200 for $U_\infty = 5.0$ m/s.

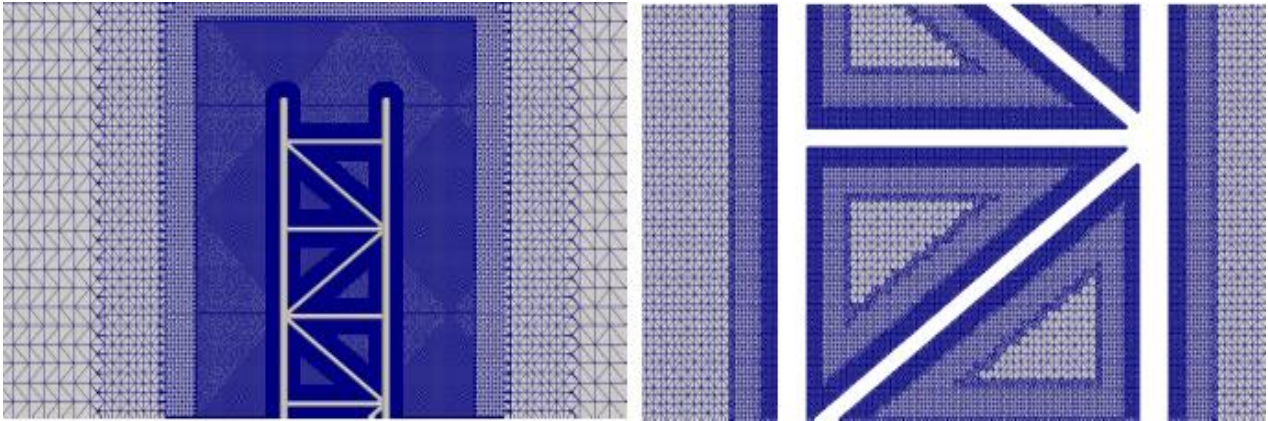


Figure 3.4 Mesh around the triangular lattice mast structure, vertical cross-section.

In order to estimate the extent to which the structure of a lattice CCM affects the speed distribution of wind flow around it, we first consider the interaction of wind flow with a metrological mast with the side width 0.74 m. Figure 3.5 shows a contour map of wind flow speed distribution around a lattice mast for wind speed $U = 10.0$ m/s and the angle of wind direction $\alpha = 0^\circ$ relative to the triangular lattice mast.

The position of sensor S is fixed on the mast by a boom at a distance of 3.0 m relative to the triangular mast centre, to which one-metre-step concentric octagons are attached. The boom length corresponds to the red point in Figure 3.3 for a mast with side width $L = 0.74$ m and solidity $t = 0.35$.

In turn, Figure 3.6 demonstrates the speed distribution of a wind flow around a lattice CCM mast with side width 0.74 m for wind speeds $U = 5.0$ and 10.0 m/s and the angles of wind direction $\alpha = 0^\circ$ and 180° relative to the position of a boom with sensor S .

Grey area in Figure 3.5, Figure 3.6, and Figure 3.7 corresponds to $100 \pm 1\%$ of the undisturbed wind flow speed values. Green area corresponds to 101–101.5%, red area to more than 101.5%, while violet area corresponds to 98.5–99% and brown area to less than 98.5% of the undisturbed wind flow speed values. The contour maps show the wind flow speed that would satisfy the IEC standard requirements in grey, green and violet areas, while in the red and brown regions the deviations would exceed the allowed error margin.

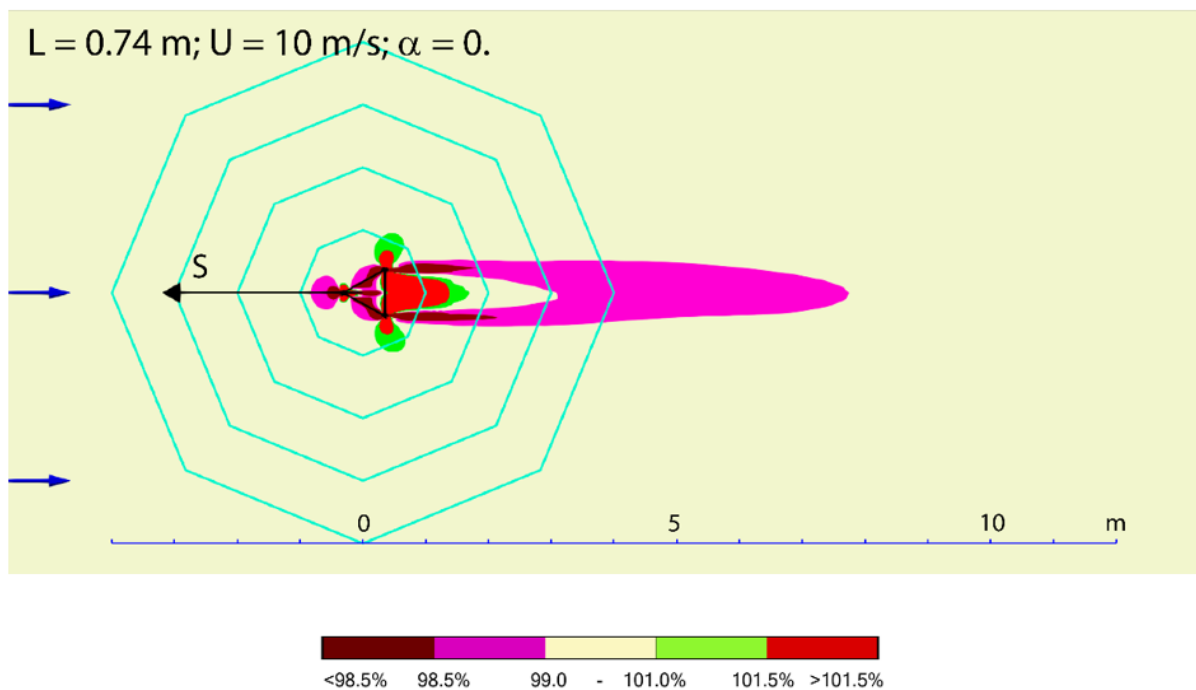


Figure 3.5 CFD model of the wind flow interaction with a triangular lattice metrological mast, side width $L = 0.74$ m, at the wind speed $U = 10.0$ m/s and angle $\alpha = 0^\circ$ relative to the position of a boom with sensor S .

The use of CFD models shows that the presence of cable lines inside a triangular lattice CCM slows down wind flow speed by more than 1.5% and causes the appearance of a narrow tail with the length of 7.0 – 9.0 m and angular dimensions of less than 10° . Within the boundaries of the remaining 350° sector, the length of the region with wind speed distortions beyond $\pm 1.5\%$ does not exceed 1.5 – 2.0 m from the mast centre.

CFD modelling results indicate that in order to perform wind measurements using a mast with side width $L = 0.74$ m and solidity $t = 0.35$ (i.e. complying with IEC standard [100]), it suffices to use a 2.0 m long boom. In this case, within the limits of 350° sector wind speed will be measured with deviation not greater than $\pm 1.5\%$.

However, within the sector of less than 10° for measurements with the same accuracy the sensor should be placed at a distance of 9.0 m from the mast centre. It would require considerable additional resource related to boom fastening at a longer distance from the centre in order to ensure that the IEC standard is followed also in the problematic 10° region. It is noteworthy to mention that in the considered case, the share of observations obtained from this sector amounts to 2.5% of the total amount of measurements. The performed calculations make it possible to refine the results of other authors' studies indicating that the requirements of the IEC standard [100] regarding the length of the boom are overestimated. At the same time, the simulation results allow to conclude that the standard does not guarantee the measurement accuracy of $100 \pm 1.0\%$ in the shadow area of the mast ($\alpha = 180^\circ$).

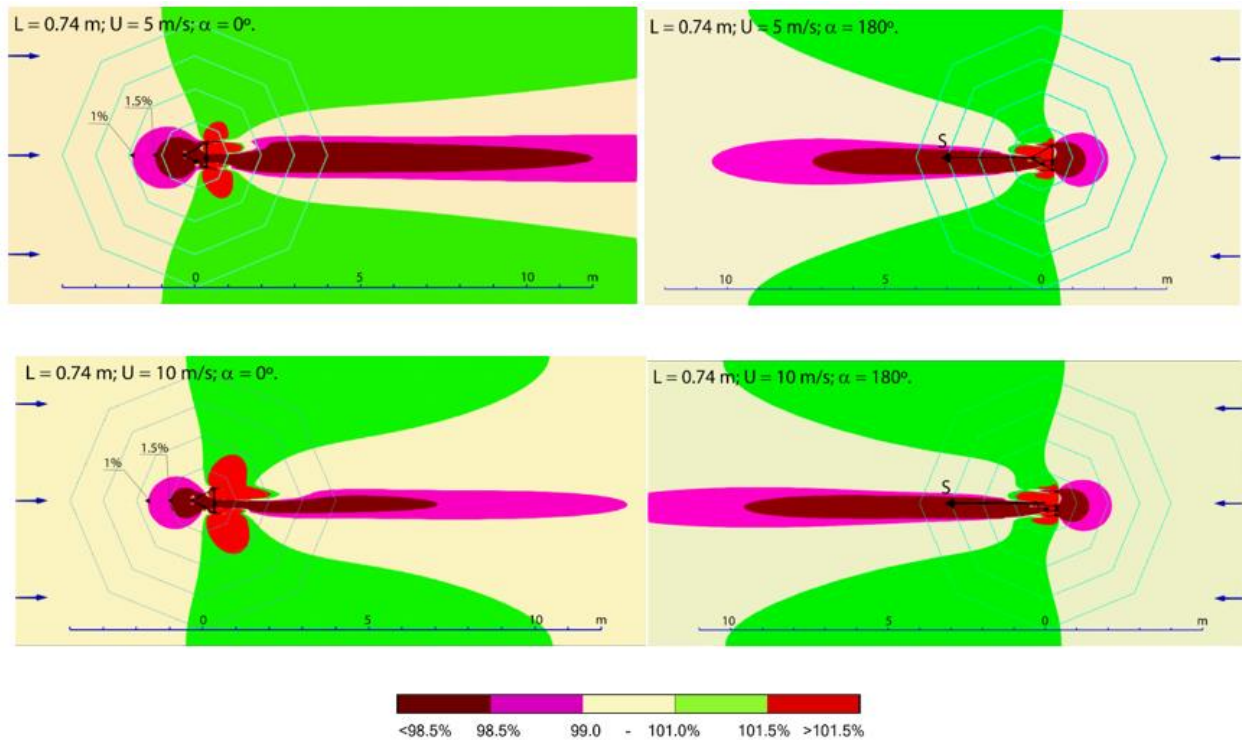


Figure 3.6 CFD modelling results of the wind flow field around a triangular lattice CCM, side width $L = 0.74$ m, for wind speeds $U = 5$ and 10 m/s and angles $\alpha = 0$ and 180° relative to the position of a boom with sensor S .

The results of these calculations for wind speeds $U = 5.0$ and 10.0 m/s are presented in Figure 3.7 a, b, where the sizes of grey area correspond to the speed of $100 \pm 1\%$. Green area corresponds to $101-101.5\%$, red area to more than 101.5% , while violet area corresponds to $98.5-99\%$ and brown area to less than 98.5% of the undisturbed wind flow speed values.

On the contour maps, distances from the mast centre to the boundaries of the fields corresponding to the 1.0 and 1.5% wind speed deviations are marked by black triangles.

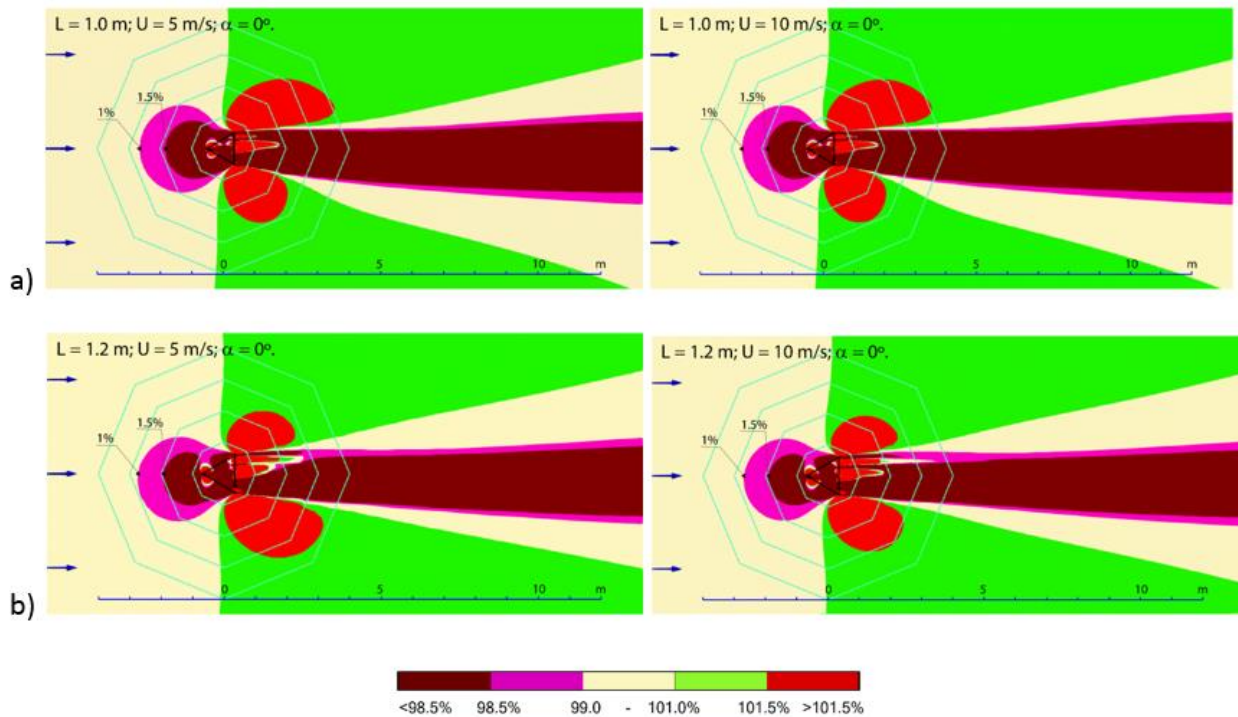


Figure 3.7 CFD modelling results of the wind flow field around a triangular lattice CCM, a) side width $L = 1.0$ m and b) side width $L = 1.2$ m, for wind speeds $U = 5.0$ and 10.0 m/s and the angle $\alpha = 0^\circ$ relative to the position of a boom with sensor S .

The modelling results are presented in Figure 3.8 as curves of distance R , m, in dependence on the wind speed U , m/s, for masts with the side widths $L = 0.74$ m and 1.2 m. A distinctive feature of these curves is the presence of peaks in the value of R in the wind speed range from 4.0 to 5.0 m/s. This indicates that when a measuring sensor S is positioned at the point corresponding to the boundary of the region where the wind speed deviation is not more than 1.0% and calculated for a speed of 5.0 m/s, the wind speed variations will not affect the measurement accuracy.

The analysis of obtained results allows expressing the value of R as being dependent on the width of a triangular lattice cellular communication mast side L . The relationship between R and L presented in Figure 3.9 allow determining the appropriate boom length for placing sensors in the area where the measurement error would not exceed 1.0 - 1.5% for the wind flow from the side of the sensor at an angle $\alpha = 0^\circ$.

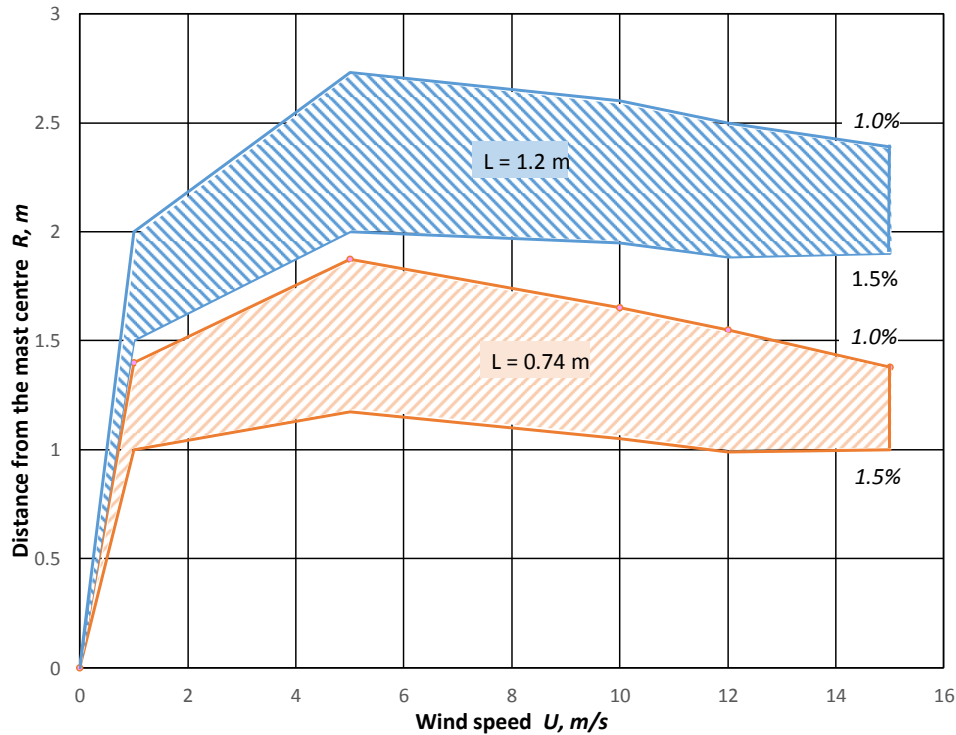


Figure 3.8 Distance from the center of a triangular lattice CCM, R , m, to the boundaries of areas where the wind flow speed decreases by 1.0 - 1.5%, for masts with side widths $L = 0.74$ and 1.2 m, angle $\alpha = 0^\circ$, relative to the position of a boom with sensor S , depending on the wind flow speed U , m/s.

Overall, an important conclusion can be made, that the requirements of the IEC standard on wind measurements can be satisfied only if two sensors arranged in anti-phase are used simultaneously. Moreover, at the data processing stage it is necessary to consider only those measurements that do not come from a sensor located in the shadow of the mast.

Such method of wind speed measurements would allow considerably lowering the requirement with respect to the minimum boom length. The relaxation of the requirements would result in much easier sensor installation process of sensors on measurement masts.

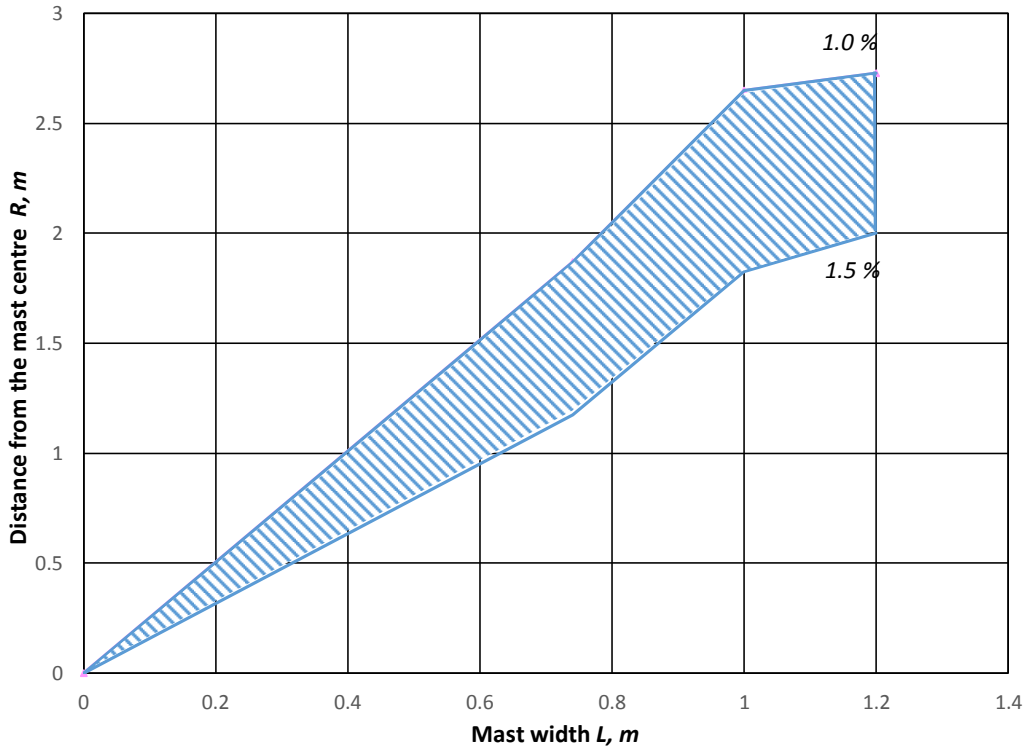


Figure 3.9 Distance from the center of a triangular lattice CCM, R , m, to the boundaries of areas where the wind flow speed decreases by 1.0 –1.5%, for wind speed $U = 5.0$ m/s, depending on the width L , m, of the mast side.

It is noteworthy, that the use of paired sensors for wind measurements creates an opportunity to employ the existing network of triangular lattice CCM. That considerably lowers the costs of data collection necessary for performing the assessment of wind energy resource potential.

3.2. The use of lattice CCM for wind shear assessment

3.2.1. The description of experimental site and wind measurement equipment

For wind energy resource assessment on the shores of the Baltic Sea, a program of physical experimental studies was developed, which involves the use of three 100 m CCMs to carry the measuring sensors of the Symphonie PLUS3 wind measuring complex.

During the experiment, wind speed is measured at four levels at several points around the mast, taking into account the requirements of an international standard IEC [100] with respect to the procedure of wind speed measurements and the modelling of wind shear.

The experimental site locations of the three masts were selected on the shore of the Baltic Sea in Ventspils, Pāvilosta and Ainaži regions as it shown in Figure 3.10. The map shows the location of the masts are at Site 1 – Staļdzene, Ventspils, Site 2 – Tebra, Pāvilosta and Site 3 – Rozēni, Ainaži, indicating the nearest locations of the Meteorological Station of the National Hydrometeorological and Climatological Service of the Latvian Environment, Geology and Meteorology Center (LEGMC).

On Figure 3.11 NRG Symphonie PLUS3 data logger used for measured data recording and transmission is presented. Left image shows data logger with battery, programming console and channels configuration diagram. On the right image, side view of the same unit is shown with GSM module (iPACK), terminals for 15 analog or digital sensors and extremal power connection.

During the experiment, three-second values of wind velocity, wind direction, temperature and air humidity were measured and the 10-min average values were recorded using NRG Symphonie PLUS3 logger. On Figure 3.12, the following installed sensors for measuring the atmospheric parameters on each mast are shown:

1. Cup anemometer of WindSensor P2546A-OPR type – 9 sensors on four levels;
2. Wind direction NRG # 200P – 2 sensors on two levels;
3. Thermometers NRG # 110S - 2 sensors on two levels;
4. Hygrometer RH-5X: 4414-1 sensor.

The listed above sensors and GSM data transfer unit (NRG Symphonie iPACK) are designed to work with NRG Symphonie PLUS3 data logger and require a power supply of 12–18 V. Therefore, a 20 W photovoltaic solar panel was used for the autonomous operation of the measuring system, taking into account short light time in the winter in Latvian latitudes.

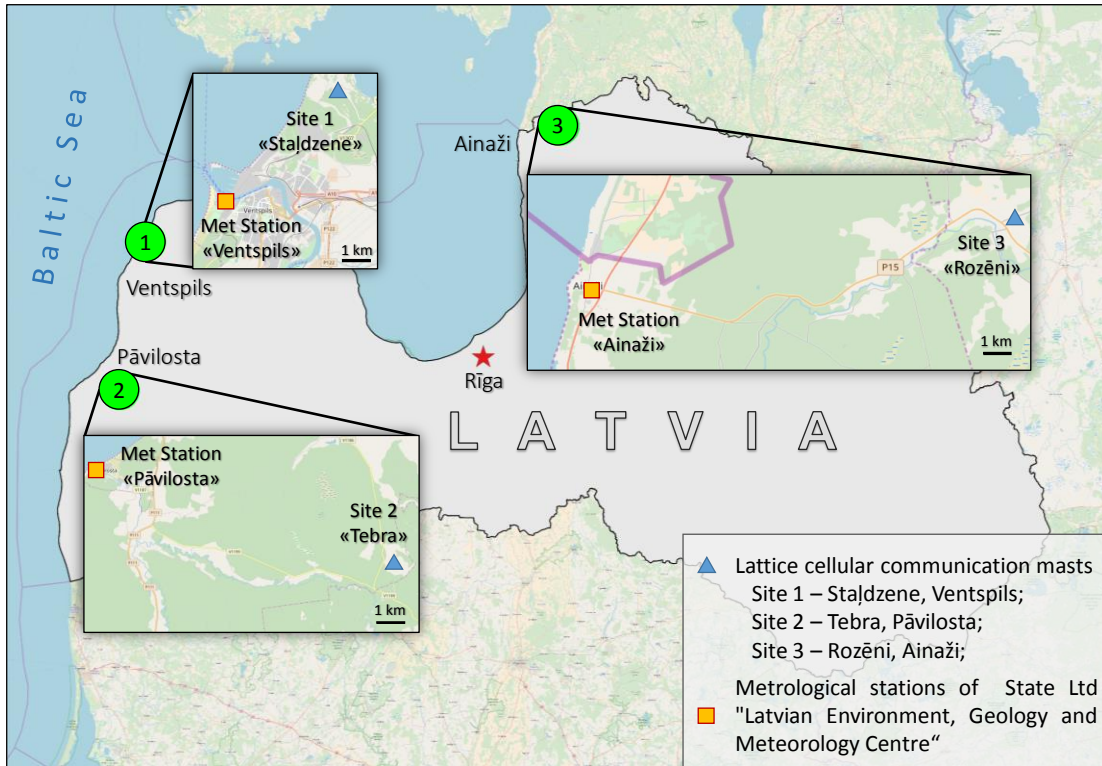


Figure 3.10 The map location of three tall triangular lattice CCM and LEGMC Met Stations on the shore of the Baltic Sea at sites Stalīdzene, Tebra and Rozēni in Ventspils, Pāvilosta and Ainaži regions.



Figure 3.11 NRG Symphonie PLUS3 logger with battery, programming console and channels configuration diagram (left) and its side view with GSM module (iPACK), terminals for 15 analog or digital sensors and external power connection (right).



Figure 3.12 Wind measurement cup anemometer of WindSensor P2546A-OPR type placed at the end of the boom (bottom left), wind direction sensor NRG #200P (top right), hygrometer RH-5X: 4414 installed on the mast (bottom right) and thermometer NRG #110S (top left).

3.2.2. The installation of measuring sensors on CCM

The guyed type lattice triangular mast with height of about 100 m and with the side length of 1.4 m, which was used to place the metrological sensors and the measuring complex in the Site 3 (Rozēni, Ainaži) is shown on Figure 3.13. For the estimation of influence of a lattice mast structure on the airflow, a method of physical measurement of wind speed using cup anemometers installed around the mast at an angle of 120° at four levels was used.



Figure 3.13 Guyed type lattice triangular CCM in the Site 3 – Rozēni, Ainaži, which has a height of about 100 m with the side length of 1.4 m.

The layout of cup anemometers and wind direction sensors installation at the height of 40 m is shown on Figure 3.14. On this vector diagram the arrangement of a wind direction sensor S_{Dir} on a 1.6 m boom with an angle of offset β with respect to the northward vector N and anemometers S_A , S_B , S_C on 2.8 m long booms are displayed. Given that an anemometer is installed on a 2.8 m long boom, its distance from the mast centre O with a mast side width $L = 1.2$ m is 3.2 m.

The installation of metrological sensors and the Symphonie PLUS3 measuring complex on the masts is carried out according to the scheme on Figure 3.15, where five levels correspond to reference heights of 2, 10, 40, 64 and 84.5 m. Reference heights are the heights allocated by

the mobile operator at the stage of the project approval. The diagram also shows the four reference heights where metal guys supporting the mast are mounted.

Technical data and description for the three sites - Ventspils, Pāvilosta and Ainaži, including summary information about site location and metrological sensor connection properties to the data loggers is given in Annex 1 Table A.1. In the Annex, for each sensor, the actual height of arrangements on the mast and the sensor direction with respect to the northward direction N is indicated.

The position of the wind direction sensor S_{Dir} with respect to the northward direction N is adjusted by setting the offset angle β in the data logger settings. The map of the terrain and the location of the CCM, indicating the angular position of the wind direction sensor S_{Dir} relative to the northward direction N at the Staļdzene, Tebra, and Rozēni sites, is shown on Figure 3.16.

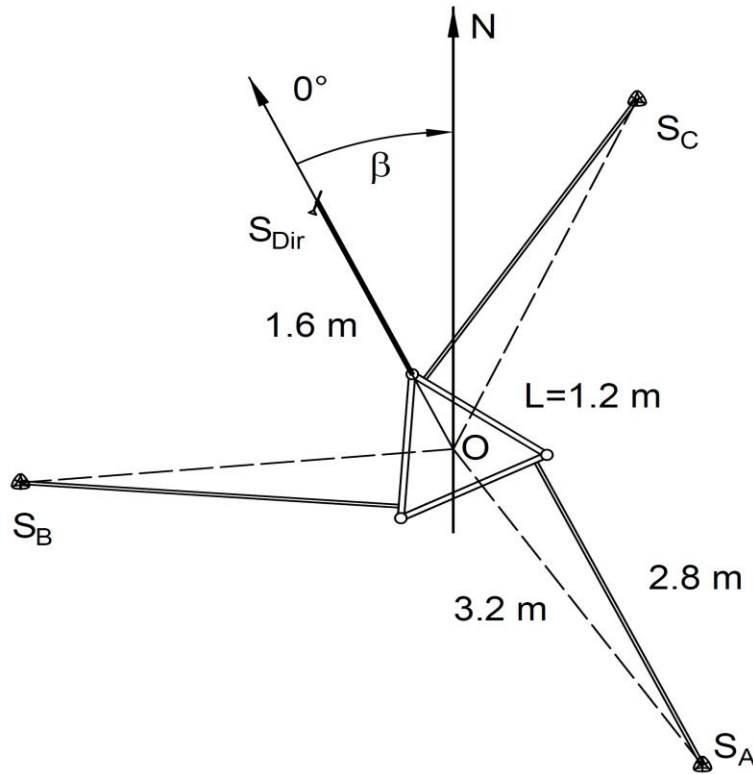


Figure 3.14 The vector diagram of the arrangement of a wind direction sensor S_{Dir} on a 1.6 m boom with an angle of offset β with respect to the northward vector N and anemometers S_A , S_B , S_C on 2.8 m long booms that are located at a 3.2 m distance from the centre O of the triangular CCM with a side length $L = 1.2$ m.

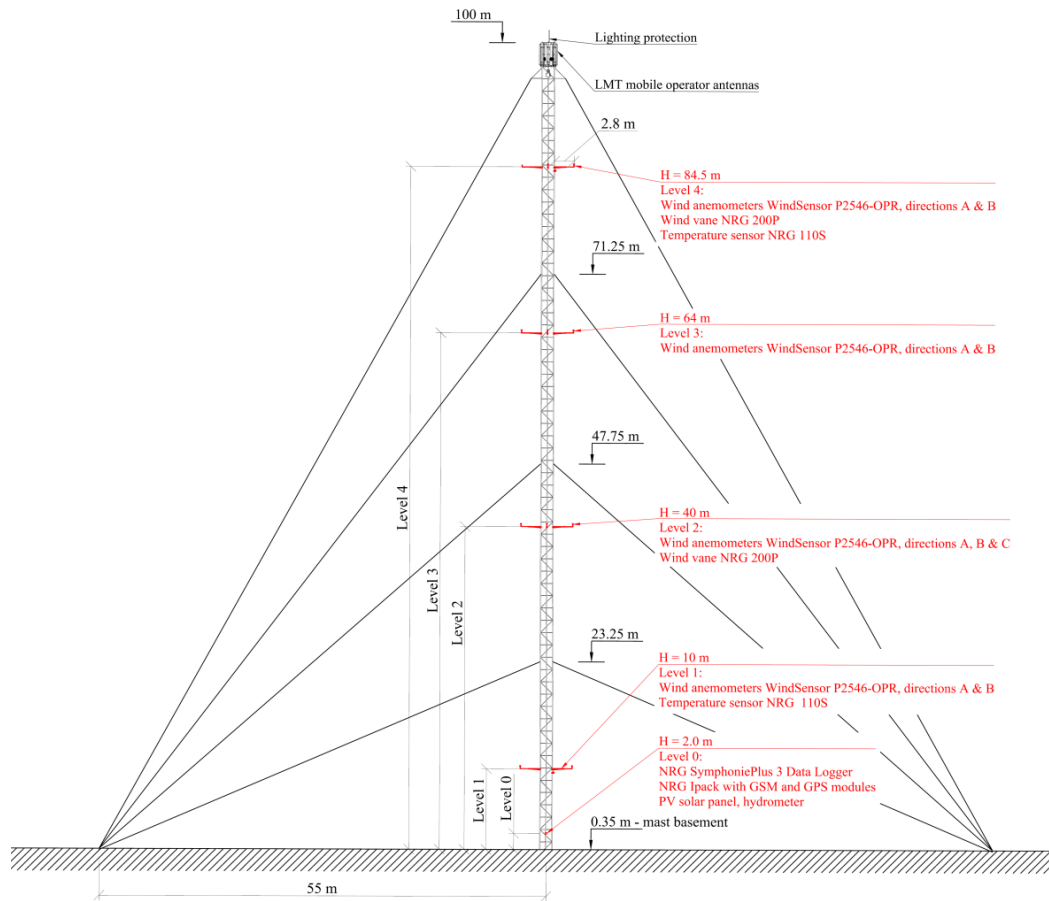


Figure 3.15 Placement of metrological sensors and the Symphonie PLUS3 measuring complex on the triangular lattice CCM with 100 m height located in Ventspils, Pāvilsta and Ainaži regions, where five levels correspond to reference heights of 2, 10, 40, 64 and 84.5 m.

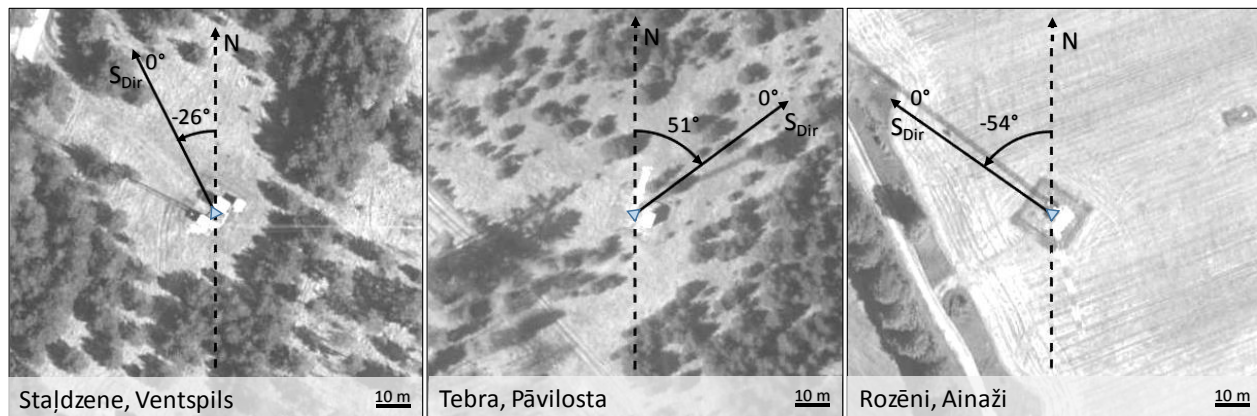


Figure 3.16 The map of the terrain and the location of the CCM, indicating the angular position of the wind direction sensor S_{Dir} relative to the northward direction N, respectively, at the Staļdzene: -26° , Tebra: 51° , and Rozēni -54° sites.

The view of mounted sensors is depicted on Figure 3.17, where left image shows installed Level 2 (40 m) anemometers S_A , S_B , S_C and wind direction sensor S_{Dir} . Respectively, on Figure 3.17 right image corresponds to Level 4 (84.5 m) with anemometers S_A , S_B and wind direction sensor S_{Dir} . On the images, one can see that the attachment of the anemometers on the mast is performed using 2.8 m long booms strengthened by three guys and cap screws. A steel cable with a diameter of 3.0 mm in a plastic protective coating was used as a brace.



Figure 3.17 Metrological sensors and a data logger mounted on a triangular lattice CCM. Level 2 (40 m) – anemometers S_A , S_B , S_C and wind direction sensor S_{Dir} (left), Level 4 (84.5 m) – anemometers S_A , S_B and wind direction sensor S_{Dir} (right).

3.3. The analysis of measurement results

3.1.1. Lattice mast structure impact on measurement results

The practical implementation of the project related to the wind speed measurements using CCM made it possible to assess the technical and economic issues that should be solved in order to implement such type of studies. During the project realization, a considerable part of time was spent on choosing the location of the masts, negotiating available heights on the mast for sensor mounting and obtaining permission from the mobile operator to use their masts for scientific purposes.

Summarizing the financial costs of the conducted experiments allows concluding that in specific cases for each site the cost of performing wind speed measurements at four levels during

the year may be by an order of magnitude lower than the costs needed for erecting and decommissioning a generic 100 m metrological mast.

The transfer of data from the measuring complexes was performed once a day via GSM mobile communication channels. Overall, the process of obtaining daily data for all 10-min measurements of wind parameters does not pose a technical problem. The received information is stored in a database, which allows to quickly monitor the operation of the complexes at a distance and analyze the information received.

In a related study [113], where the results of airflow modelling around a triangular lattice mast are discussed, it can be seen that when measuring wind speed using two or three sensors with offset by 120° from each other, at each moment only one sensor can be in the shadow of the mast. Therefore, if the calculations of average wind speed from the database excluded measurements made by the sensor located in the shadow of the mast, it would be possible to increase the reliability of the result of calculations.

According to the analysis of the results of 10-min measurements for two sensors located at the same height, it can be assumed that the ratio of their values should characterize the deviation of the airflow velocity in the corresponding sector around the mast. Therefore, the results of wind speed measurements of all sensors were grouped by time of measurement and in the direction from 0° to 360° with the steps of 1°.

The results of simultaneous wind speed measurements by two anemometers installed at the same height with 120° displacement makes it possible to estimate the degree of wind flow distortion caused by the mast structure. For the quantitative evaluation of the average value of wind flow distortion indicator, the equation of relative wind speed can be used:

$$V_{w_avg} = \frac{1}{n} \sum_{k=0}^n \left(\frac{V_{A_k}}{V_{B_k}} \right) = \frac{1}{n} \sum_{k=0}^n V_{w_k}, \quad (3.5)$$

where V_{A_k} and V_{B_k} are simultaneous 10-min wind speed measurements, for sensors S_A and S_B , at the same height, $k = 1, 2, \dots, n$ is the number of wind measurement step, where n is the total size of the samples.

The ratios calculated using Eq. (3.5) for sensors S_A and S_B and sensors S_A and S_C in relationship to the angle of wind direction, averaged in steps of one degree for Staldzene site at the Levels 1 - 4, corresponding to the heights 12.4, 40.4, 61.4 and 83.9 m above the ground, in relationship to the angle of wind direction are shown in Figure 3.18. A characteristic feature of these curves are peaks corresponding to the wind direction angles 105° and 225° with respect to the angle 0° of the direction sensor S_{Dir} .

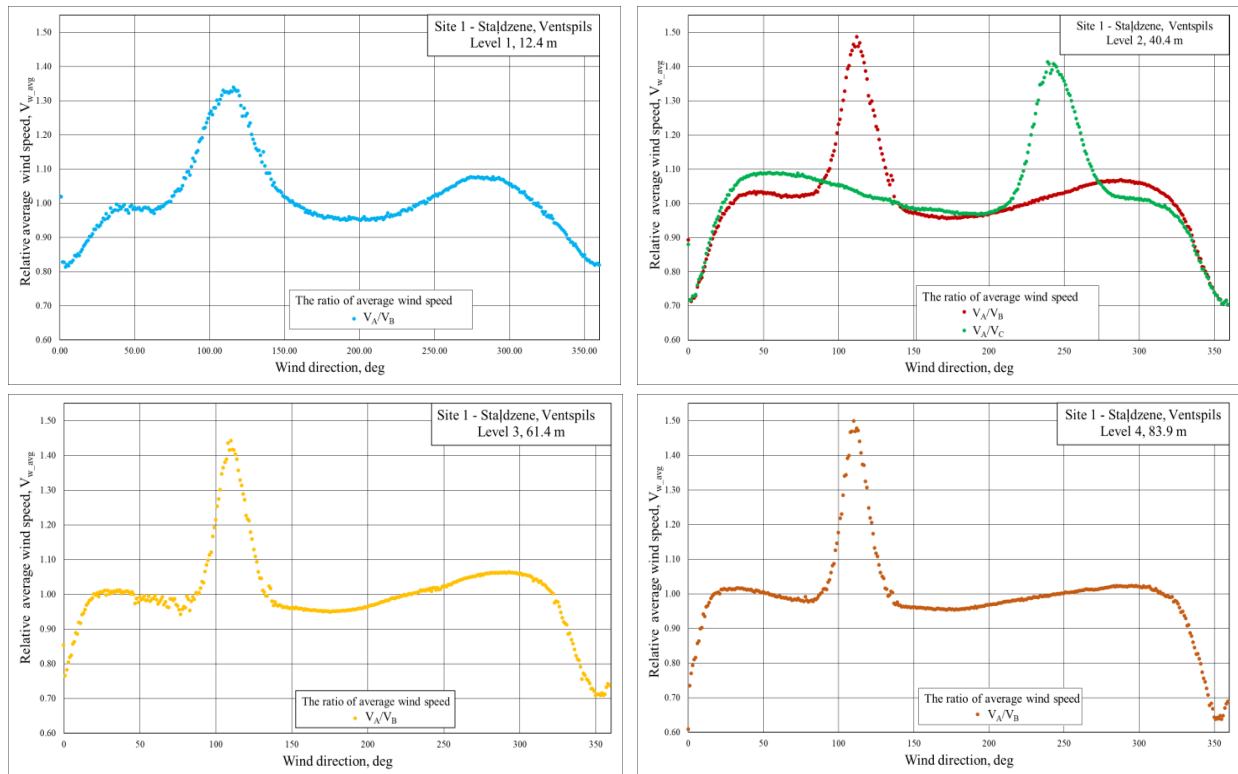


Figure 3.18 Relative average wind speed V_{w_avg} from sensors S_A , S_B and S_C installed on the CCM with side length 1.2 m in Ventspils site at a Levels 1 – 4 in relationship to the angle of wind direction

Similar calculations were performed for Pāvilsta and Ainaži sites and are shown in Figure 3.19 and Figure 3.20 in the form of relative average wind speed V_{w_avg} obtained for anemometers S_A , S_B and S_C installed at a Levels 1 - 4 above the ground, in relationship to the angle of wind direction.

It is important to note that the wind flow velocity in these directions at different heights is reduced by almost 50%. The mathematical modelling results given in papers [102], [104] for met masts indicate that the speed drop can reach 30 - 35%. The difference between modelled and

observed deviations can be attributed to the presence of cable lines inside the cellular communication mast that cannot be fully considered in the modelling framework.

Based on the simulation results and experimental studies presented above, it can be concluded that for each sensor on the mast there is a sector within which the results of wind speed measurements will not meet the requirements of the standard. However, the size of this sector does not exceed 70° .

It means that in order to measure wind speed in accordance with the requirements of the standard, two sensors offset by an angle of at least 120° must be used and the results of measurements should be related to the direction of the wind flow. In this case, the measured values of wind speed, which are obtained in the area shaded from the wind, must be excluded from calculations.

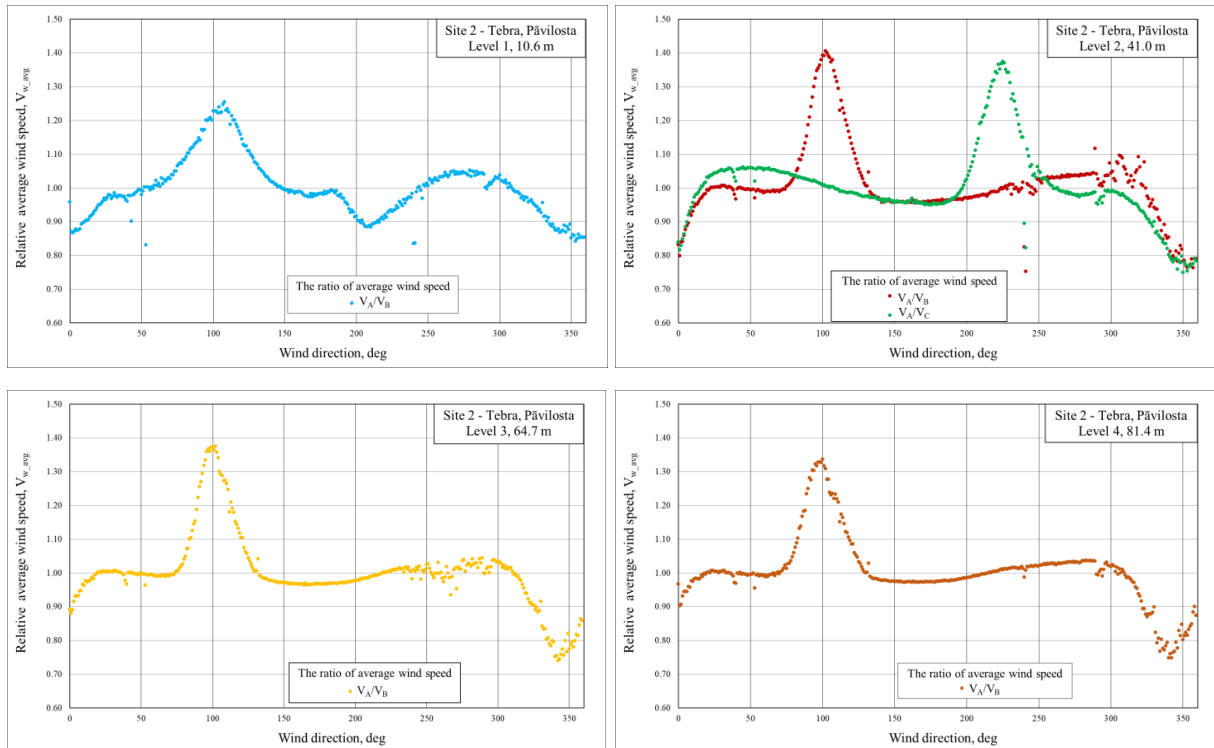


Figure 3.19 Relative average wind speed V_{w_avg} of measured wind speeds from sensors S_A , S_B and S_C installed on the CCM with side length 1.4 m in Pāvilosta site at a Levels 1 – 4-in relationship to the angle of wind direction

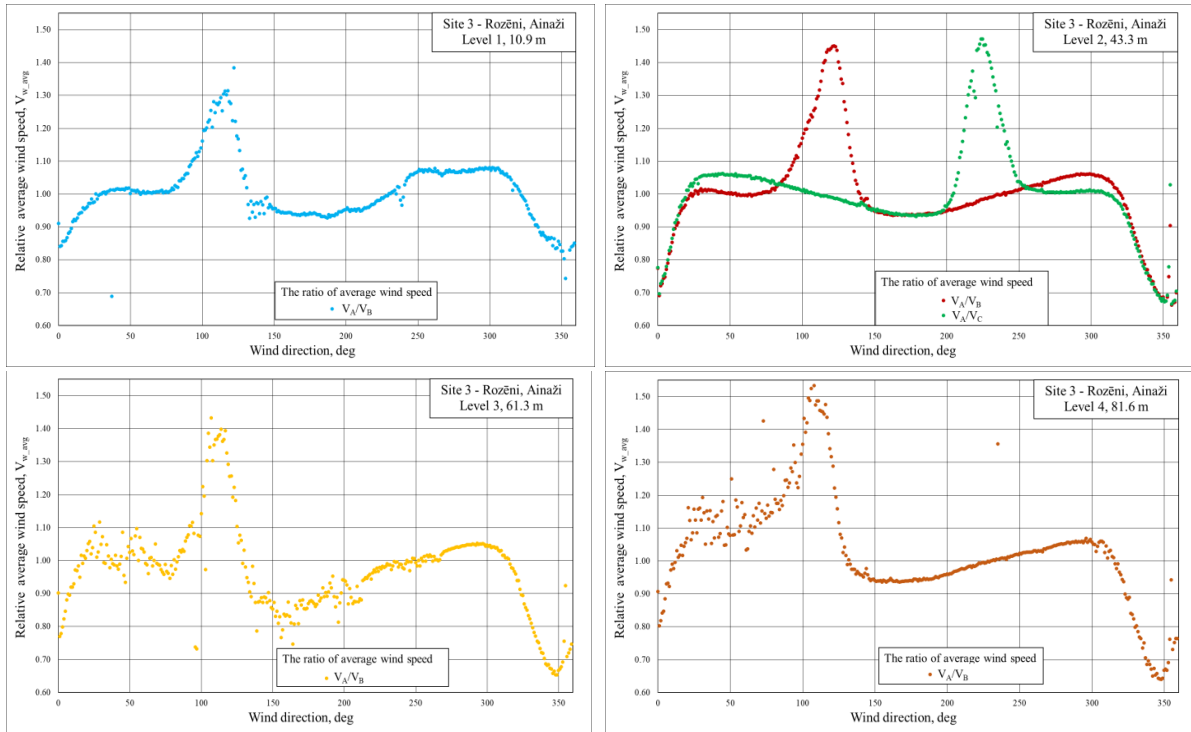


Figure 3.20 Relative average wind speed V_{w_avg} of measured wind speeds from sensors S_A , S_B and S_C installed on the CCM with side length 1.4 m in Ainaži site at a Levels 1 – 4 in relationship to the angle of wind direction

3.1.2. The method of wind speed measurement uncertainty reduction

The results of long-term wind speed measurements, performed simultaneously by three anemometers S_A , S_B , and S_C , at the height of 40.4 m at site 1 for 24 hours period, are shown in Figure 3.21. In the figure, the time period highlighted in grey corresponds to the weather conditions when sensors S_A , and S_C , were open to the flow of wind, while sensor S_B , was located in the shadow area created by the mast structure. It is noteworthy that the figure also illustrates that the results of wind speed measurements during this period differ by ~ 2.0 times.

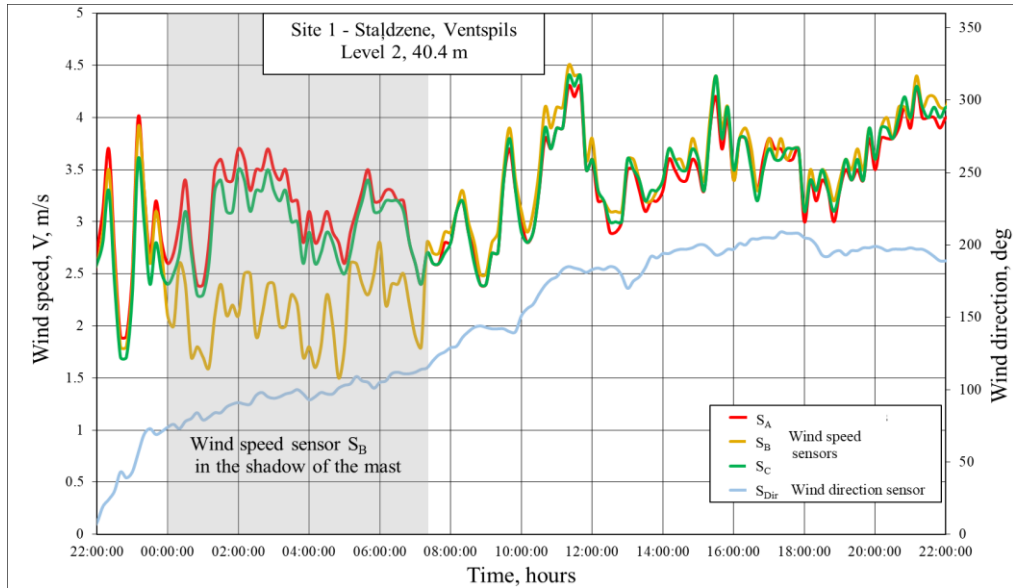


Figure 3.21 Average wind speed data with 10 min increments from anemometers S_A , S_B , S_C and wind direction from sensor S_{Dir} . The grey area indicates the period when sensor S_B was in the shadow, which corresponds to the wind direction $75^\circ - 115^\circ$.

Comparing the wind speed and wind direction sensor curves, it can be seen that the shadow area corresponds to the direction of $75^\circ - 115^\circ$. Thus, the extent of the effect of the mast on the measuring sensors can be represented as a vector diagram on Figure 3.22, which shows the wind flows with directions 106° , -14° and -124° , as well as the respective shadow areas behind the mast of sensors S_A , S_B , S_C .

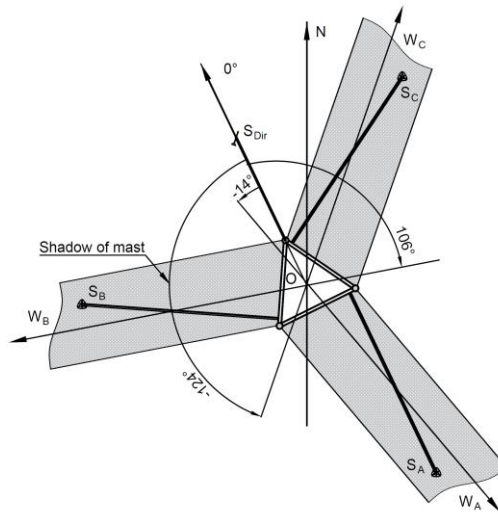


Figure 3.22 The vector diagram of wind flows W_A , W_B , W_C and their shadows of sensors S_A , S_B , S_C .

The average wind speed values V_{avg} obtained from measurements and corrected average wind speeds V_{avg_corr} , for anemometers S_A , S_B , S_C at Levels 1 - 4 for the entire measurement periods on each site are given in Annex 1 Table A2, where one can see mean wind speed values for each height and difference in percent between raw and corrected values.

Based on the measurement results it is possible to conclude that wind speed values recorded from anemometers for one height differ among themselves within several percent. In this case, the real value of the wind speed differs from the measured values by same level.

The comparison of the wind speed measurements results shows that, as a result of the correction, the average speed at all heights increased by $\sim 1.9 - 3.9 \%$. Since distorted values were excluded from the calculations, this means that the reliability of the measurement results has increased by a similar amount.

Despite the fact that the logger receives measurement data from the sensors every 3-second, it actually records the averaged 10-min values. This leads to the fact that the sensors, separated from each other by several meters do not record the exactly the same value of the wind speed. On some occasions, within 10-m intervals wind flow can significantly change its direction. This leads to the fact that, a scatter of the points appears on the curves, which can be seen on Figure 3.23, where an example of calculated wind flow distortion values V_w in relationship to the angle of wind direction for each 10-minute simultaneous wind speed measurements from two anemometers S_A , S_B registered in site Ventspils, Level 4 is presented.

It should be pointed out that the appearance on the curve points grouped in vertical lines is caused by the icing of the wind direction sensor. This particular phenomenon can also be seen in Figure 3.24, which shows the snapshot of temperature, humidity and wind direction measurements on Site 1, Ventspils for a short time period when wind direction sensors were frozen.

The icing of the wind direction sensors was preceded by a combination of certain factors: wet snow and rain, a sharp increase in humidity from 60 to 98%, and a temperature drop below 0° . The sensors was not responding for about 40 hours. As a result, the information necessary to correct the wind speed data was lost for this period.

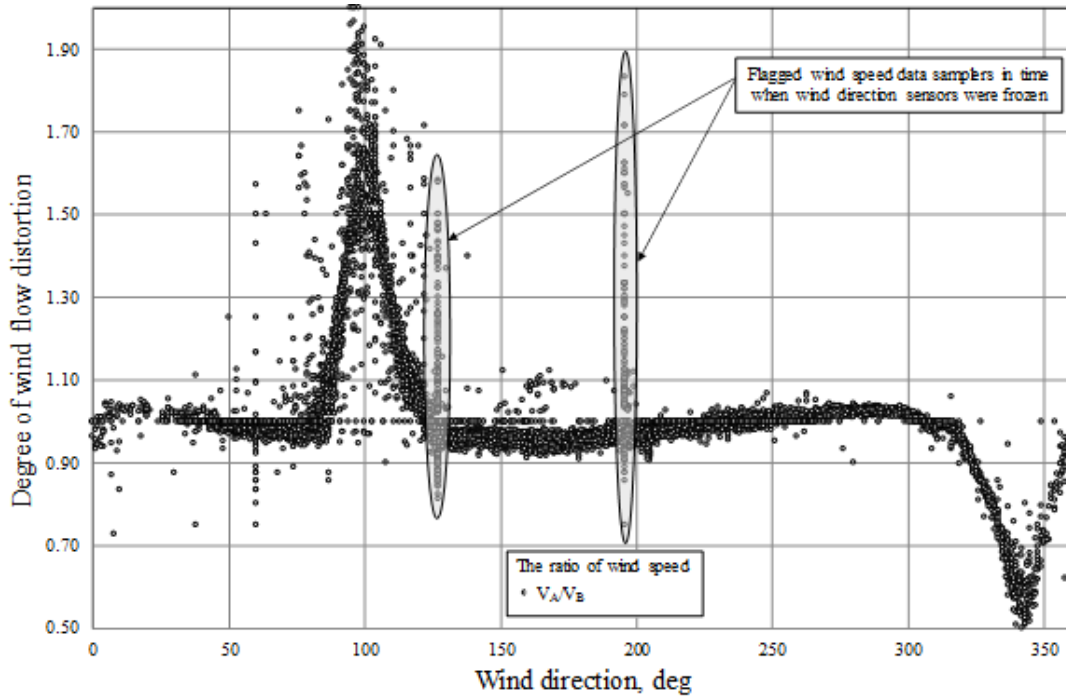


Figure 3.23 An example wind flow distortion V_{w_avg} calculated for each 10-minute simultaneous wind speed measurements from two anemometers S_A , S_B installed on the mast with side length 1.2 m in Ventpils site at Level 4, in relationship to the angle of wind direction

The diagram shows the models of average wind speed V_{avg} with relationship to the height, calculated from raw measurements and corrected data. In this case, the wind shear model does not take into account the roughness of the terrain, the properties of which can be seen in Figure 3.25.

It is worth comparing the wind shear curves obtained as a result of the simultaneous measurements of wind speed at three sites on the shores of the Baltic Sea. It can be seen that the parameters γ and α in Eq. 3.6 of power law function for Sites 1 and 2 have similar values and the curves have similar shape. However, for Site 3, the curve of the wind shear differs in the nature of the slope and has an intersection with the curves for Sites 1, 2, reflecting different wind conditions in northern Latvian coast compare to south-western Latvian coast.

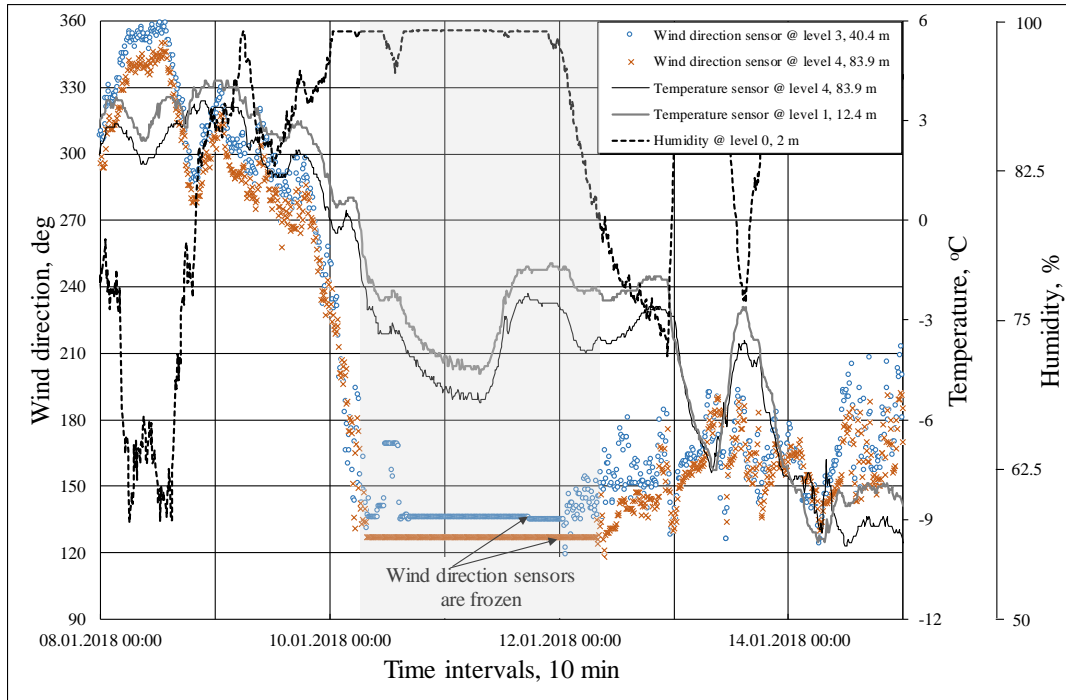


Figure 3.24 A snapshot of temperature, humidity and wind direction measurements on Site 1, Ventspils for a short time period when wind direction sensors were frozen.

Based on the wind speed measurements given in Annex 1 Table A.2, for the measurement period from 01.2018 to 01.2019, were calculated wind shear models for Ventspils, Pāvilsta and Ainaži sites, which are shown in Figure 3.25. In order to extrapolate the measured wind speed values, the power law function is used, which approximates the mean wind speed values with a sufficiently high index of R^2 [114]. Obtained wind speed values are well approximated by the Eq.

$$V_{avg} = V_{avg_H} \left(\frac{h}{H} \right)^\alpha = \frac{V_{avg_H}}{H^\alpha} h^\alpha = \gamma h^\alpha, m/s, \quad (3.6)$$

where V_{avg} – average wind speed at height h , m;

V_{avg_H} - the average wind speed, measured at height H m/s;

H – the height of wind speed measurement, m;

h – the estimation height, m;

γ equal to: 0.638; 0.561 – for Sites 1, 2 and 1.05 – for Site 3; and

α – app. coefficients equal to: 0.524; 0.513; 0.364, corresponding to Sites 1, 2 and 3.

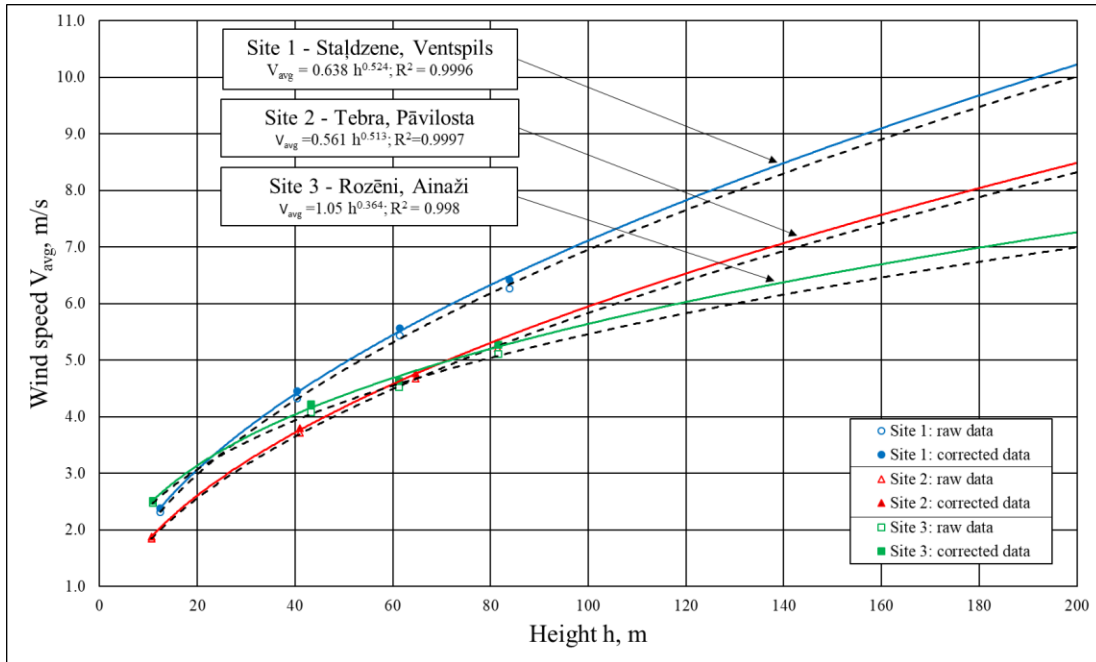


Figure 3.25 Wind shear models for average wind speed V_{avg} for Ventspils, Pāvilosta and Ainaži sites, calculated using raw measurements (dashed lines) and corrected data (solid lines), for the period 01.2018 - 01.2019.

3.4. Conclusions

The study has shown that the implementation of IEC standard [100] for calculating the boom length does not guarantee the accuracy of the wind speed measurement $100 \pm 1\%$ in the shadow area of the mast, whereas in all other directions the boom length is overestimated.

In order to meet the requirements of the standard it is proposed to use two sensors arranged in anti-phase. Furthermore, at the data processing stage, the obtained measurement results should be considered in combination with the wind flow direction. Specifically, in order to obtain mean the wind speed values only the indications from a sensor outside of the shadow area should be used.

The proposed method of measuring wind speed allows significantly lowering the requirements with respect to the boom length that reduces the cost of installing sensors on measurement masts. The performed calculations make it possible to refine the results of other authors' studies indicating that the requirements of IEC standards regarding the length of the boom are overestimated.

Based on the analysis of the contour maps of wind flux interaction with a triangular lattice CCM obtained using CFD modelling it can be concluded that these masts can be used to measure

wind speed with the accuracy that meets the requirements of IEC regulation in case two sensors placed in anti-phase are used for that purpose. Thus, the study provides the basis for a better substantiation of the boom length requirements that would be applicable in a wide range of wind speed conditions.

In order to study the airflow interaction with lattice triangular mast, a method of physical wind speed measurement using several sensors with offset by 120° from each other, at four height levels was used. At each height level two anemometers were mounted, while at the level of 40 m above the ground three anemometers were installed.

The results of the physical studies of long-term wind speed measurements using lattice CCM with height up to 100 m allow estimating the efforts associated with the installation of the metrological sensors and measuring complex Symphonie PLUS3 on the mast. Furthermore, the experiment provides an insight in the magnitude of costs and time necessary for organizing preparatory works in the scope of wind power projects.

In order to make wind speed measurements compliant with the requirements of IEC standard, using typical lattice CCM with side width of 1.2 and 1.4 m and a height up to 100 m, anemometers should be located at a distance of at least 3.2 m from the center of the mast.

At the same time, the analysis of the results of wind speed measurements using two anemometers shows that at a distance of 3.2 m from the mast center, the wind speed in the shadow area of this mast decreases up to 1.5 times and this values should be excluded from calculations.

The use of measurement results from two anemometers, located with offset angle at least 120° , allows identifying the wind speed measurements made in the mast shadow area. Furthermore, the data comparison method provides objective grounds for excluding these values from calculations, thus improving the accuracy of wind speed measurements.

The reliability of the estimations of average wind speed increases after the exclusion of distorted measurements from the calculations. Subject to such correction, the speed values at all heights increased by $\sim 1.9 - 3.9\%$ on average.

The use of stationary CCM for wind speed measurements provides a valid option for significantly reducing the time and material resources required to study the potential of wind energy at the height of up to 100 meters above ground level.

4. The assessment of wind energy potential in Latvia

4.1. Wind energy resource spatial distribution modelling

4.1.1. The landscape of the territory of Latvia

The territory of Latvia does not possess any significant reserves of fossil fuels. Therefore, the needs of the national economy are mainly met through the import of electricity and energy carriers. This creates the dependency of the country's economy on external supplies. Hence, the state is interested in the development of power plants using available national energy resources [114].

The availability of financial support from the European development funds stimulates the construction of power generating stations [115]. This fact also encourages investors to consider the commercial use of alternative renewable energy sources, which are available for use on the industrial scale.

Favourable geographical location of the country on the shore of the Baltic Sea makes its territory open from the western direction for southwestern winds, which are prevailing in this region. The western part of Latvia is dominated by forest-covered plains, while in the eastern part of the country there are hilly areas of up to 300 m high.

Wind flows from the sea possess a significant energy potential, which can be used to produce electricity. Wind speed measurement results performed with 1 min increments provide necessary data for calculating the density of wind energy that a wind current in a given region can carry. Based on this information, an estimate of the average annual power production for the projected WPP can be made [116], [117].

When choosing a construction site for a WPP, it is necessary to take into account the natural specificities of the landscape and estimate the density of wind energy in the given area. In this regard, information on the spatial distribution of the resource of wind energy on the entire territory of the country is of utmost importance for the national economy.

4.1.2. The network of meteorological stations

In Latvia, for more than 100 years, there has been a network of meteorological observation stations that perform the collection and archiving of high quality representative

meteorological data. In accordance with international requirements, the stations use only calibrated sensors and certified equipment for the measurements. The monitoring of climate and weather conditions is carried out at 22 stations, shown in Figure 4.1. A majority of the stations are currently operating in an automated mode.



Figure 4.1 Map of Latvia with the locations of 22 meteorological stations and the mean elevation above sea level (*m*) with a 1x1 *km* resolution.

The stations continuously measure and record the speed and direction of wind, measure atmospheric pressure, humidity and air temperature, as well as other meteorological parameters. In order to measure wind speed over the considered time period, 10 stations were equipped with Vaisala WAA 151 anemometers, while 8 stations had Vaisala WMT 702 ultrasonic wind sensors and at 4 stations anemometers were replaced by ultrasonic sensors.

In order to calculate the average wind speed with 1 min increments, an anemometer measures the actual wind speed every 2 s, while the ultrasonic sensor – every 3 s. All wind speed sensors are installed at the height of 10 m, except for Riga (36 m), Kolka (20 m) and Pāvilosta (since December 2015 – 18 m) meteorological observation stations. Prior to the analysis, outliers were removed from the dataset.

There is a number of publications devoted to the issue of estimating the magnitude of wind energy resource potential and its distribution on the territory of Latvia [118]–[121]. However, the reliability of these studies is not high, as they are based on the analysis of

accessible public wind speed data, which is designed to study climate change. The correct estimates can be done only based on the analysis of the results of wind speed measurements performed simultaneously and at the same height above the ground in different regions of the country for a period of at least one year.

This research is based on data obtained using certified measuring sensors installed at meteorological observation stations belonging to LEGMC. The results of physical measurements are recorded as discrete values of wind speed with 1 min increments from 22 observation stations at 10 m height above the ground, over a period from 01.01.2015 to 31.12.2016.

The presentation of the results of physical measurements in the form of a model of the spatial distribution of wind speed allows to consider, as an alternative, other methods related to wind speed prediction. For instance, already exist other models of the spatial distribution of wind speed at the heights of 10, 54, 100 and 136 m, developed by using climatological reanalysis datasets ERA5 from 2015 to 2016 for the Latvian territory [122].

4.1.3. Wind types in the territory of Latvia

The study of wind properties is typically based on the analysis of wind speed measurement results obtained over a long period of time [108]. As a part of the analysis, measurement results are grouped into bins, which correspond to the selected speed intervals with a certain step. For each bin, the total recurrence time of this rate is determined and expressed as a percentage of the total measurement time.

On Figure 4.2 frequency distribution functions for wind speed measurement results obtained at meteorological observation stations in Ainaži, Daugavpils, Priekule, Saldus and Ventspils areas during the measurement period from 01.01.2015 to 31.12.2016 are presented.

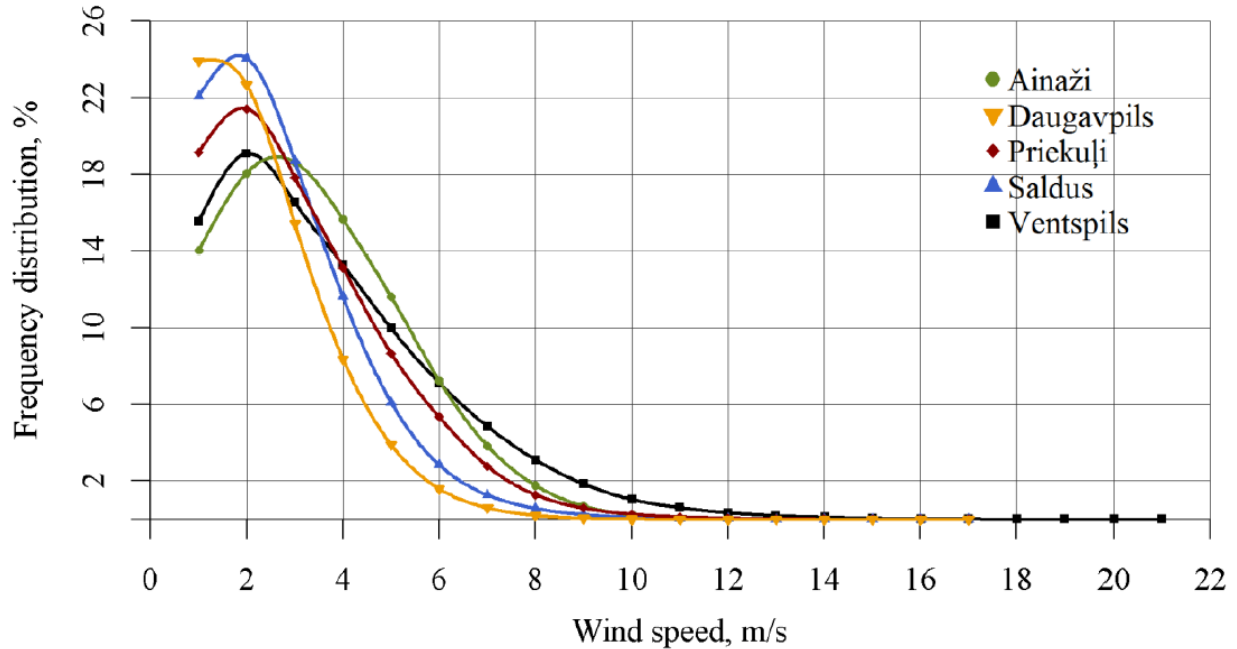


Figure 4.2 Frequency distribution functions of average wind speed V_{avg} over the period of observations from 01.01.2015 to 31.12.2016 for five meteorological observation stations at a height of 10 m above the ground.

The points on the curves of the frequency distribution of wind speed correspond to the discrete values of wind speed V_{avg} representing bins with the interval of 1 m/s. The figure shows that the type of wind considerably varies depending on the area in the country.

For the analysis of wind speed distribution the most often used approximation is Weibull probability density function. This function is considered to be a good approximation of the wind speed frequency distribution and is described by the following equation:

$$F(V) = \frac{k}{c} \left(\frac{V}{c}\right)^{k-1} \exp\left[-\left(\frac{V}{c}\right)^k\right] \quad \text{for } V > 0, \quad (4.1)$$

where c – is scale factor;

k – is shape factor; and

V – is wind speed, m/s.

Parameters c and k of the Weibull wind speed frequency distribution functions [109] for 22 stations were estimated using the maximum likelihood method. The maximum likelihood estimator was derived by maximizing the likelihood function [102] and was estimated using functions from the R package MASS [123].

Once the distribution parameters are estimated, it is necessary to perform a goodness of fit test, which checks the conformity between observations and the theoretically fit distribution. This is done by applying the Kolmogorov-Smirnov test, which measures the maximum distance between the empirical and the fitted distribution functions.

The hypothesis that the two distributions are equal is rejected if the distance exceeds a certain critical value [124]. Following the estimation of the parameters of the fitted distribution, it is necessary to assess critical values by applying the bootstrap procedure [125]. Hypothesis was not rejected for any of the stations at 5% significance level, thus confirming the applicability of the Weibull distribution for the average wind speed data.

The way properties of the wind flow differ across various regions of the country can be represented in the form of a spatial distribution map of Weibull distribution function parameters, as are shown in [126]. The Weibull distribution parameter values depend on regional topography and site proximity to the Baltic Sea and the Gulf of Riga.

4.1.4. The model of wind speed spatial distribution

The uniform distribution of observation stations on the territory of the country and a long measurement period allow us to present the results as a visual model in Figure 4.3. The colour palette used in the model allows identifying areas in the territory of Latvia with the same level of wind speed. In this case, the spatial distribution of the average value of the wind speed V_{avg} is depicted in steps of 0.5 m/s. The value of the average wind speed for the measurement period at the measurement points was calculated as follows:

$$V_{avg} = \frac{1}{n} \sum_{i=1}^n V_i, \quad (4.2)$$

where V_i – is the average wind speed with 1 min increments, m/s;

n – is the number of measurements for the observation period from 01.01.2015 to 31.12.2016; and

i – is observation 1, 2, 3, ..., n ;

In order to estimate the value of the meteorological parameter between the observation stations, a spatial interpolation of measured data was used and a geostatistical method – universal kriging – was applied [127], [128].

Apart from the observed values from the nearest stations, this method also uses additional spatial factors that influence meteorological parameters. The most relevant factors for average wind speed interpolation are geographical coordinates in metric system LKS-92, elevation above the sea level and distance from the Baltic Sea or the Gulf of Riga. Spatial interpolation is performed on a grid with a resolution of 1x1 km.

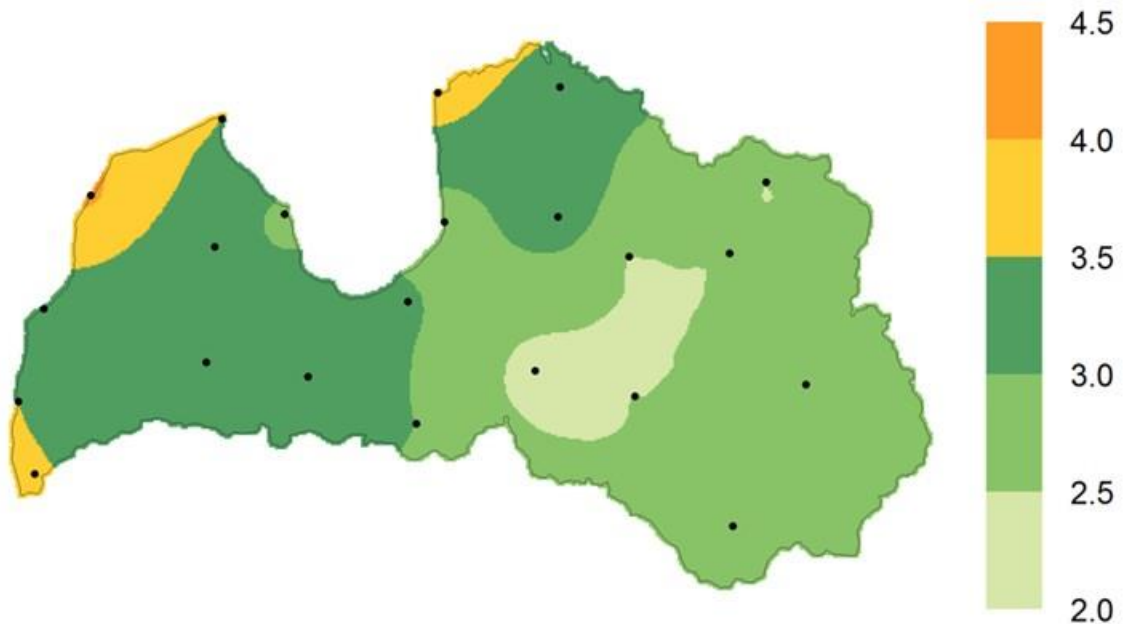


Figure 4.3 Model of the spatial distribution of average values of wind speed V_{avg} m/s at an altitude of 10 m above the ground on the territory of Latvia.

Modern weather modelling techniques allow predicting the magnitude of wind speed above the surface of land and sea. For example, climatological reanalysis dataset ERA5, created by the European Centre for Medium-Range Weather Forecasts (ECMWF), provides information for a variety of meteorological parameters. ERA5 covers the Earth with a 31 km grid and stratifies the atmosphere into 137 levels from the surface up to the height of 80 km. The first 7-year segment of the ERA5 dataset is now available for public use [129].

The information available to users allows obtaining the average wind speed with 2 h increments for any point on the surface of the Earth. The models of spatial distribution of wind speeds in the territory of Latvia for the heights of 10, 54 m and 100, 136 m, respectively, which are estimated using the ERA5 dataset over a time period from 01.01.2015 to 31.12.2016 are presented in Figure 4.4 and Figure 4.5.

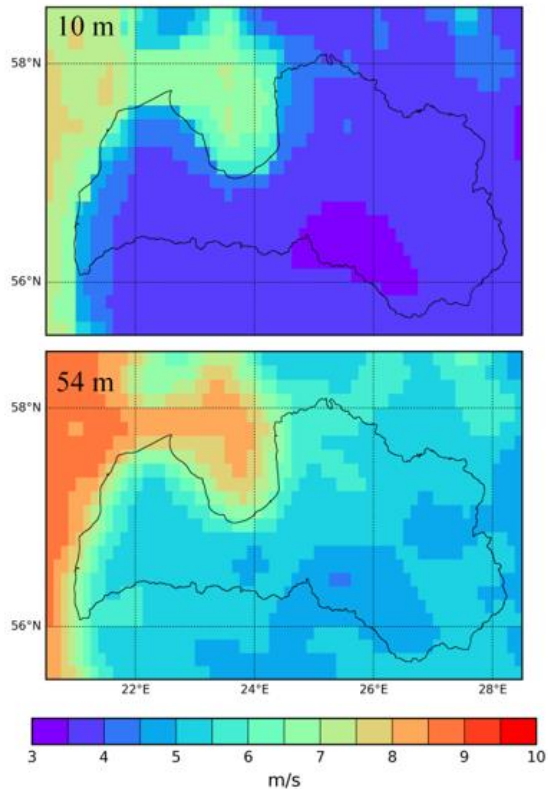


Figure 4.4 Models of spatial distribution of average wind speed at the heights for 10 m and 54 m, estimated using ERA5.

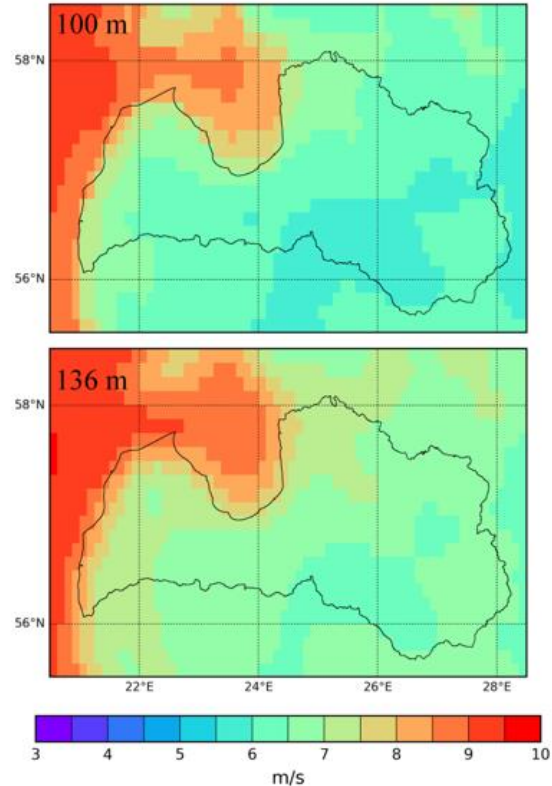


Figure 4.5 Models of spatial distribution of average wind speed at the heights for 100 m and 136 m, estimated using ERA5.

The use of these models does not guarantee high accuracy and resolution, in contrast to physical measurements obtained at the observation stations, but it shows how the boundaries of the wind speed distribution regions change with an increasing altitude. The models also allow identifying the presence of areas that have relatively low and high potentials for wind energy. Specifically, wind speed on the coast of the Baltic Sea in the western part of the country is much higher than in the east, while the lowest values of wind speed are observed in the central part of the country.

The results of wind speed measurements at meteorological observation stations in the area of Ainaži, Daugavpils, Priekule, Saldus and Ventspils and ERA5 simulations are given in Table 4.1. Comparative analysis of these data shows that the results of ERA5 simulation consistently exceed the measured historical values in all regions by ~ (20–50)%. It is likely that ERA5 modelling results are strongly influenced by the structure of the terrain.

Table 4.1

Average Wind Speed V_{avg} , $V_{avg.cub}$. m/s and Wind Energy Density in Relative Units P'_{avg} Obtained as a Result of Physical Measurements at Selected Meteorological Observation Stations and Based on Estimations Using ERA5 Dataset

Station	Results of measurements			Results of ERA5 modelling			
	$V_{avg 10m}$, m/s	$V_{avg.cub 10m}$, m/s	$P'_{avg 10m}$	$V_{avg 10m}$, m/s	$V_{avg 54m}$, m/s	$V_{avg 100m}$, m/s	$V_{avg 136m}$, m/s
Ventspils	4.1	5.4	1.00	6	7.4	8.1	8.5
Ainaži	3.8	4.7	0.66	4.7	6.7	7.2	7.9
Priekule	3.4	4.5	0.58	3.9	5.5	6.5	7.1
Saldus	3.0	3.9	0.38	3.8	5.3	6.4	6.9
Daugavpils	2.5	3.3	0.23	3.6	4.9	5.9	6.4

However, modelling results presented in the form of contour maps can serve as a basis for estimating and comparing the intensity of wind speed in the central part of the country and on the shores of the Baltic Sea. That makes them useful at the planning stage of energy projects – in the process of selecting the most suitable sites for WPP construction and predicting the distribution of wind energy potential on the territory of Latvia.

In order to estimate the reliability of ERA5 simulation, the values of wind speed at the heights of 54, 100 and 136 m can be crosschecked with the results of physical measurements at the heights of up to 200 m above the ground in the time period from 01.03.2014 to 01.03.2015 obtained using laser measuring complex Pentalum SpiDAR [108]. Historical wind speed measurements used for the comparison were carried out in the coastal zone of Latvia, in Ventspils region.

The performed comparison shows that the deviation of the results of physical wind speed measurements at the altitudes of 54, 100 and 136 m from the estimates of the average wind speed values obtained using ERA5 technology does not exceed 20 %. As the altitude above the ground level increases, the turbulence of airflows decreases; therefore, the use of simulation technology gives higher accuracy in determining wind speed.

An important observation with respect to the models of spatial distribution of wind speed at the heights of 54, 100 and 136 m is the continuous evolution of the boundary pattern, which determines the transition of the velocity levels. This indicates the preservation of the regularity of the change in the magnitude of the wind speed with increasing altitude.

4.2. Wind energy assessment methods

4.2.1. Long-term wind speed measurements and wind shear assessment

Most of the Latvian territory can be characterised as a plain field covered by forests with up to 10–15 m high trees. Therefore, the impact of the terrain on the wind flows is clearly noticeable only up to 30 m, and the wind shear tends to have similar properties across the entire territory. Consequently, these areas are suitable for the construction of wind farms and individual wind WTs.

However, prior to the construction of WPP it is necessary to evaluate the efficiency of WTs with different rated power curves and at different possible heights of the rotor hubs. In order to perform the evaluation it is necessary to analyse wind energy streams using the results of wind speed measurements and the models of wind energy density distribution depending on the altitude.

In Latvia, systematic long-term measurements of the wind speed that also take into account its height distribution are being carried out since 2007 at two sites on the north-western shore of the Baltic Sea in Ventspils region and on the north of the country in Matiši village, near the Burtnieku lake (35 km from the seashore) [130], [131].

At the Matiši site, the on-site measurements of wind speed were carried out using certified sensors for wind speed and sensors indicating the direction of air streams. In order to collect the wind data, measurement sensors were mounted at several levels on a 60 m high metallic mast [133].

The charts of monthly fluctuations of the average wind speed V_{avg} , m/s, for heights 20, 40, and 60 m at the Matiši site are presented in Figure 4.6. Average monthly wind speed is calculated by averaging the measured 10-min wind speed values V for the time interval T from 04.2009 to 04.2013. The time series of average daily wind speed values, $V_{avg,d}$, are shown in Figure 4.7 for the height of 60 m above the ground.

The continuous recording of wind speed values with 10-min intervals made it possible to construct wind speed frequency distribution curves $F(V)$ with high precision [130]. The curves plotted in Figure 4.8 are constructed based on the measured values of wind speed V in the time period of 04.2009 - 04.2013. Having the real frequency distribution of wind speed shown in this figure, it is possible to proceed with the model of Weibull's probability density function $F(V)$ using the parameters k (shape factor) and c (scale factor). Figure 4.9 displays similar curves of Weibull's probability density function $F(V)$ constructed by the classical method [109] for the same time span.

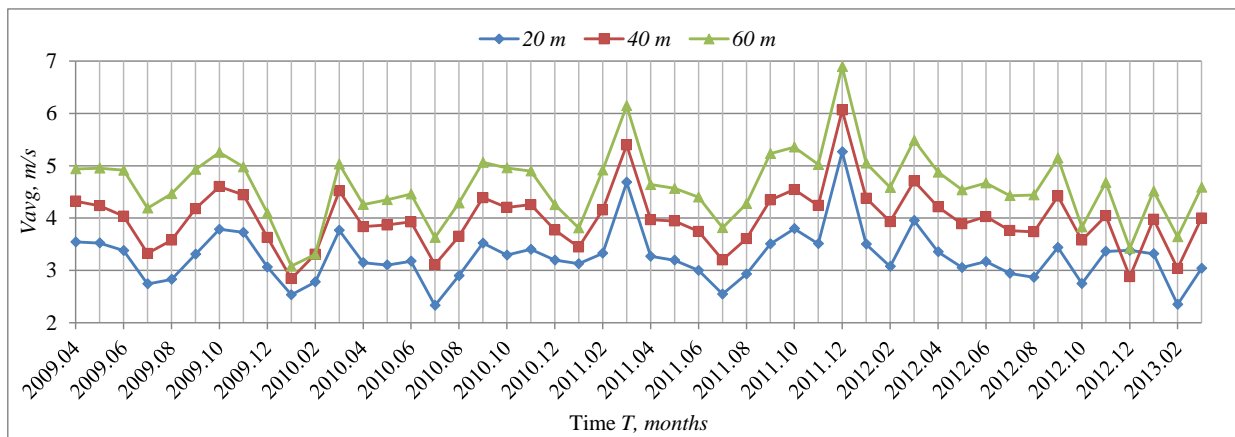


Figure 4.6 Monthly fluctuations of the average wind speed V_{avg} , m/s for the heights of 20, 40 and 60 m above ground in the measurement time interval T from 04.2009 to 02.2013.

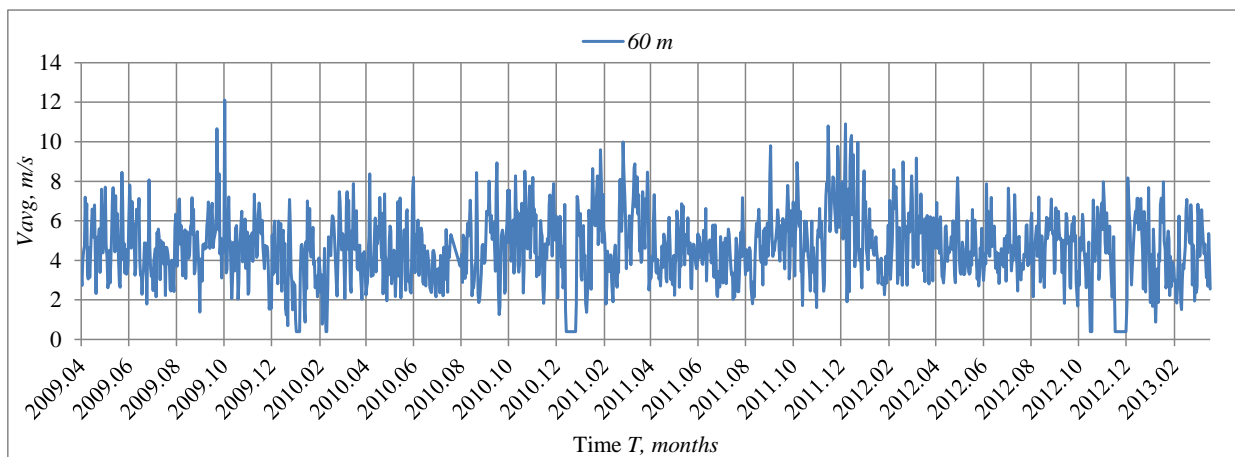


Figure 4.7 Daily fluctuations of the average wind speed $V_{avg,d}$ (m/s) for the height of 60 m above ground in the measurement time interval T from 04.2009 to 02.2013.

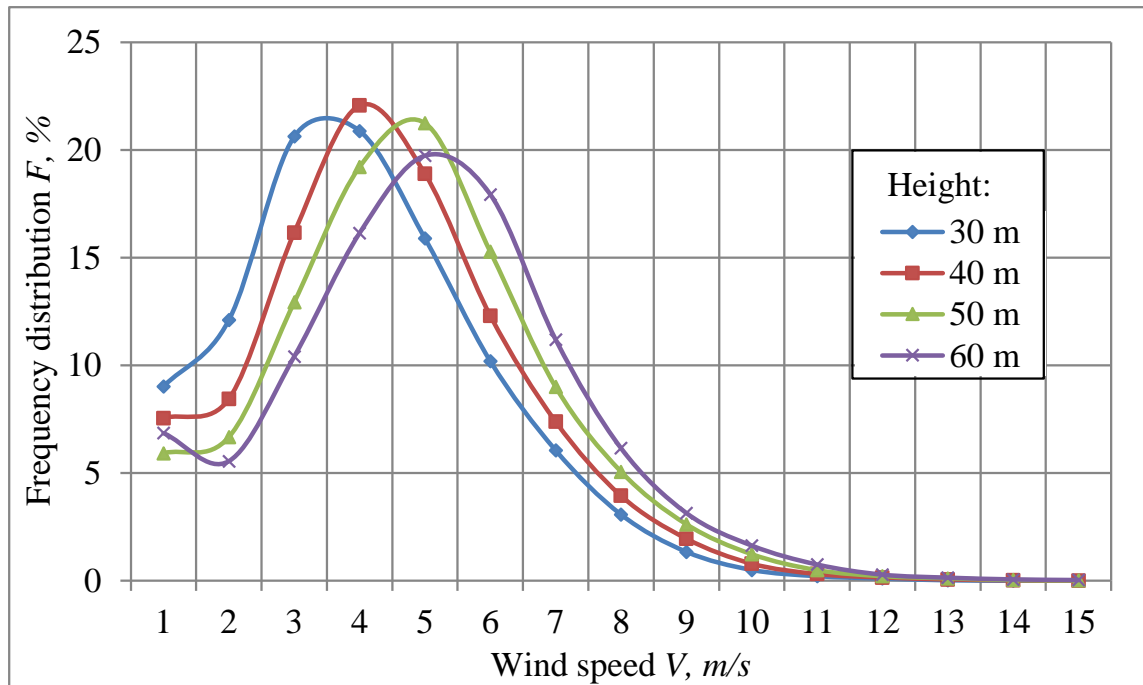


Figure 4.8 Wind speed frequency distribution curves, $F(V)$, for the period 04.2009 - 04.2013.

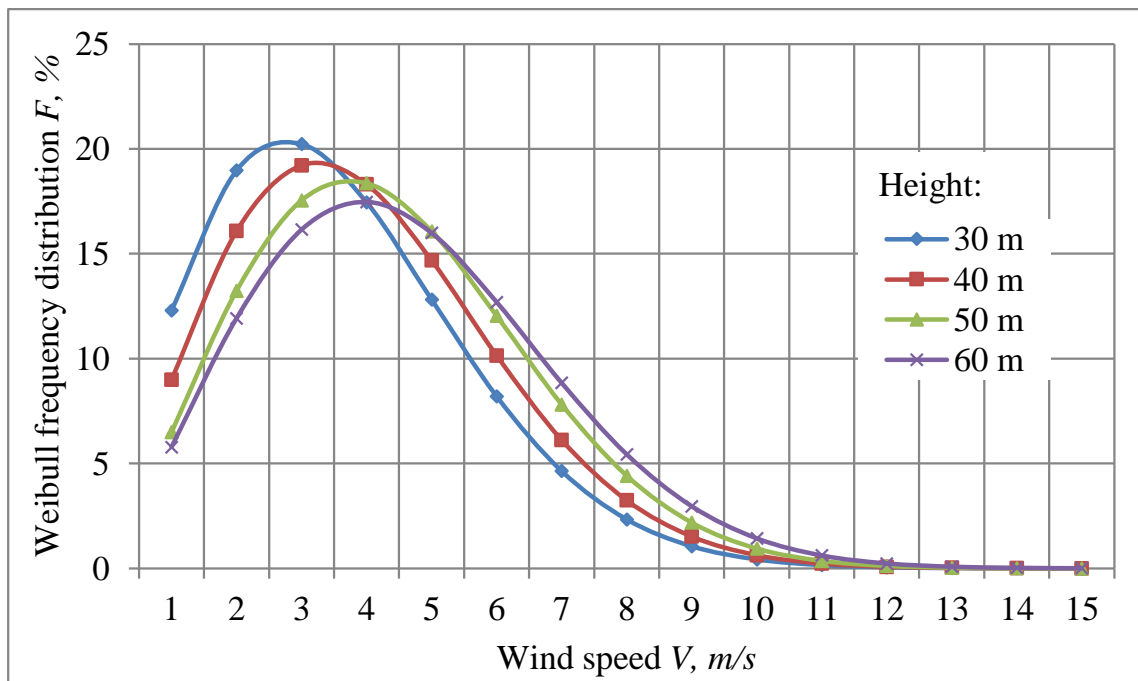


Figure 4.9 Weibull probability density function curves, $F(V)$, for the period 04.2009 - 04.2013.

The measured values of average wind speed, V_{avg} , and their standard deviations, SD, for heights 10, 20, 30, 40, 50 and 60 m presented Table 4.2. Based on these data, the values of parameters k and c corresponding to these heights were calculated.

Table 4.2

Average wind speed at the Matiši site for the measurement heights 10, 20, 30, 40, 50, 60 m and parameters k and c of Weibull's distribution

Period of measurements	Height above the ground, m	$V_{avg}, m/s$	SD	Weibull coefficients	
				k	c
04.2009 - 04.2013	10	2.72	0.70	1.63	3.05
	20	3.28	0.70	1.85	3.70
	30	3.63	0.74	2.01	4.10
	40	4.02	0.72	2.19	4.54
	50	4.38	0.73	2.31	4.94
	60	4.65	0.73	2.34	5.25

4.2.2. Weibull distribution parameters' approximation

The distribution of Weibull parameters (k – shape factor and c – scale factor) as a function of height (see Figure 4.10) is well approximated by the power law curves [108]. The expressions for c and k based on the wind speed measurement results at the Matiši site using power law approximation are as follows:

$$c = c_H \left(\frac{h}{H}\right)^{\alpha_c}, \quad (4.3)$$

$$k = k_H \left(\frac{h}{H}\right)^{\alpha_k}, \quad (4.4)$$

where c_H, k_H are the values of the Weibull's distribution coefficients calculated for the reference height H ;

h is the rotor hub height, m; and

α_c, α_k are the values of approximation coefficients.

The modelling of c and k parameters of Weibull distribution as a function of height h using Eq. (4.5) and (4.6) allows the extrapolation of their values to the heights up to 150 m, where the mentioned relationship is expected to hold. The results of wind speed measurements from Table 4.2 allow to calibrate parameters c and k in expressions Eq. (4.3) and (4.4) for the Matiši site:

$$c = c_H \cdot \left(\frac{h}{H}\right)^{0.359} = \frac{c_r}{H^{0.359}} \cdot h^{0.359} = 1.205 \cdot h^{0.359}, \quad (4.5)$$

$$k = k_H \cdot \left(\frac{h}{H}\right)^{0.226} = \frac{k_r}{H^{0.226}} \cdot h^{0.226} = 0.937 \cdot h^{0.226}. \quad (4.6)$$

Measurements at 10 and 20 m heights are significantly affected by the landscape and were not included in the models; therefore, these models were constructed using wind speed data from 30 to 60 m.

From c and k parameter values calculated based on the results of physical measurements at the heights where sensors can be placed, it is possible to proceed to the model of Weibull's distribution of the wind speed. The extrapolation curves allow calculating wind energy at the heights exceeding those of the sensors fixed on the mast. In Figure 4.10 coefficients c and k up to the height of 150 m obtained using power law approximation are presented.

As it is shown in a related study [89] and in Figure 4.10, at the heights above 50 m the character of approximating curve Eq. (4.6) does not coincide with the measured k - factor values. Therefore, for the calculation of wind speed frequency distributions by Weibull method, the value of k coefficient for heights above 50 m can be considered constant and independent of height. In the diagram, this section of curve is shown by a dotted line.

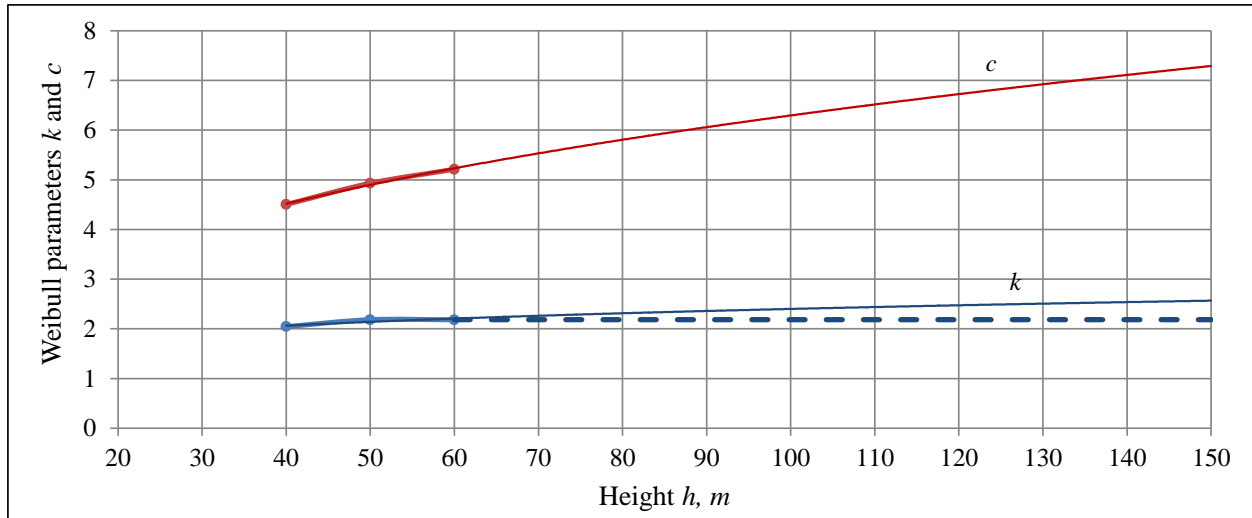


Figure 4.10 Weibull parameters k (shape factor) and c (scale factor) for the measurement heights of 40, 50 and 60 m (points) and their extrapolations up to 150 m using power law. Dashed blue line is the assumed constant parameter k above 60 m height.

According to such methodology – that is by calculations using the models considered above – the necessary information on the wind speed frequency distribution can be obtained for the heights of rotor hubs corresponding to the types of WTs chosen for the research. This would enable the calculation of the AEP by generators, making it possible to estimate the efficiency of WT.

4.3. Wind energy potential assessment models

4.3.1. Modelling of the spatial distribution of Weibull parameters

The scale parameter values (see Figure 4.11), which stretch or shrink the distribution, are decreasing with the distance from the sea, indicating that coastal stations have wider probability density functions. The spatial distribution of the shape parameter values (see Figure 4.12) is influenced by topography as the lowest values are observed in the highlands. Overall, the shape parameter values vary from 1.6 to 2.1, indicating that the density function has a positively skewed bell shape.

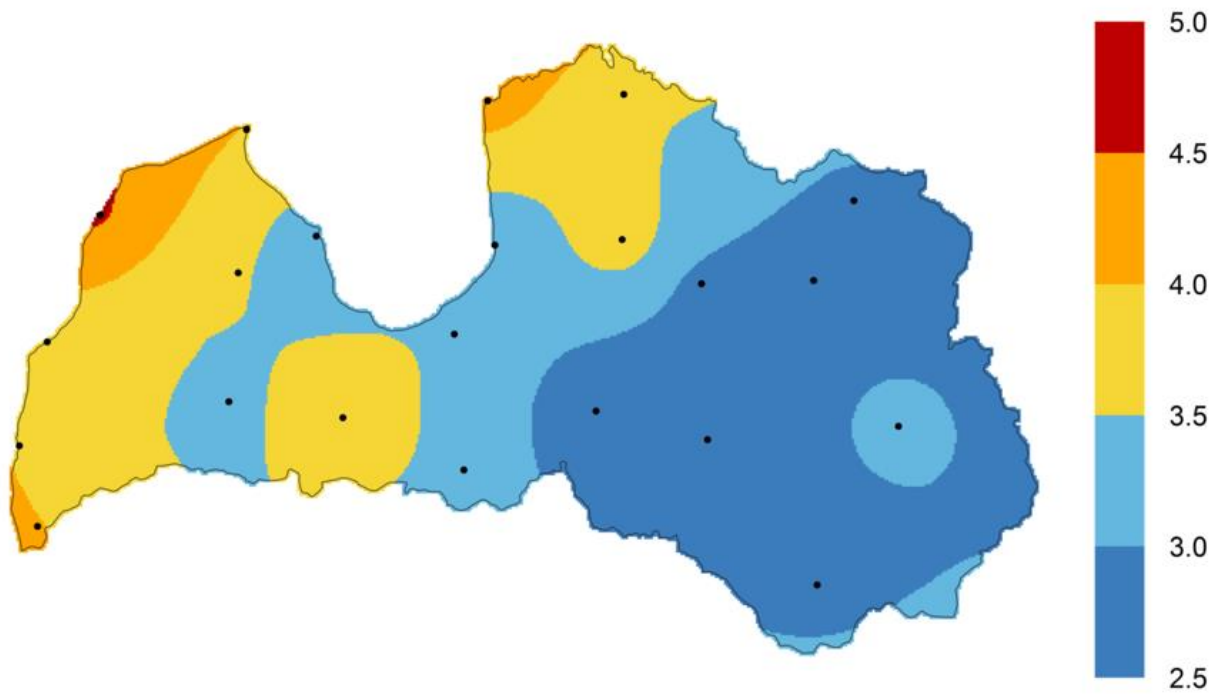


Figure 4.11 Model of the spatial distribution of the scale parameter c of Weibull wind speed probability density at the height of 10 m above the ground.

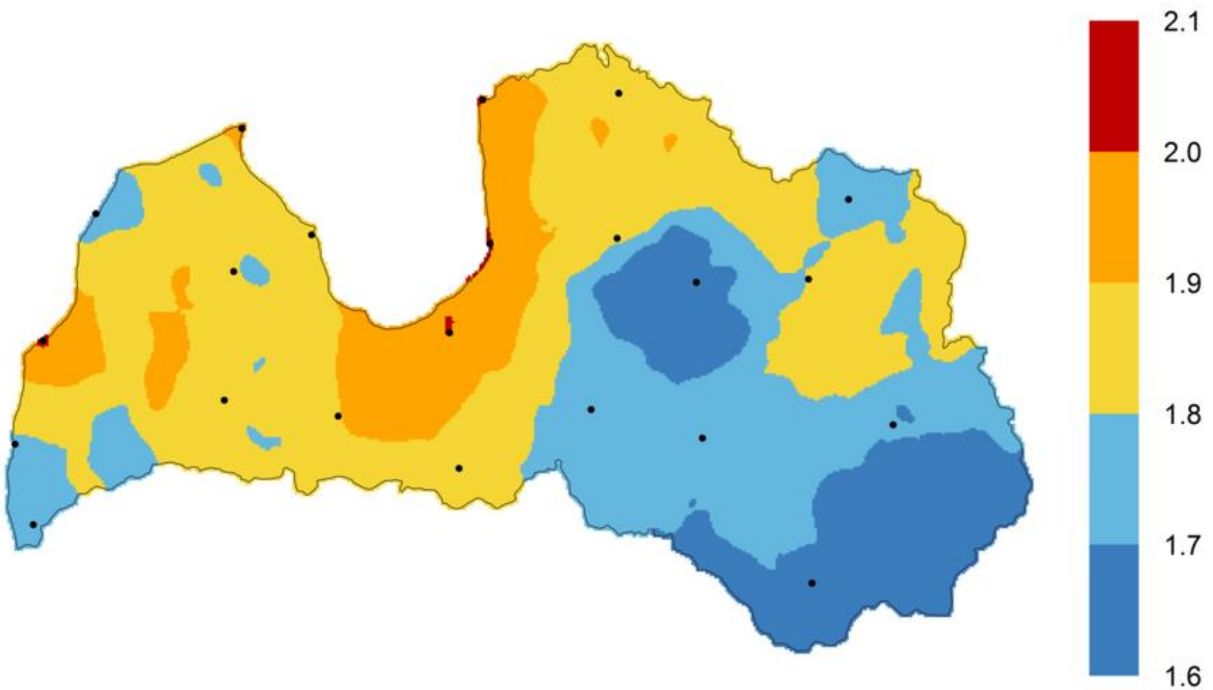


Figure 4.12 Model of the spatial distribution of the shape parameter k of Weibull wind speed probability density at the height of 10 m above the ground.

The estimates of parameters c and k presented in the form of contour maps allows estimating the frequency characteristics of the wind speed distribution for any point on the territory of Latvia at the height of 10 m above the ground using Eq. (4.1). This greatly simplifies the assessment of the amount of wind energy that can be produced when choosing the location for a small wind turbine generator (SWTG) installation.

4.3.2. The spatial distribution of wind energy resource

Due to the cyclical nature of the wind and nonlinear relationship between wind speed and energy it carries, it is not possible to perform an assessment of the wind energy potential based on Eq. (4.2). In order to perform a more accurate assessment, it is necessary to take into account the frequency distribution function from Eq. (4.1). In this case, the value of the average energy density that the airflow carries over an area of 1 m^2 is calculated from [108]:

$$P_{avg} = \frac{1}{2} \rho V_{avg.cub}^3, \quad (4.7)$$

where ρ – is air density (1.23 kg/m^3 for standard condition at the sea level and temperature 15°C);

$V_{avg.cub}$ – is average cubic wind speed, m/s.

Average cubic wind speed can be calculated either based on actual wind speed measurements according to Eq. (4.8) or using the frequency of wind speed occurrence obtained in accordance with Weibull distribution function following Eq. (4.9).

$$V_{avg.cub} = \sqrt[3]{\frac{1}{n} \sum_{i=1}^n V_i^3}, \quad (4.8)$$

where V_i – is average wind speed for 1 min measurement interval, m/s;

n – is the number of measurements for the entire measurement period; and

i – is the number of a measurement interval 1, 2, 3 ... n .

$$V_{avg.cub} = \sqrt[3]{\frac{1}{100} \sum_{i=1}^n V_i^3 F(V_i)}, \quad (4.9)$$

where V_i – is wind speed in bin i , m/s;

$F(V_i)$ – is Weibull cumulative distribution function for wind speed V_i , %; and

i – is the number of bins with 1 m/s interval, 1, 2, 3 ... n .

As can be seen from Eq. (4.7) the amount of energy that the wind carries is proportional to the value of the average cubic wind speed Eqs. (4.8) and (4.9). At the same time, the division of the territory of Latvia into five regions according to the level of the average cubic wind speed makes it possible to make an estimate of the resource of wind energy that these regions have.

Assuming that the maximum value of the average energy density, which the wind carries on the shore of the Baltic Sea, is taken as 1.0, then the values of the average energy density in relative units for each station will be determined by Eq. (4.10):

$$P^*_{avg.i} = \frac{V_{avg.cub.i}^3}{V_{avg.cub.max}^3}, \quad (4.10)$$

where $V_{avg.cub.max}$ – is average cubic wind speed at Ventspils station;

$V_{avg.cub.i}$ – is average cubic velocity at each of the 22 stations; and

i – is observation station 1, 2, 3 ... 22.

By interpolating the obtained values, it is possible to create a map of the spatial distribution of the average density of wind energy $P^*_{avg.i}$ on the territory of Latvia in relative units, which is shown in Figure 4.13.

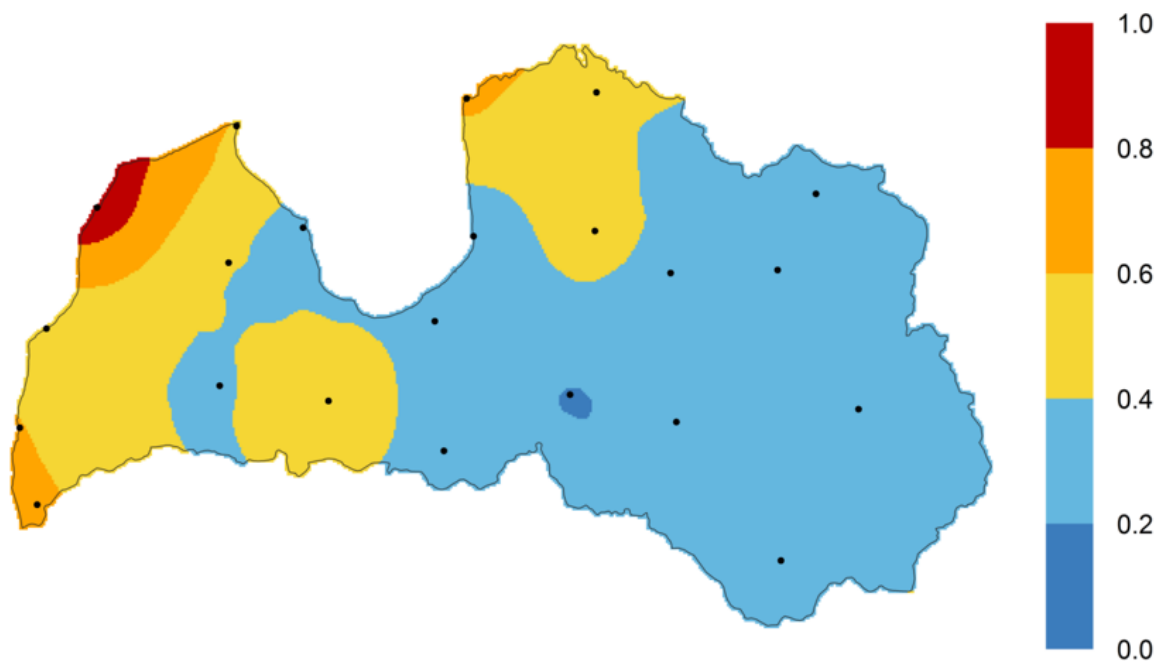


Figure 4.13 Model of the spatial distribution of the average wind energy density in relative units P^*_{avg} at the height of 10 m above the ground in the territory of Latvia.

The values obtained using Eqs. (4.2), (4.7), and (4.10) and the values of the parameters of the Weibull wind speed frequency distribution function, calculated on the basis of measurements at the meteorological observation station in Ainaži, Daugavpils, Priekule, Saldus and Ventspils for the measurement period from 01.01.2015 to 31.12.2016 are given in Table 4.3.

Table 4.3

The values of parameters c and k of the Weibull wind speed frequency distribution function, average wind speed V_{avg} , $V_{avg.cub.}$ and wind energy density in relative units $P^*_{avg.i}$ for selected meteorological observation stations

Stations	Measurement results				
	c	k	V_{avg}	$V_{avg.cub.}$	$P^*_{avg.i}$
Ainaži	4.3	2.0	3.8	4.7	0.66
Daugavpils	2.8	1.6	2.5	3.3	0.23
Priekule	3.9	1.8	3.4	4.5	0.58
Saldus	3.4	1.8	3.0	3.9	0.38
Ventspils	4.6	1.7	4.1	5.4	1.00

4.4. Forecasting the efficiency of SWTG

4.4.1. Types and power curves of the SWTG

The study presents the results of the analysis of the efficiency of using low-power wind generators. A distinctive feature of these generators is that they are designed to transform the energy that wind carries at an altitude of 10 - 25 m above the ground. In most cases, SWTGs are used to power an autonomous load or serve as a backup power source in a private farm, the operation of which does not depend on the power grid.

Forecasting the efficiency of work and determining the AEP of the SWTG can be done only on the basis of long-term measurements of wind speed. However, the need to perform these measurements and calculate the AEP creates a problem for small households.

The author proposes to use historical records of long-term measurements of wind speeds that are available in the archives of the National Meteorological Observation Service for forecasting the efficiency of low-power wind generators. The study of the SWTG performance was carried out using the power curves of two types of SWTG: Horizontal Axis WTs (HAWT) with rated power 0.75, 2.5, 5.0, 20.0 kW and Vertical Axis WTs (VAWT) 0.75, 2.5, 6.0 kW. The two types of generators are shown in Figure 4.14 and Figure 4.15 respectively.

The main technical and design characteristics of the SWTG wind power converters are summarized in Table 4.4. The information provided in the summary table is in line with the models presented in the Catalogue of European Urban Wind Turbine Manufacturers [133].

The efficiency of a wind converter depends on the aerodynamic properties of the wind turbine and the wind type prevailing in the region. Therefore, it is of interest to evaluate the advantages of using both convector types in the specific conditions of the Latvian landscape. For comparison, Figure 4.16 shows the power curves of HAWT 0.75, 2.5 kW and VAWT 0.75, 2.5 kW.

From the analysis of the power curves, it follows that a distinctive feature of a wind turbine with a vertical axis of rotation is a low starting torque that is associated with the starting turbine rotation speed of more than 3 m/s. At the same time, as it can be seen from Table 4.4 and Figure 4.16, the rated wind speed for VAWT type converters reaches 14 m/s, while for HAWT the rated speed is 11–12.5 m/s. That means that the operating range of the considered VAWT type generators is between 3 and 14 m/s while for HAWT type converters it is between 2 and 11–12.5 m/s.



Figure 4.14 Horizontal Axis Wind Turbine 0.75 kW.



Figure 4.15 Vertical Axis Wind Turbine Darrieus H-type 0.75 kW.

Table 4.4

Technical characteristics of HAWT and VAWT Darrieus H-type SWTG with rated power 0.75, 2.5, 5.0, 20.0 kW and 0.75, 2.5, 6.0 kW

Turbine type	Rated power, kW	Rotor height, m	Rotor diameter, m	Rated wind speed, m/s
VAWT	0.75	1.50	1.50	14.0
	2.50	2.88	1.99	14.0
	6.0	5.00	3.30	14.0
HAWT	0.75	-	2.40	12.0
	2.50		5.00	11.0
	5.0		5.40	11.0
	20.0		8.00	12.5

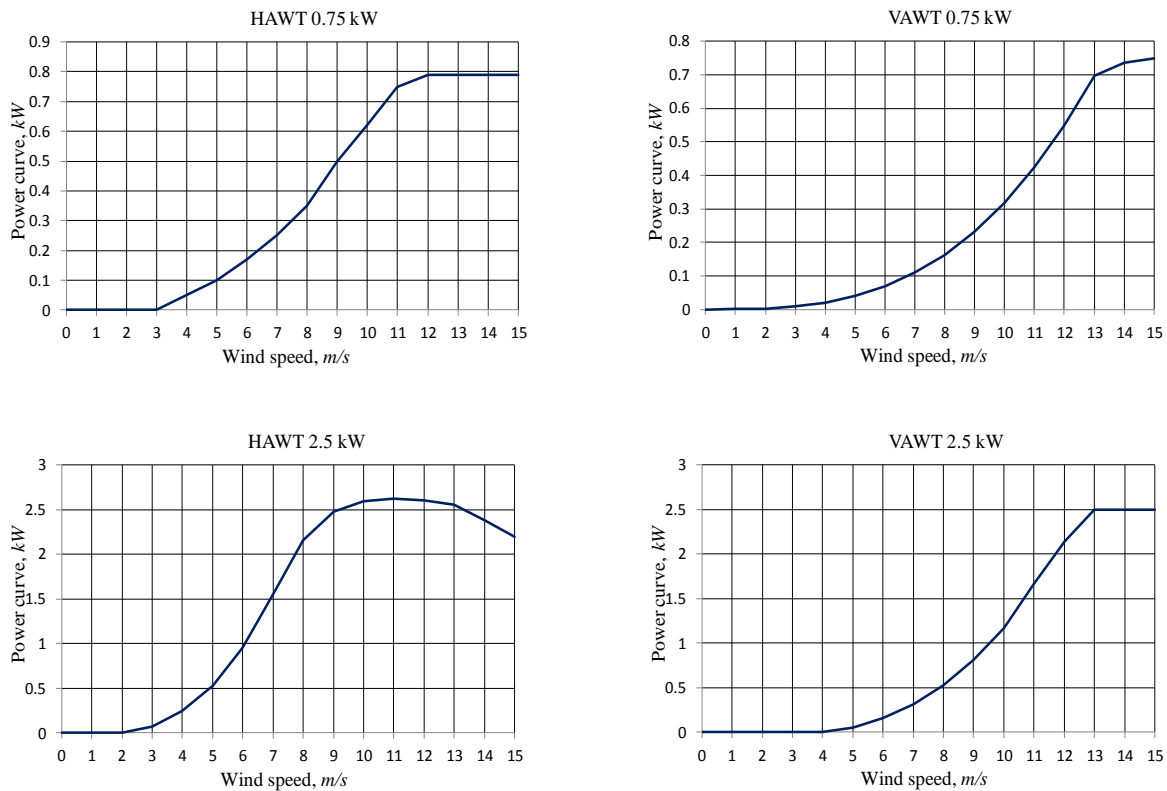


Figure 4.16 Power curves $P(V)$ of HAWT 0.75, 2.5 kW and VAWT 0.75, 2.5 kW Darrieus H-type.

4.4.2. The modelling of power production of HAWT and VAWT

The amount of power produced by a converter in a certain period is determined by the following relationship [109]:

$$W(V) = \sum_{i=1}^n (P(V_i) \cdot F(V_i)), \quad (4.11)$$

where V_i – generator power curve value for wind speed V_i ; and

$F(V_i)$ – Weibull frequency distribution function value for wind speeds V_i .

Weibull wind speed frequency distribution function $F(V)$, corresponding to the wind type observed in Ventspils region is presented in Figure 4.17 along with the power curve $P(V)$ for HAWT 2.5 kW. In Figure 4.17, the area represented by Eq. (4.11) corresponds to the AEP of HAWT 2.5 kW in Ventspils region and equals to $W = 4.6 \text{ MWh}$. Functions $P(V)$ and $F(V)$ were used in the form of discrete bins with 1.0 m/s step length. Wind speed for the i -th step is determined from the expression:

$$V_i = \Delta V \cdot i, \quad (4.12)$$

where: ΔV – bin size 1 m/s; and

$i = 1, 2 \dots n$.

The efficiency of wind converters is characterized by the capacity factor C_e , which is defined as a ratio of the estimated value of W to the potential value of the energy produced by the generator W_r , assuming that it operates at the rated capacity during the entire consider period. Thus, in order to calculate the value of the capacity factor, the following expression is used:

$$C_e = \frac{W}{W_r} 100 (\%). \quad (4.13)$$

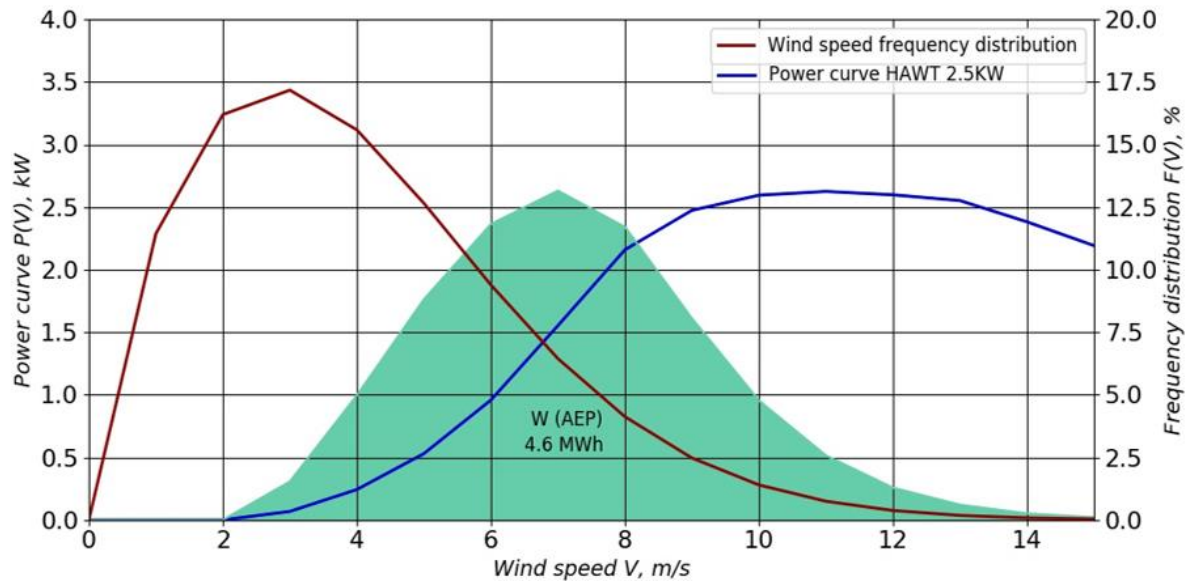


Figure 4.17 Weibull wind speed frequency distribution function $F(V)$, the power curve $P(V)$ for HAWT 2.5 kW and the value of AEP $W = 4.6 \text{ MWh}$, corresponding to wind type at Ventspils meteorological observation station.

The results of the SWTG operational efficiency forecasts, depending on the type of wind turbine, rated generator power and the location of its installation for selected meteorological observation stations: Ainaži, Daugavpils, Priekuļi, Saldus and Ventspils are summarized in Table 4.5.

The summary of the estimates of capacity factor C_e for wind converters of HAWT and VAWT type in Ventspils region are presented in Figure 4.18. The comparison shows that regardless of the type, the efficiency of the wind turbine operation decreases with increasing converter rated power.

The results of the study suggest that the SWTG wind power converters of HAWT type, mounted on a mast with the height of at least 10 m above the ground, are more suitable for operating in the conditions of Latvia compared to VAWT type generators.

Moreover, it is expected that among the wind energy converters of HAWT type considered in the study, generator with the rated power of 2.5 kW will tend to operate with the highest efficiency.

Table 4.5

Capacity factor C_e , for HAWT and VAWT type of the SWTG with rated power 0.75, 2.5, 5.0, 20.0 kW and 0.75, 2.5, 6.0 kW at selected meteorological observation stations

Stations	Capacity factor C_e , %						
	HAWT				VAWT		
	0.75 kW	2.5 kW	5.0 kW	20.0 kW	0.75 kW	2.5 kW	6.0 kW
Ainaži	9.89	16.77	11.27	5.94	4.56	3.07	3.41
Daugavpils	3.08	5.53	3.84	1.87	1.60	0.67	1.10
Priekule	8.06	13.67	9.25	4.88	3.79	2.49	2.82
Saldus	5.08	8.91	6.11	3.02	2.46	1.24	1.76
Ventspils	13.33	21.24	14.56	8.49	6.45	5.24	4.96

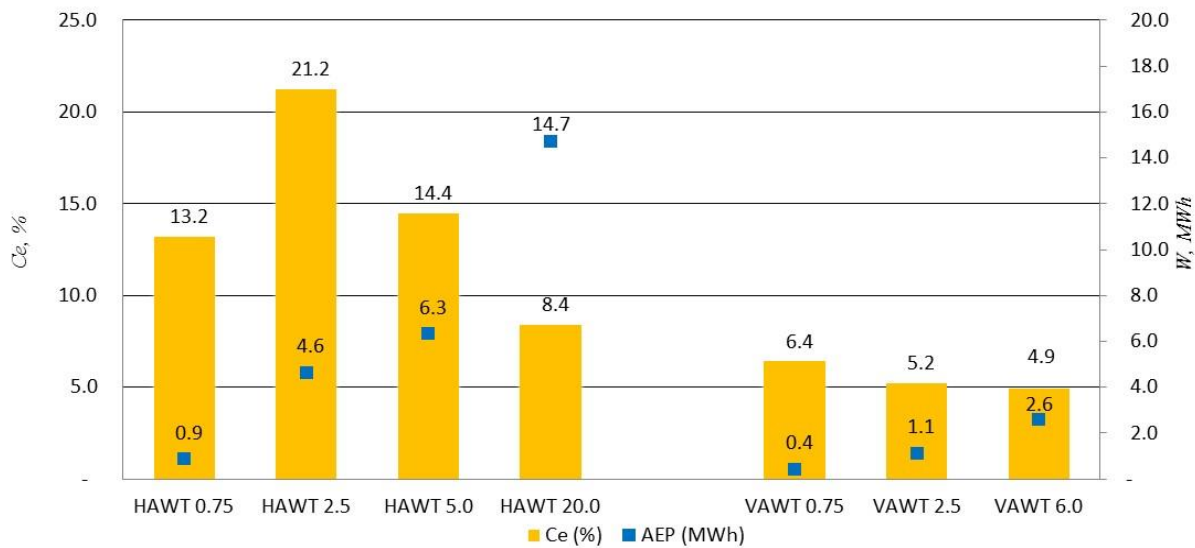


Figure 4.18 Forecasted capacity factor C_e and AEP for HAWT converters with rated power 0.75, 2.5, 5.0, 20.0 kW and VAWT Darrieus H-type 0.75, 2.5, 6.0 kW for Ventspils.

The efficiency of wind energy converters in the territory of Latvia can be represented as a model of the spatial distribution of the capacity factor C_e in relative units. Taking the maximum value of the capacity factor $C_{e\ max}$ to serve as the basis, relative capacity factor C_e^* for each meteorological observation station can be determined from Eq. (4.14):

$$C_{e\ i}^* = C_{e\ i} / C_{e\ max}, \quad (4.14)$$

where $C_{e\ max}$ – is value of the capacity factor corresponding to the performance of HAWT 2.5 kW wind power converter for the type of wind observed at the Ventspils station; and

C_{ei} – is value of the capacity factor corresponding to the efficiency of the HAWT 2.5 kW wind type converter for the wind type at each of the 22 stations.

In this case, the maximum value of the capacity factor corresponds to the SWTG of HAWT type with rated power 2.5 kW, which technical characteristics are summarized in Table 4.4, operating in the meteorological conditions observed at the Ventspils observation station.

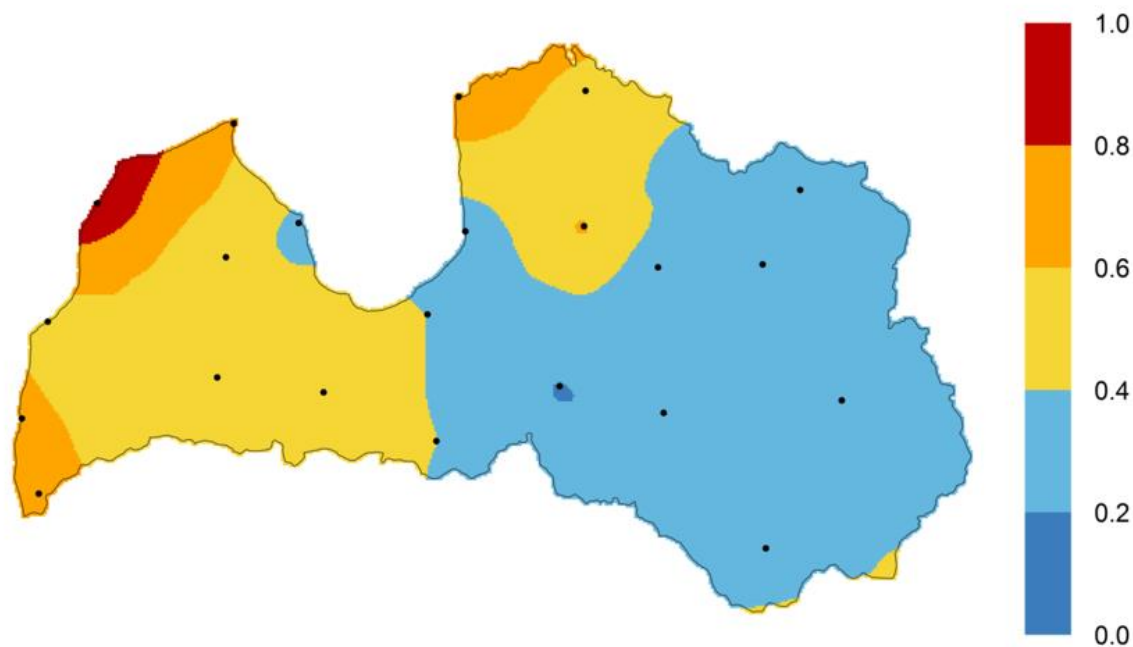


Figure 4.19 Model of the spatial distribution of relative capacity factor C_e^* for HAWT type generator with rated power 2.5 kW at the height of 10 m above the ground.

The developed model of the spatial distribution of factor C_e^* in relative units is presented in the form of a color contour map in Figure 4.19. The figure identifies areas within which HAWT 2.5 kW is expected to work with the certain level of efficiency relative to the one projected for the Ventspils region. Thus, the results of the presented study can serve as a tool for estimating and forecasting the feasibility of the commercial use of small wind energy converters at an altitude of 10 m in the territory of Latvia.

4.5. The assessment of WT efficiency in Latvia under low-wind conditions

Depending on the wind speed and the magnitude of the turbulence an international standard defines three wind classes [134, 135]. The properties of the fourth (non-standard) class are specified by turbine designers.

However, turbine wind class is just one of the factors that need to be considered during the complex process of the WPP design. Wind classes determine which turbine is suitable for the typical wind conditions of a particular site. They are mainly defined by the average annual wind speed (measured at the turbine’s hub height), the speed of extreme gusts that could occur over 50 years, and how much turbulence there is at the wind site. The wind classes for wind turbines corresponding to high, medium and low wind conditions are presented in Table 4.6.

The results of the wind shear studies show that Latvia is characterized by low wind speed streams. In order to estimate the AEP of a set of chosen WT types the author uses wind speed frequency distribution function $F(V)$ for the heights corresponding to the rotor hubs approximated by power law models in combination with power curves $P(V)$ of the generators. The AEP (W, MWh) into which the wind stream energy can be converted in a definite period of time is determined by the Eq. (4.11).

Table 4.6.

Wind classes defined based on IEC 61400-1 standard

Wind Turbine Class	Annual average wind speed at hub height, m/s	Extreme 50-year gust, m/s	Turbulence classes	
			a, %	b, %
IEC I High Wind	10.0	70.0	18.0	16.0
IEC II Medium Wind	8.5	59.5	18.0	16.0
IEC III Low Wind	7.5	52.5	18.0	16.0
IV (not standardized)	6.0	42.0		

In order to compare the performance of wind turbines in terms of the AEP at different heights under Latvian conditions, five WT generators from the leading European turbine designers were chosen. These turbines are designed to operate in wind class conditions II and III. Turbines of the types are equipped with generators having the rated power of 2300, 3000, 3200, 3050 and 3450 kW, which could be mounted on the masts with heights given in Table 4.7.

The table also shows the values of parameters c and k calculated based on Eq. (4.3) and (4.4) for the respective heights of rotor hub, as well as the values of the coefficient of efficiency C_e for each WT.

The efficiency coefficient C_e for each WT type is estimated based on the AEP obtained from Eq. (4.11) and the theoretically possible power output for the same period. The theoretical maximum power output is assumed to be the amount of energy that can be obtained from a generator during 8760 hours of its uninterrupted operation with the rated power P_R (kW). The efficiency % of a particular WT can be expressed as:

$$C_e = \frac{W}{P_R \cdot 8760} 100. \quad (4.15)$$

where W is the amount of energy (kW/h) produced in 1 year period.

The values of the parameter C_e calculated by Eq. (4.15) using power law models for the WT types under consideration are presented in Table 4.7.

Table 4.7

Forecasted power production and the WT operational efficiency at the heights of rotor hub for Nordex N131/3000, Enercon E101, Vestas V136-3.45 and Siemens SWT-3.2-113, SWT-2.3-108

Type of WT	Rated power of generator, P_R , kW	Wind class IEC	Height of rotor hub, m	Forecasted power production		Weibull parameters	
				AEP, MWh	C_e , %	k	c
N131/3000	3000	IIIa	114	8771	33.4	2.18	6.60
			131	9667	36.8	2.18	6.94
E101	3050	IIa	124	6540	24.5	2.18	6.81
			135	7046	26.4	2.18	7.02
V136-3.45	3450	IIIa	112	10883	35.5	2.18	6.56
			132	12094	39.4	2.18	6.96
SWT-3.2-113	3200	II	122	8065	28.8	2.18	6.76
			142	9043	32.3	2.18	7.14
SWT-2.3-108	2300	II	90	4636	23.0	2.18	6.06
			100	5116	25.4	2.18	6.30

The power curves $P(V)$ for following WT types: Nordex N131/3000, Enercon E101, Vestas V136-3.45 and Siemens SWT-3.2-113 and SWT-2.3-108 [136 – 140] and the curves of

Weibull's probability density function $F(V)$ are presented in Figure 4.20– Figure 4.24. The values of Weibull coefficients calculated using the power law models and the step length $\Delta V=1.0$ m/s. In the diagrams, results are shown for two height options available for the corresponding WT.

The calculation results of forecasted efficiency C_e , % for the considered WTs from Table 4.7 are summarized in Figure 4.25.

The analysis of the results shows that Vestas V136-3.45 and Nordex N131/3000, which power curves correspond to wind class III, have the highest estimated efficiency among the considered WT types. Vestas V136-3.45 with hub height 132 m could achieve maximum efficiency equal to 39.4%. The efficiency of Nordex N131/3000 with height 131 m could reach 36.8%. For the Enercon E101 and Siemens SWT-3.2-113, SWT-2.3-108 WTs, which are designed for wind class II, values of efficiency coefficient would not exceed 32.2% for hub height 142 m and only 23% for 90 m.

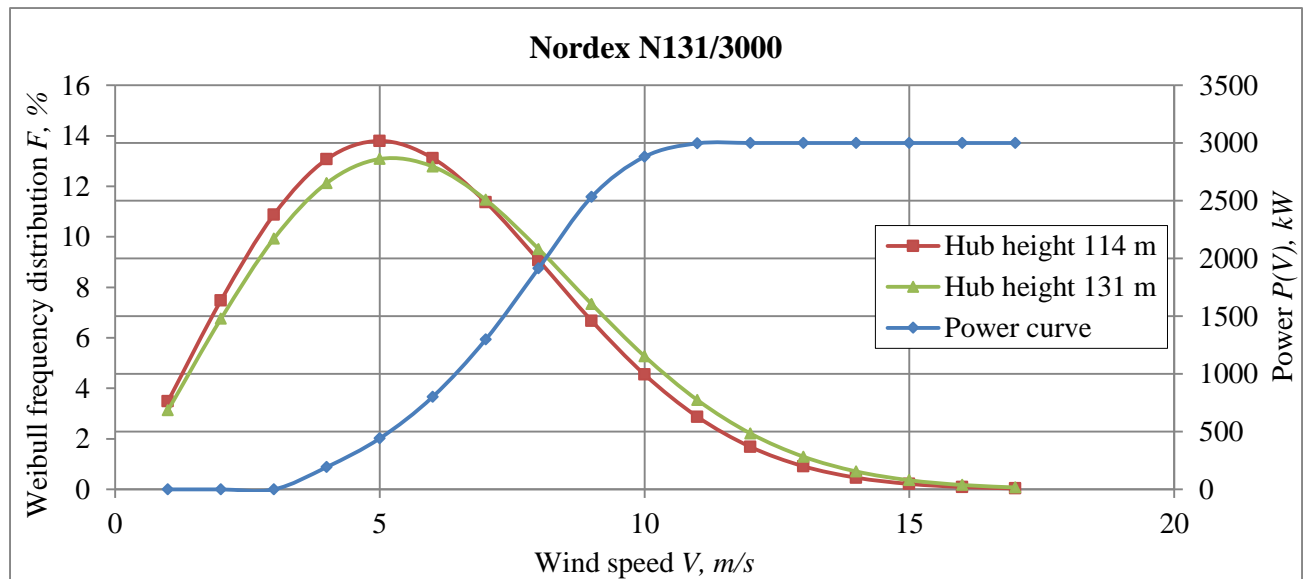


Figure 4.20 Power curve $P(V)$ for generator of Nordex N131/3000 type 3000 kW and Weibull probability density function $F(V)$ curves for wind speeds V , m/s at heights 114 and 131 m.

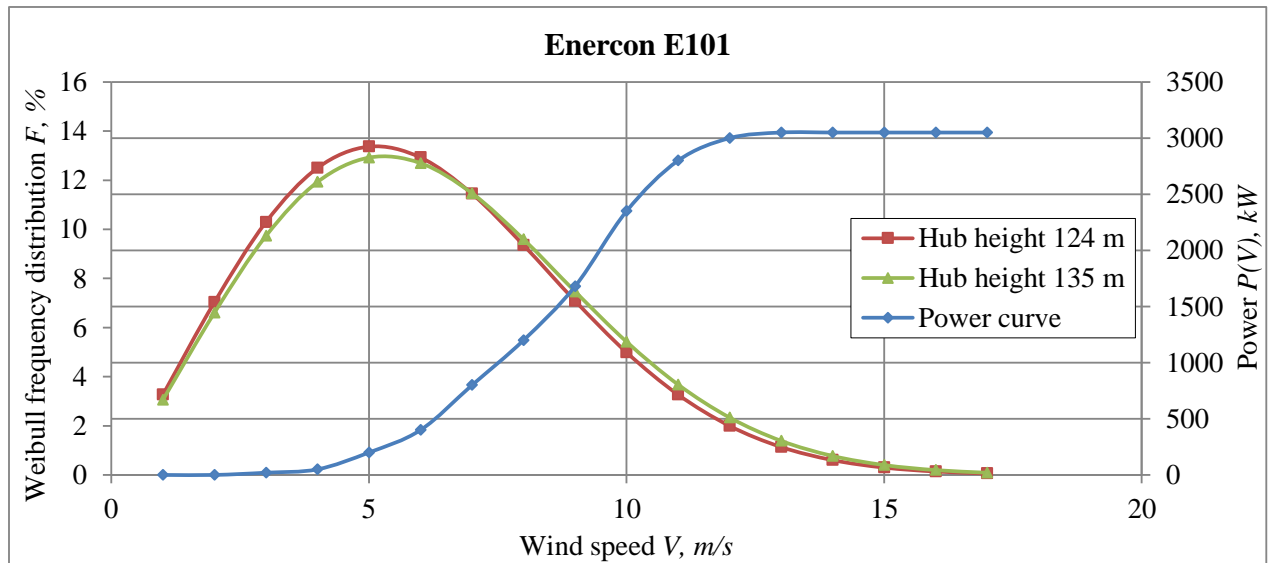


Figure 4.21 Power curve $P(V)$ for generator of Enercon E101 type 3050 kW and Weibull probability density function $F(V)$ curves for wind speeds V , m/s at heights 124 and 135 m.

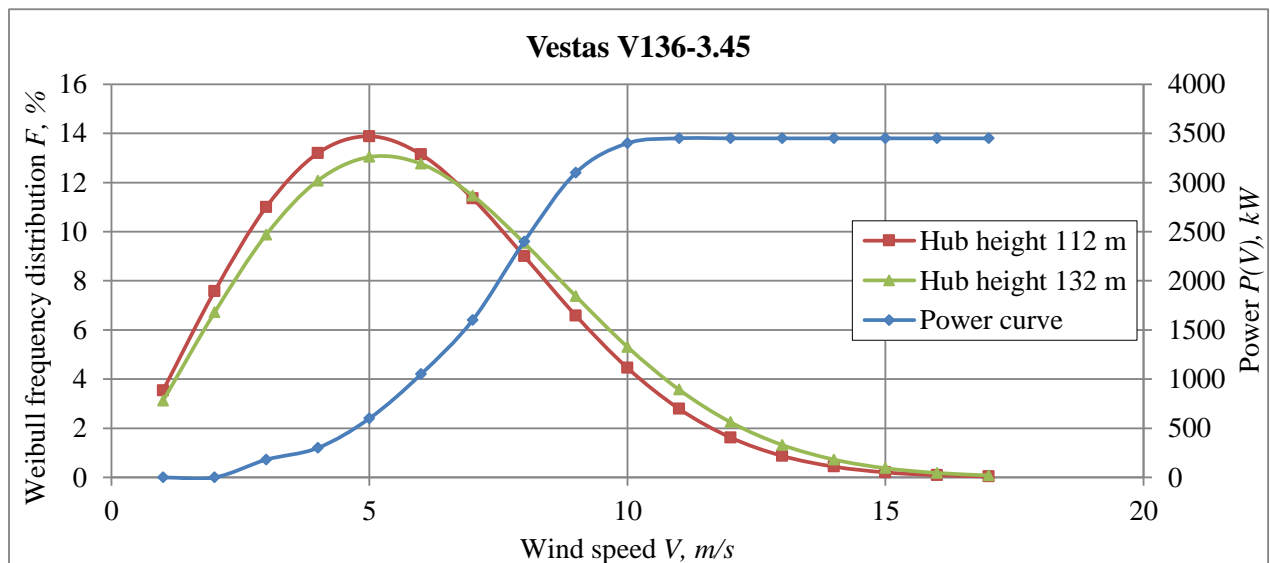


Figure 4.22 Power curve $P(V)$ for generator of Vestas V136-3.45 type 3450 kW and Weibull probability density function $F(V)$ curves for wind speeds V , m/s at heights 112 and 132 m.

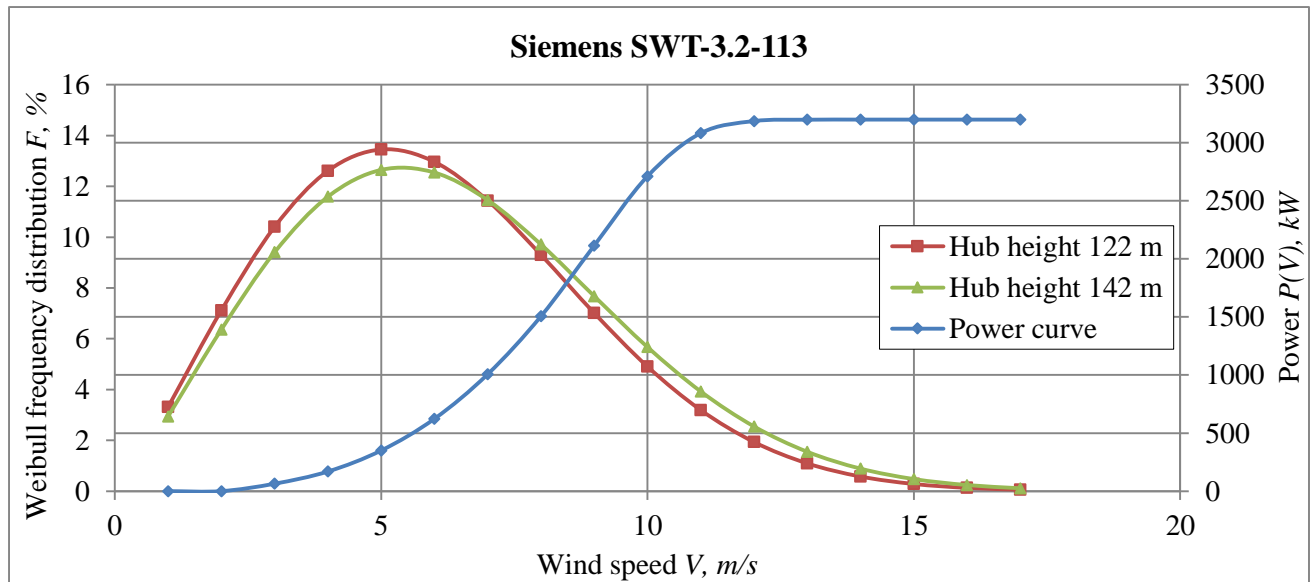


Figure 4.23 Power curve $P(V)$ for generator of Siemens SWT-3.2-113 type 3.5 MW and Weibull probability density function $F(V)$ curves for wind speeds V , m/s at heights 122 and 142 m.

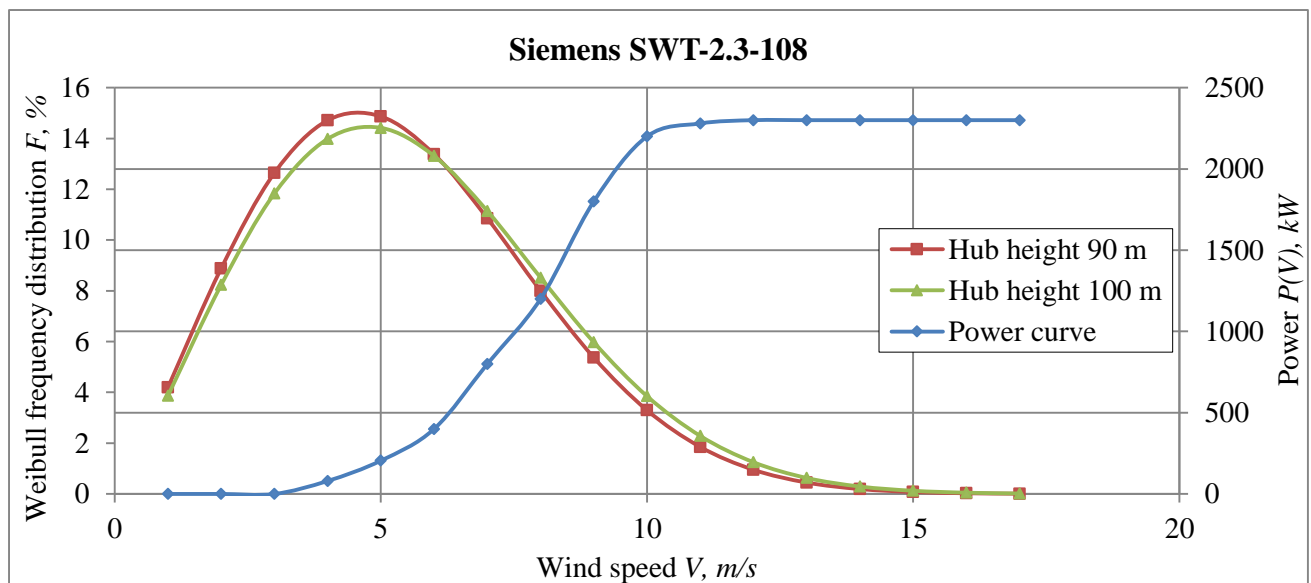


Figure 4.24 Power curve $P(V)$ for generator of Siemens SWT-2.3-108 type 2 MW and Weibull probability density function $F(V)$ curves for wind speeds V , m/s at heights 90 and 100 m.

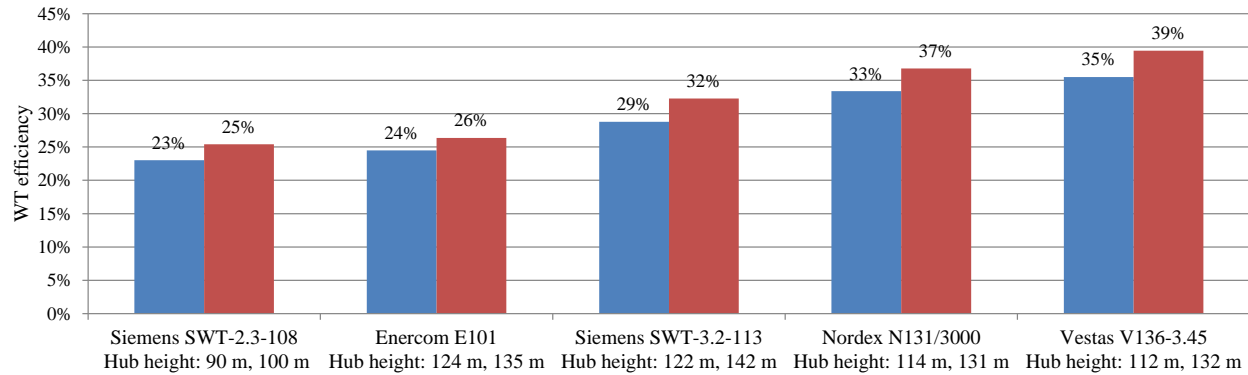


Figure 4.25 Forecasted efficiency C_e , %, for Nordex N131/3000, Enercon E101, Vestas V136-3.45 and Siemens SWT-3.2-113, SWT-2.3-108 WTs for different heights of rotor hubs (height in meters) performing under the low-wind conditions in Latvia.

The study results suggest that in Latvia WT of wind class III should be used for wind power parks as their power curve is specially tailored to operate in low-wind conditions.

4.6. Conclusions

The study developed the models of the spatial distribution of wind speed and wind energy on the territory of Latvia. The models were created based on the generalisation of physical wind speed measurements results at the altitude of 10 m above the ground.

The models were constructed using the method of spatial interpolation based on measured values and presented in the form of colour contour maps with a 1x1 km resolution. Physics measurements were carried out for the period of 01.01.2015 - 31.12.2016 at 22 meteorological observation stations belonging to the LEGMC.

The author provided a comparative analysis of the results of physical measurements and modelling of average wind speed for meteorological observation stations in Ainaži, Daugavpils, Priekule, Saldus and Ventspils. On top of it, the results of an alternative modelling approach towards obtaining the spatial distribution of wind speed using the ERA5 weather modelling technology at the altitudes of 10, 54, 100 and 136 m with a 31x31 km resolution are presented.

The study presented the spatial distribution models of average wind speed, parameters of Weibull wind speed distribution, relative wind energy density and operational efficiency of SWTG at the height of 10 m above the ground. The spatial models were presented in the form of colour contour maps. The visual representation of the distribution of wind energy resource makes it possible to estimate the efficiency of wind generators on the entire territory of Latvia. Thus, the

developed models of the spatial distribution of wind speed and wind energy can serve as a practical tool and reference material for analysing the prospects of using wind generators in various regions of Latvia and assessing the possibility of commercial use of wind energy at a height of 10m.

The study provided the comparative analysis of two type of the SWTG: HAWT type with rated power 0.75, 2.5, 5.0, 20.0 kW and VAWT Darrieus H-type with rated power 0.75, 2.5, 6.0 kW. The results of the comparison suggest that HAWT type generators with rated power 2.5 kW tend to perform better than other considered wind energy converters under Latvian meteorological conditions in terms of efficiency. The results of the study can serve as a tool for forecasting AEP and estimating the feasibility of the commercial use of wind energy at the height of 10 m in the territory of Latvia.

In order to investigate the effectiveness of WTs in low-wind conditions typical for Latvia, 10-min data collected by the wind measuring complex NRG LOGGER Symphonie 9200 mounted on the 60 m mast in Matiši site for the period 04.2009-04.2013 was used together with WTs power curves of the leading European WT manufacturers such as Nordex, Vestas, Enercon and Siemens.

The forecast of the AEP was performed using the Weibull frequency distribution of wind speed by modelling of Weibull distribution coefficients c and k by the power law approximations for two heights for each corresponding WT type.

It can be noted that in the conditions of Latvia, high operational efficiency can be reached by Vestas V136-3.45 and Nordex N131/3000, which power curves corresponds to wind class III. Vestas V136-3.45 with hub height 132 m could achieve maximum efficiency equal to 39.4%. The efficiency of Nordex N131/3000 with height 131 m could reach 36.8%. For Enercon E101 and Siemens SWT-3.2-113, SWT-2.3-108 WTs, which are designed for wind class II, the estimate values of efficiency coefficient would not exceed 32.2% for hub height 142 m and only 23% for 90 m.

5. Implications and proposals

Based on an overview of a broad range of material on modern energy supply, it can be argued that the development of RES should not be considered in isolation, but as part of a broader process of “energy transition” taking the form of a long-term change in the structure of energy systems. The process of energy transition, triggered by growing concerns over global climate change, has led to the development of targeted government support plans aimed at making electricity production from RES sustainable and economically attractive.

Although at this point the cost of "green" energy remains higher compared to traditional sources, the feasibility of alternative energy is persistently increasing. This is facilitated by the improvement of technology, declining WT production costs and an extensive construction of WPP in mountains and offshore regions.

Overall trends in the power production suggest that the transition to RES in electricity production is feasible, and wind is going to play a leading role in the new paradigm of electricity supply. However, wind, as an energy source, has several drawbacks that need to be address before it can independently challenge traditional sources – high volatility, relatively low efficiency and strong geographical linkage. That makes the task of increasing the technical and economical efficiency of WPP especially relevant nowadays.

This thesis has pursued the goal of lowering the cost of wind energy generation and increasing penetration of this source of energy by reducing the uncertainty associated with the design of WPP projects. The analysis covered economical, operational and informational aspects of projects involving small- and large-scale wind turbines.

Following the outcomes of the study, economical risks associated with the use of wind energy under free market conditions can be better assessed based on systematic update and validation of SDE models used for forecasting. The probabilistic modelling of project revenues using Monte Carlo simulations involved separate treatment of wind speed measurements and market electricity price data in combination with generator specific power curves. The results indicated that project revenues are sensitive to the choice of generator type and hub height, but overall income can be optimized subject to the size of the initial investment and expected operational cost structure.

Furthermore, the study show that forecasted efficiency is highly dependent on the initial choices of the generator model and can range from 12% for old, but still operational in Latvia,

wind generators Nordex N54/1000 to 52% for new Nordex N131/3000 model at high altitudes of operation. The results of the analysis imply that Siemens generators SWT-2.3-101 installed at the largest Latvian wind farm, accounting for one third of wind energy capacity installed in Latvia, might not be optimal generator type for the Latvian weather conditions.

The modelling efforts emphasised the importance of high-quality wind speed data availability at higher altitudes. Therefore, in the course of the study, an investigation of wind shear based on long-term wind speed measurements was performed. The study used the power law function to extrapolate the values of the Weibull distribution function parameters to the height corresponding to the location of wind turbine axis.

Moreover, a set of mathematical CFD modelling and physical experiments were carried out in order to test a method of performing wind shear estimations using CCM by installing wind speed measuring complexes at multiple height levels of existing network of tower, densely covering the entire territory of Latvia. In the course of the experiments, the impact of lattice masts' structural design on the results of wind speed measurements was quantified.

Using CFD modelling techniques it has been shown that the implementation of the IEC standard for calculating boom length does not guarantee the accuracy of wind speed measurement $100 \pm 1\%$ in the shadow area of the mast, whereas in all other directions the boom length is overestimated.

Consequently, based on the experiment results the study provided a methodology for quantifying the uncertainty of wind measurements obtained from CCM and proposed a method of improving the accuracy of measurements by comparing the results of estimations obtained from two sensors installed at the same height and offset by at least 120° with respect to each other. The reliability of the estimations of wind speed increased $\sim 1.9 - 3.9\%$ on average after the exclusion of distorted measurements from the calculations.

Thus, in the course of the study, it has been shown that the use of CCM for wind speed measurements is a viable and cost-efficient alternative to the construction of tall meteorological masts. The proposed approach can provide necessary high-quality experimental data on wind speed that meets the requirements of the IEC regulation

In order to reduce the costs of obtaining information necessary for estimating operational efficiency of low-power wind generators, the study proposed making spatial distribution models of average wind speed and Weibull parameters of wind speed distribution at the height of 10 m in

Latvia. The contour maps with resolution 1x1 km were created based on the interpolation of physical wind speed measurement results at the altitude of 10 m above the ground performed by LEGMC at 22 meteorological stations across the country. Based on this information, it is possible to make an estimate of the average annual electricity generation for the projected wind power plants.

Based on an in-depth knowledge of wind conditions in the Latvian territory at low altitudes the study performed an assessment of the operational efficiency of low-power wind generators for wind turbines with vertical and horizontal axes and developed the model of the spatial distribution of the relative capacity factor for a HAWT type generator.

Visual representation of the distribution of wind energy resource makes it possible to estimate the efficiency of wind generators at any point of the entire territory of Latvia. Thus, the developed models of the spatial distribution of wind speed and wind energy can serve as a practical tool and reference material for analysing the prospects of using the SWTG in various regions of Latvia and assessing the possibility of commercial use of wind energy at the height of 10m. The results increase information accessibility and lower barriers to market entry.

To sum up, the improvement of technical and economic efficiency of WPP can be achieved by increasing the power of WTs and hub height, using storage devices and energy storage facilities, developing offshore and shallow water zones, improving the quality and accessibility of wind speed data, the use of advanced wind power production forecasting methods and search for non-conventional solutions.

References

1. International Energy Agency (EIA) (2007): Annual Energy Review 2006. Report No. DOE/EIA-0384(2006). Washington, D.C.: U.S. Department of Energy. Available online at <https://www.eia.gov/totalenergy/data/annual/archive/>; accessed January 2018.
2. Ачкасов В.А., Ланцов С.А. (2011): Мировая политика и международные отношения М.: Аспект Пресс, 2011. — 480с.
3. International Energy Agency (EIA) (2018): Global Energy & CO2 Status Report 2017, Global energy transformation
4. IRENA (2017): Renewable Energy Benefits: Leveraging Local Capacity for Solar PV, International Renewable Energy Agency (IRENA) and Lawrence Berkeley National Laboratory (LBNL), Abu Dhabi.
5. IRENA (2018): Global Energy Transformation: A roadmap to 2050, International Renewable Energy Agency, Abu Dhabi.
6. REN21 (2018): Renewables 2018 global status report. Available from: http://www.ren21.net/wp-content/uploads/2018/06/17-8652_GSR2018_FullReport_web_1.pdf
7. ENERDATA (2018): Statistical yearbook of world energetics 2018. Available from: <https://yearbook.enerdata.ru/renewables/renewable-in-electricity-production-share.html>
8. Лукутин Б.В. (2008): Возобновляемые источники электроэнергии., 2008. — 187 с.
9. GWEC (2018): Global wind report. Available from: http://www.tuulivoimayhdistys.fi/filebank/1191-GWEC_Global_Wind_Report_April_2018.pdf
10. Power Technology (2018): Global wind power market value expected to near \$100bn by 2025. Available from: <https://www.power-technology.com/comment/global-wind-power-market-value-expected-near-100bn-2025/>
11. Wind Europe (2017): Wind in power 2017. Available from: <https://windeurope.org/wp-content/uploads/files/about-wind/statistics/WindEurope-Annual-Statistics-2017.pdf>
12. WWEA (2017): Wind power capacity reaches 546 GW, 60 GW added in 2017. Available from: <http://wwindea.org/blog/2018/02/12/2017-statistics/>

13. Delloite (2018): Global renewable energy trends. Available from:
<https://www2.deloitte.com/insights/us/en/industry/power-and-utilities/global-renewable-energy-trends.html>
14. European Commission (2014): Subsidies and costs of EU energy. Available from:
https://ec.europa.eu/energy/sites/ener/files/documents/ECOFYS%202014%20Subsidies%20and%20costs%20of%20EU%20energy_11_Nov.pdf
15. General Electric (2018). Available from: <https://www.ge.com/renewableenergy/wind-energy/turbines/haliade-x-offshore-turbine>.
16. Econet (2018). Available from: <https://econet.ru/articles/168309-vetrovaya-energetika-stanet-deshevle-atomnoy-energii>
17. Bezrukov V., Domburs L., Pugachev V. (1995): The performance evaluation of the efficiency of the TW 600 wind power converter in the Ainaži region. Latvian Journal of physical and technical sciences, 1995, Nr.2. pp 35-45.
18. Central Statistical Bureau of Latvia, (2016): Available from:
<https://www.csb.gov.lv/en/statistics/statistics-by-theme/economy/gdp/search-in-theme/116-statistical-yearbook-latvia-2016>
19. Jalonsom (2016). Available from:
https://commons.wikimedia.org/wiki/File:Wind_turbine_schematic.svg
20. Tennet (2018): Available from: <https://www.tennet.eu/our-grid/offshore-projects-netherlands/net-op-zee-borssele/>
21. Krohn S., Morthorst P., Awerbuch S. (2009): The Economics of Wind Energy, A report by the European Wind Energy Association 2009. p 156.
22. IRENA (2015): Wind Costs 2010-2015. Available from:
<http://resourceirena.irena.org/gateway/dashboard/?topic=3&subTopic=31>
23. Fraunhofer (2018): Levelized cost of electricity renewable energy technologies. Available from:
https://www.ise.fraunhofer.de/content/dam/ise/en/documents/publications/studies/EN2018_Fraunhofer-ISE_LCOE_Renewable_Energy_Technologies.pdf
24. Renewables First (2018). Available from:
<http://www.renewablesfirst.co.uk/windpower/windpower-learning-centre/how-much-does-a-farm-wind-turbine-small-wind-farm-turbine-cost/>

25. Heimiller D., Ho J., Moné C., Hand M., Bolinger M., Rand J. (2015): Cost of Wind Energy Review. U.S. Department of Energy Office of Scientific and Technical Information. p.115.
26. IRENA (2018): Renewable Power Generation Costs in 2017. Available from:
https://www.irena.org/-/media/Files/IRENA/Agency/Publication/2018/Jan/IRENA_2017_Power_Costs_2018.pdf
27. Rolik J. (2017): Management in Implementing Wind Energy Project. The 16th International Scientific Conference October 19-22, 2016, Riga, Latvia, Procedia Engineering 178 (2017) p.278 – 288.
28. Final report on Project DiaCore (2016): The impact of risks in renewable energy investments and the role of smart policies, Contract N°: IEE/12/833/SI2.645735.
29. Blanco, M. I. (2009): The Economics of Wind Energy, Renewable and Sustainable Energy Reviews, 13: p.1372-1382.
30. Boomsma, T. K., Meade, N., Fleten, S. E. (2012): Renewable Energy Investments Under Different Support Schemes: A Real Options Approach, European Journal of Operational Research, 220: p. 225-237.
31. Gatzert N., Kosub T. (2015): Risks and Risk Management of Renewable Energy Projects: The Case of Onshore and Offshore Wind Parks .Presented to the Actuaries Institute ASTIN, AFIR/ERM and IACA Colloquia 23-27 August 2015 Sydney. p. 34.
32. Bullough C. (2004): Advanced Adiabatic Compressed Air Energy Storage for the Integration of Wind Energy European, Wind Energy Conference and Exhibition, London, 22-25 Nov 2004.
33. International Electrotechnical Commission, (2011): Electrical Energy Storage, White Paper, p. 78.
34. Baltputnis K., Broka Z., Sauhats A., Petričenko R. (2016): Short-Term Optimization of Storage Power Plant Operation under Market Conditions. No: 2016 IEEE 16th International Conference on Environment and Electrical Engineering (EEEIC 2016): Conference Proceedings, Itālija, Florence, 7.-10. jūnijs, 2016. Piscataway: IEEE, 2016, pp. 250.-256.
35. Martí Perez, I. (2002): Wind Forecasting Activities. Proceedings of the First IEA Joint Action Symposium on Wind Forecasting Techniques, Norrköping, Sweden, pp. 11-20. Published by FOI - Swedish Defence Research Agency.

36. Frías, L., E.Pascal, U.Irigoyen, E.Cantero, Y.Loureiro, S.Lozano, PM. Fernandes, I.Martí (2009): Support Vector Machines in the wind energy framework. A new model for wind energy forecasting. Proc. Of the 2009 European Wind Energy Conference EWEC'09 Marseille (FR).
37. Giebel G., Brownsword R., Kariniotakis G., Denhard M., Draxl C. (2011): The State-Of-The-Art in Short-Term Prediction of Wind Power : A Literature Overview, 2nd edition. ANEMOS.plus, 2011. 109 p.
38. Pinson P.; Chevallier C., Kariniotakis G. (2007): Trading Wind Generation From Short-Term Probabilistic Forecasts of Wind Power. IEEE Transactions on Power Systems (Volume: 22, Issue: 3, Aug. 2007). p. 1148 – 1156.
39. Eenergy & Meteo Systems (2018). Available from: https://www.energymeteo.com/products/power_predictions/wind_power_prediction.php
40. Fraunhofer (2018). Available from: https://www.energy-charts.de/power_inst.htm
41. Nord Pool (2018). Available from: <https://www.nordpoolgroup.com/Market-data1/#/nordic/table>
42. Wang, J., Jiang, H., Han, B. and Zhou, Q. (2015): An experimental investigation of FNN model for wind speed forecasting using EEMD and CS. Mathematical Problems in Engineering Volume 2015, Article ID 464153, p.13.
43. Directive (EU) 2018/2021 of the European Parliament and of the Council of 11 December 2018 on the promotion of the use of energy from renewable sources (Text with EEA relevance.) Available from: <https://eur-lex.europa.eu/eli/dir/2018/2001/oj>
44. Wind Europe (2017): Wind energy in Europe: Scenarios for 2030. Available from: <https://windeurope.org/wp-content/uploads/files/about-wind/reports/Wind-energy-in-Europe-Scenarios-for-2030.pdf>
45. CSB (2018): Latvian Energy Balance in 2017. Available from: https://www.csb.gov.lv/sites/default/files/publication/2018-08/Nr_25_Latvijas_energobilance_2017_%2818_00%29_LV.pdf
46. Review of RES perspective in Baltic countries till 2030 (2015). Available from: http://elering.ee/public/Infokeskus/Uuringud/Review_of_RES_perspective_in_Baltic_countries_till_2030.pdf

47. CSB (2018): Electrical capacity and produced electricity from renewables. Available from: http://data1.csb.gov.lv/pxweb/en/vide/vide__energetika__ikgad/ENG090.px/?rxid=a39c3f49-e95e-43e7-b4f0-dce111b48ba1
48. Möhrlen, C., (2004): Uncertainty in wind energy forecasting. PhD Thesis, University College Cork. P.174.
49. Schwartz, M.N, and Bailey B.H. (1998): Wind Forecasting Objectives for Utility Schedulers and Energy Traders (1998): Presented at Windpower '98, Bakersfield, CA, April 27-May 1, 1998. NREL/CP-500-24680. Available from OSTI.gov.
50. Costello, R., D. McCoy, P. O'Donnell, A.G. Dutton, G.N. Kariniotakis (2002): Potential Benefits of Wind Forecasting and the Application of More-Care in Ireland. Paper presented on the 3rd MED POWER conference 2002, Athens (GR), November 4-6, 2002.
51. Berge, E., F. Nyhammer, L. Tallhaug, F. Villanger, J.b. Bremnes, M.Ø. Kjøltzow, J. Smits, A. Knauer (2003): Forecasting wind and wind energy production in Norwegian wind farms. Final report of the NFR project: 138848/212 "Korttidsprognoser for energiproduksjon fra vindkraft". Kjeller Vindteknikk Report number KVT/EB/2003/005, Kjeller (NO), 2003. P.61.
52. Nordhaus, William D. (1987): "Forecasting Efficiency: Concepts and Applications," *The Review of Economics and Statistics*, MIT Press, vol. 69(4), pp. 667-674, November.
53. Iversen, E.B.; Morales, J.M.; Møller, J.K.; Madsen, H. (2015): Short-term probabilistic forecasting of wind speed using stochastic differential equations. *Int. J. Forecast.* 2015, 32, pp.981–990.
54. Messner, J. W., Zeileis, A., Broecker, J., & Mayr, G. J. (2013): Probabilistic wind power forecasts with an inverse power curve transformation and censored regression. *Wind Energy*, 17, pp. 1753–1766.
55. Pinson, P., Nielsen, H., Møller, J., Madsen, H., & Kariniotakis, G. (2007): Non-parametric probabilistic forecasts of wind power: required properties and evaluation. *Wind Energy*, 10(6), pp. 497–516.
56. R. Billinton and W. Wangdee (2007): "Reliability-based transmission reinforcement planning associated with large-scale wind farms," *IEEE Trans. Power Systems*, vol. 22, pp. 34-41, Feb. 2007.

57. Schefzik, R., Thorarinsdottir, T. L., & Gneiting, T. (2013): Uncertainty quantification in complex simulation models using ensemble copula coupling. *Statistical Science*, 28(4), 616–640.
58. Giebel, G., Brownsword, R., & Kariniotakis, G. (2004): The state-of-the-art in short-term prediction of wind power. A literature overview. Version 1.1. ANEMOS Project.
59. Giebel G., Kariniotakis G, Brownsword R. (2003): The state-of-the-art in short term prediction of wind power from a danish perspective. 4th International Workshop on large scale integration of wind power and transmission networks for offshore wind farms, Oct 2003, Billund, Denmark. 2003. P.8.
60. Nielsen, T.S., Joensen A., Madsen H., Landberg L., and Giebel G. (1998): A New Reference for Predicting Wind Power. *Wind Energy* 1, pp. 29-34.
61. Makarov, Y., Hawkins, D., Leuze, E. and Vidov, J (2003): California ISO Wind Generation Forecasting Service Design and Experience. Proceedings of American Wind Energy Association Conference, Oregon, USA
62. Kamal, L. and Y.Z. Jafri (1997): Time series models to simulate and forecast hourly averaged wind speed in Quetta, Pakistan. *Solar Energy* 61(1), pp. 23-32.
63. Sfetsos A. (2001): A novel approach for the forecasting of mean hourly wind speed time series. *Renewable Energy* 27 , pp. 163-174.
64. Torres, J.L., A. Garcia, M. De Blas and A. De Francisco (2005): Forecast of hourly average wind speed with ARMA models in Navarre (Spain). *Solar Energy* 79(1), pp. 65-77.
65. Lin L., Eriksson J.T., Vihriälä H., and Söderlund L. (1996): Predicting wind behaviour with neural networks. Proceedings of the EUWEC, Göteborg (SE), pp. 655-658.
66. Salcedo-Sanz S., Pérez-Bellido A. M., Ortiz-García E.G., Portilla-Figueras A., Prieto L., Correoso F. (2009): Accurate short-term wind speed prediction by exploiting diversity in input data using banks of artificial neural networks. *Neurocomputing* 72, pp. 1336-1341.
67. Mohandes, M.A., T.O. Halawani, S. Rehman, A.A. Hussain (2004): Support Vector Machines for Wind Speed Prediction. *Renewable Energy* 28(4), pp. 939—947.
68. Moon, D., N. Lincoln, D. Christenson, R. Chevallez-Perrier (2004): Support Vector Machine Technology Coupled with Physics-based Modeling for Wind Facility Power Production Forecasting. Proceedings of the Global Wind Power Conference and Exhibition, Chicago (US), 28-31 March 2004

69. Foley, A. M., Leahy, P. G., Marvuglia, A., & McKeogh, E. J. (2012): Current methods and advances in forecasting of wind power generation. *Renewable Energy*, 37 (1), 1–8.
70. Costa, A., Crespo, A., Navarro, J., Lizcano, G., Madsen, H., & Feitosa, E. (2008): A review on the young history of the wind power shortterm prediction. *Renewable and Sustainable Energy Reviews*, 12(6), 1725–1744.
71. Monteiro C., Bessa R., Miranda V., Botterud A., Wang J., Conzelmann G., et al. (2009): Wind power forecasting: state-of-the-art 2009. Tech. rep. Argonne National Laboratory (ANL).
72. Soman S. S., Zareipour H., Malik O., and Mandal P. (2010): A review of wind power and wind speed forecasting methods with different time horizons, in *North American Power Symposium (NAPS)*, 2010, Sept 2010, pp. 1–8.
73. Chang, W. (2014): A Literature Review of Wind Forecasting Methods. *Journal of Power and Energy Engineering*, 2, 161-168.
74. Chen, P., Pedersen, T., Bak-Jensen, B., & Chen, Z. (2010): ARIMA-Based Time Series Model of Stochastic Wind Power Generation. *IEEE Transactions on Power Systems*, 25(2), 667-676.
75. Ekstrom, J., Koivisto, M. J., Mellin, I., Millar, J., & Lehtonen, M. (2017): A Statistical Model for Hourly LargeScale Wind and Photovoltaic Generation in New Locations. *IEEE Transactions on Sustainable Energy*, 8(4), [7879358].
76. Sklar, M. (1959): Fonctions de re'partition a` n dimensions et leurs marges, *Publications de l'Institut de Statistique de L'Université de Paris*. Vol. 8, pp. 229-231
77. Nelsen, R. B. (2007): *An introduction to copulas*, Springer Science & Business Media. 225 pp.
78. McNeil AJ, Frey R, Embrechts P (2015): *Quantitative risk management: concepts, techniques, tools*. Princeton University Press, Princeton. 720 pp.
79. Cherubini U, Luciano E, Vecchiato W (2004): *Copula methods in finance*. Wiley, New York 2004. p. 310.
80. Hu Wei, Yong Min, Yifan Zhou, Qiuyu Lu (2017): Wind power forecasting errors modelling approach considering temporal and spatial dependence. *J. Mod. Power Syst. Clean Energy*. <https://doi.org/10.1007/s40565-016-0263-y>

81. Papaefthymiou G., Kurowicka D. (2009): "Using copulas for modeling stochastic dependence in power system uncertainty analysis," *IEEE Trans. Power Syst.*, vol. 24, no. 1, pp. 40–49, February 2009.
82. Hagspiel S., Papamannouil A., Schmid M., Andersson G. (2012): Copula-based modeling of stochastic wind power in Europe and implications for the Swiss power grid. *Appl. Energy* 2012, 96, 33–44.
83. Louie H (2014): Valuation of bivariate archimedean and elliptical copulas to model wind power dependence structures. *Wind Energy* 17(2):225–240
84. Xie K., Li Y., and Li W. (2012): Modelling wind speed dependence in system reliability assessment using copulas, *IET Renewable Power Generation*, vol. 6, no. 6, pp. 392–399, November 2012.
85. Iversen, E.B.; Morales, J.M.; Møller, J.K.; Madsen, H. (2015): Short-term probabilistic forecasting of wind speed using stochastic differential equations. *Int. J. Forecast.* 2015, 32, 981–990.
86. Giebel, G., Sørensen, P. E., & Holttinen, H. (2007): Trade Wind Deliverable 2.2: Forecast error of aggregated wind power. *Risø-I, Vol.. 256*
87. Madsen, H., Pinson P., Kariniotakis G., Nielsen H.Aa., Nielsen T.S. (2005): Standardizing the Performance Evaluation of Short-term Wind Power Prediction Models. *Wind Engineering* 29(6), pp. 475-489, 2005
88. Jens Tambke, Matthias Lange, Ulrich Focken, Jörg-Olaf Wolff, John A. T. Bye (2005): Forecasting offshore wind speeds above the North Sea. *Wind Energy* 8(1), pp. 3-16, 2005
89. V. Bezrukovs, A. Zacepins, Vl. Bezrukovs, V. Komashilovs (2016): Comparison of methods for evaluation of wind turbine power production by the results of wind shear measurements on the Baltic shore of Latvia. *Renewable Energy, Volume 96, Part A*, October 2016, pp. 765–774.
90. Brigo, D., Dalessandro, A., Neugebauer, M. and Triki, F. (2009): A stochastic processes toolkit for risk management: Geometric Brownian motion, jumps, GARCH and variance gamma models. *Journal of Risk Management in Financial Institutions*, 2: pp. 365–393
91. Kwiatkowski, D., P.C.B. Phillips, P. Schmidt, Y. Shin (1992): Testing the Null Hypothesis of Stationarity against the Alternative of a Unit Root, *Journal of Econometrics*, 54, pp. 159-178, North-Holland.

92. Uhlenbeck G.E., Ornstein L.S. (1930): On the theory of Brownian motion *Phys. Rev.* , 36 (1930) pp. 823–841
93. N. Wax (ed.) *Selected papers on noise and stochastic processes* , Dover, reprint (1954)
94. Vasicek, O. (1977): An Equilibrium Characterization of the Term Structure. *Journal of Financial Economics*, 5, pp. 177–188.
95. Seifert, Jan, Uhrig-Homburg, Marliese (2007): Modelling Jumps in Electricity Prices: Theory and Empirical Evidence, *Review of Derivatives Research*, Vol. 10, pp. 59-85, 2007.
96. Lucia, Julio J., Schwartz, Eduardo, *Electricity Prices and Power Derivatives* (2002): Evidence from the Nordic Power Exchange, *Review of Derivatives Research*, Vol. 5, Issue 1, pp. 5-50, 2002.
97. Escribano, Alvaro, Pena, Juan Ignacio, Villaplana, Pablo, (2002): Modeling Electricity Prices: International Evidence, Universidad Carlos III de Madrid, Working Paper 02-27, 2002.
98. Brown, B.G., Katz R.W., and Murphy A.H. (1984): Time Series Models to Simulate and Forecast Wind Speed and Wind Power. *Journal of Climate and Applied Meteorology* 23(8), pp. 1184-1195, August 1984
99. Bezrukovs V., Bezrukovs Vl.(2014): Wind Speed and Energy at Different Heights on the Latvian Coast of the Baltic Sea, *Journal of Energy and Power Sources*. Vol. 1, (2014), No. 2, pp. 105-112.
100. *Wind Turbines – Part 12-1: Power Performance Measurements of Electricity Producing Wind Turbines*. IEC 61400-12-1:2017, Geneva, Switzerland. P.558.
101. Hansen M., Pedersen B. Influence of the Meteorology Mast on a Cup Anemometer, *Journal of Solar Energy Engineering*, Vol. 121, (1999), pp. 128-131.
102. Stickland, M., Scanlon, T., Fabre, S., Oldroyd, A., & Kindler, D. (2013): Measurement and simulation of flow field around a triangular lattice meteorological mast, *Journal of Energy and Power Engineering*, Vol. 7, (2013), Issue 10, pp. 1934-1939.
103. Fabre S et al. (2011): Computational and Experimental Study on the effect of flow field distortion on the accuracy of the measurements made by anemometers on the Fino3 Meteorological mast. EWEA Offshore 2011, Amsterdam.

104. Orlando S., Bale A., Johnson D.A. (2011): Experimental study of the effect of tower shadow on anemometer readings. *Journal of Wind Engineering and Industrial Aerodynamics*, 2011, Vol. 99, Issue 1, 2011, P. 1-6.
105. Farrugia R.N., Sant T. (2013): Modelling wind speeds for cup anemometers mounted on opposite sides of a lattice tower: A case study, *Journal of Wind Engineering and Industrial Aerodynamics*, Vol. 115, (2013), pp. 173–183.
106. Gioffrè, M., Gusella, V., Materazzi, A. L., Venanzi, I. (2004): Removable guyed mast for mobile phone networks: wind load modeling and structural response, *Journal of wind engineering and industrial aerodynamics*, Vol. 92, (2004), pp. 463–475.
107. Perrin, D., McMahon, N., Crane, M., Ruskin, H. J., Crane, L., Hurley, B. (2007): The Effect of Meteorological Tower on its Top-Mounted Anemometer, *Applied Energy*, Vol. 84, (2007), Issue 4, pp. 413-424.
108. Bezrukovs V., Bezrukovs Vl., Zacepins A., Komashilovs V. (2015): Application of optical measurement complex Pentalum SpiDar for wind shear measurement onshore Baltic sea. EWEA, Paris, 17 - 20 November 2015.
[//proceedings.ewea.org/annual2015/conference/allposters/PO.155.pdf](http://proceedings.ewea.org/annual2015/conference/allposters/PO.155.pdf)
109. Manwell J F, McGowan J G, Rogers A L (2009): *Wind Energy Explained: Theory, Design and Application*, John Wiley & Sons Ltd. p 689.
110. Bezrukovs V., Upnere S., Bezrukovs Vl., Zacepins A., Jekabsons N. (2017): Effect of the cellular communication mast structure on the wind speed measurement results. The 7th International ENERGY Conference & Workshop – REMOO conference, Venetia, Italia, 10.-12.05.2017.
111. Wibe Mast S1000/1200 description and drawings (2015). Available from:
www.yumpu.com/en/document/view/18287236/wibe-mast-s1000-1200-scanmast/3.
112. Davidson L. (2015): *An introduction to turbulence models*. Goteborg: Chalmers University of Technology, 2015. 48 p.
113. Bezrukovs V., Bezrukovs Vl., Upnere S., Gulbe L., Bezrukovs D. (2018): The use of cellular communication masts for wind shear research. *ENERGETIKA*. 2018. T. 64. Nr. 2. pp. 64–73.

114. Bezrukovs V., Bezrukovs V.I., Gulbe L., Bezrukovs D., Konuhova M., (2018): The experience of installing wind measuring sensors on cellular communication tall masts. *Space Research Review*, Vol. 5, 2018, pp 85-103.
115. Shipkovs, P., Kashkarova, G., Lebedeva, K., & Migla, L. (2012): Use of renewable energy resources for reduction of environmental pollutions. In the Fourth IASTED African Conference on Power and Energy Systems (AfricaPES 2012), 3–5 September 2012 (pp. 79–85). Gaborone, Botswana. CD Proceedings.
116. Bobinaite, V., & Priedite, I. (2015): RES-E support policies in the Baltic States: electricity price aspect (part II). *Latvian Journal of Physics and Technical Sciences*, 2, 13–25.
117. Bezrukovs, V.P., Bezrukovs, V.V., & Zacepins, A.J. (2014): Comparative efficiency of wind turbines with different heights of rotor hubs: Performance evaluation for Latvia. *J. Phys.: Conf. Ser.* 524 012113. doi:10.1088/1742-6596/524/1/012113
118. Turcik, M., Obuševs, A., Oļeiņikova, I., & Junghans, G. (2013): Assessment of wind production impacts to a power system and market formation in Baltic. *Power and Electrical Engineering*, 31, pp. 31–37.
119. Vēja karte un kvalitāte. (n.d.) Available from: http://www.kerveju.lv/veja_karte.php
120. Ostapenko, J., & Gamalejevs, A. (2004): *Latvian Wind Energy Guide*. Riga. p. 96.
121. Atjaunojamā enerģija Latvijā. Project No. 2/EEZLV02/ 14/GS/044 Contract No. 2/EEZLV02/14/GS/044/011 24.04.2015/ Available from: http://kphi.liepu.lv/wpcontent/uploads/2016/03/Renewable_energy_LV.pdf
122. Bezrukovs, V., Zacepins, A., Bezrukovs, V., & Komashilovs, V. (2016): Investigations of wind shear distribution on the Baltic shore of Latvia. *Latvian Journal of Physics and Technical Sciences*, 53(3), pp. 3–10.
123. Ripley, B. et al. (2017): Support Functions and Datasets for Venables and Ripley's MASS. Retrieved 11.08.2017 from <https://cran.r-project.org/web/packages/MASS/>
124. Storch, H. von, Zwiers, F.W. (2003). *Statistical Analysis in Climate Research*. Cambridge: Cambridge University Press, 2003, 484 pp.
125. Kharin, V.V., Zwiers, F.W. (2000): Changes in the extremes in an ensemble of transient climate simulations with a coupled atmosphere–ocean GCM. *Journal of Climate*. 13, pp. 3760–3788.

126. Aniskevich S., Bezrukovs V., Zandovskis U., Bezrukovs D., (2017): Modelling the spatial distribution of wind energy resources in Latvia. *Latvian Journal of Physics and Technical Sciences* N 6 (Vol. 54) 2017. pp. 10 – 20.
127. Bivand, R. S., Pebesma, E. J., & Gómez-Rubio, V. (2008). *Applied Spatial Data Analysis with R* (2nd edition). New York: Springer. p.150.
128. Hennermann, K., & Berrisford, P. (2017). ERA5 data documentation. Available from: <https://software.ecmwf.int/wiki/display/CKB/ERA5+data+documentation>
129. ERA5 Public Release 2010-2016. Available from: <https://climate.copernicus.eu/era5-public-release-2010-2016>.
130. Bezrukovs V., Bezrukovs VI. (2012): Wind speed and energy at different heights on the Latvian coast of the Baltic Sea. In WREF 2012, Denver, Colorado, May 13-17, 2012, 8 p.
131. Bezrukovs V., Bezrukovs VI., Lizuma L. (2013): The landscape influence on the wind energy distribution in height on the Latvian coast of the Baltic Sea, In International Conference on Alternative Energy in Developing Countries and Emerging Economies, Thailand, Bangkok, May 30-31, 2013, pp 614 – 619.
132. V. Bezrukovs, VI. Bezrukovs, A. Zacepins, D. Bezrukovs (2016): Forecasting of wind turbine efficiency in Latvia by long-term wind speed measurements. October 13-14, 2016 57th International Scientific Conference on Power and Electrical Engineering of Riga Technical University (RTUCON) -8 p.
133. Catalogue of European Urban Wind Turbine Manufacturers. Retrieved 30.08.2017 from http://www.urbanwind.net/pdf/CATALOGUE_V2.pdf
134. Madsen P.H. (2008): Introduction to the IEC 61400-1 standard. RISO DTU, 21.08.2008.
135. LM Windpower (2018). Available from: <https://www.lmwindpower.com/en/stories-and-press/stories/learn-about-wind/what-is-a-wind-class>
136. Nordex N 131/3000 Delta. Details and information. Available from: <http://en.wind-turbine-models.com/turbines/837-nordex-n-131-3000-delta/picture-9562>
137. Vestas 3 MW platform Available from: <http://nozebra.ipapercms.dk/Vestas/Communication/Productbrochure/3MWbrochure/3MWProductBrochure/>
138. Wind Turbine SWT-3.0-113 / SWT-3.2-113, Technical specification (2018). Available from: <https://www.siemensgamesa.com/-/media/siemensgamesa/downloads/en/products->

and-services/onshore/brochures/legacy-siemens/siemens-gamesa-onshore-wind-turbine-swt-3-2-113-en.pdf

139. Enercon product overview (2015). p. 19. Available from:
http://www.enercon.de/fileadmin/Redakteur/Medien-Portal/broschueren/pdf/en/ENERCON_Product_en_06_2015.pdf
140. Wind Turbine SWT-SWT-2.3-108. The new productivity benchmark (2017). Available from: <https://en.wind-turbine-models.com/turbines/647-siemens-swt-2.3-108>

Annex 1

Table A.1

Technical data and description about masts location, type of metrological sensors and the data loggers for three sites - Ventspils, Pāvilosta and Ainaži

Location		Site 1	Site 2	Site 3
		Ventspils	Pāvilosta	Ainaži
Site description		Staldzene	Tebra	Rozēni
Site description		Forest 5 m	Forest 10 m	Field
Site position	Lat	N 057° 26.166'	N 056° 50.602'	N 057° 53.443'
	Long	E 021° 37.143'	E 021° 25.607'	E 024° 39.788'
	Altitude, m	30	10	10
Date installation of equipment		2017.12.21.	2018.01.11.	2018.01.21.
Logger Symphonie Plus	S/N	494105786	494105789	494105784
	Ipack S/N	62207072	62207077	62207074
	Phone Nr	+371 27861349	+371 27870971	+371 2783176
	Site Number	0011	0012	0013
Technical dates of mast	Type	WIBE	Vairogs-M	Vairogs-M
	Height, m	100	99	99
	Side length, m	1.2	1.4	1.4
	Pipe diameter, mm	76	85	85
	Height of section, m	6.0	5.4	5.4
PV info	Type	MWG -20		
	Size , mm	353 x 505 x 25 mm		
	Voltage max. power	17.49 V		
	Peak power	20 W		
Channels	Sensors			
Ch1	Type	Anemometer P2546C-OPR		
	S/N	37800	37776	37777
	Level 1, m	12.4	10.6	10.9
	Position	A & 154°	A & 231°	A & 126°
	Slope	0.62074	0.619	0.6193
	Offset	0.22271	0.231	0.23045
Ch2	Type	Anemometer P2546C-OPR		
	S/N	37803	37778	37779
	Level 1, m	12.4	10.6	10.9
	Position	B & 274°	B & 351°	B & 246°
	Slope	0.62062	0.619	0.62018
	Offset	0.22834	0.231	0.23054
Ch3	Type	Anemometer P2546C-OPR		
	S/N	37798	37780	37781
	Level 2, m	40.4	41.0	43.3
	Position	A & 154°	A & 231°	A & 126°
	Slope	0.6209	0.62	0.62097
	Offset	0.22953	0.234	0.21741
Ch4	Type	Anemometer P2546C-OPR		
	S/N	37785	37795	37782
	Level 3, m	61.4	64.7	61.3
	Position	B & 274°	B & 351°	B & 246°
	Slope	0.62167	0.62	0.62059
	Offset	0.20707	0.238	0.21965
Ch5	Type	Anemometer P2546C-OPR		
	S/N	37788	37796	37783
	Level 4, m	83.9	81.4	81.6
	Position	A & 154°	A & 231°	A & 126°
	Slope	0.62	0.62	0.62086
	Offset	0.23182	0.228	0.21594
Ch6	Type	Anemometer P2546C-OPR		
	S/N	37802	37797	37787
	Level 4, m	83.85	81.4	81.6

	Position	B & 274°	B & 351°	B & 246°
	Slope	0.62008	0.62	0.62041
	Offset	0.23415	0.234	0.22689
Ch7	Type	Vane NRG 200P		
	S/N	Vane1	Vane 1	Vane 1
	Level 2, m	40.3	41.0	43.3
	Offset	-26°	51°	-54°
	Slope	0.351	0.351	0.351
Ch8	Type	Vane NRG 200P		
	S/N	Vane2	Vane2	Vane2
	Level 4, m	83.9	81.4	81.6
	Offset	-26°	51°	-54°
	Slope	0.351	0.351	0.351
Ch9	Type	Voltmeter iPACK		
	S/N	62207072	62207077	62207074
	Level 0, m	2.0		
	Slope	0.021	0.021	0.021
Ch10	Type	Hygrometer NRG RH-5X		
	S/N	4414	4414	4414
	Level 0, m	2.0		
	Slope	0.097	0.097	0.097
Ch11	Type	Thermometer NRG 110S		
	S/N	42802555	44282552	44202553
	Level 4, m	12.4	10.0	10.4
	Slope	0.1357	0.136	0.1358
	Offset	-86.47	-86.811	-86.2
Ch12	Type	Thermometer NRG 110S		
	S/N	42802554	44282549	44282550
	Level 4, m	83.9	81.4	81.6
	Slope	0.1353	0.136	0.1358
	Offset	-85.91	-86.279	-86.37
Ch13	Type	Anemometer P2546C-OPR		
	S/N	37799	37791	37788
	Level, m	40.4	41	43.32
	Position	C & 34°	C & 111°	C & 6°
	Slope	0.62129	0.62	0.62
	Offset	0.22264	0.232	0.23182
Ch14	Type	Anemometer P2546C-OPR		
	S/N	37801	37792	37789
	Level 2, m	40.4	41.0	43.3
	Position	B & 274°	B & 351°	B & 246°
	Slope	0.62073	0.62	0.61989
	Offset	0.22101	0.233	0.23449
Ch15	Type	Anemometer P2546C-OPR		
	S/N	37784	37794	37790
	Level 3, m	61.4	64.7	61.3
	Position	A & 154°	A & 231°	A & 126°
	Slope	0.62029	0.62	0.62023
	Offset	0.2202	0.235	0.22017

Table A.2

Values of average wind speeds V_{avg} before and after corrections V_{avg_corr} and their difference $(1 - V_{avg} / V_{avg_corr})$ in percents for sensors S_A , S_B , S_C , installed on cellular communication masts in Ventspils, Pāvilosta and Ainaži at the Levels 1 - 4

Level	Sensors	Location sites								
		Ventspils			Pāvilosta			Ainaži		
		Average wind speed, m/s		Diff., %	Average wind speed, m/s		Diff., %	Average wind speed, m/s		Diff., %
		V_{avg}	V_{avg_corr}		V_{avg}	V_{avg_corr}		V_{avg}	V_{avg_corr}	
1	S_A	2.27	2.29	0.9%	1.87	1.90	1.3%	2.55	2.55	0.1%
	S_B	2.22	2.31	3.6%	1.81	1.91	5.3%	2.45	2.56	4.5%
	$\frac{S_A + S_B}{2}$	2.25	2.30	2.3%	1.84	1.91	3.3%	2.50	2.56	2.3%
2	S_A	4.21	4.27	1.4%	3.60	3.67	1.9%	3.72	3.74	0.6%
	S_B	4.15	4.26	2.7%	3.53	3.69	4.3%	3.55	3.78	5.9%
	S_C	4.11	4.25	3.2%	3.62	3.65	1.0%	3.57	3.76	5.0%
	$\frac{S_A + S_B + S_C}{3}$	4.16	4.26	2.5%	3.58	3.67	2.4%	3.62	3.76	3.9%
3	S_A	5.27	5.35	1.5%	4.42	4.52	2.2%	4.19	4.21	0.5%
	S_B	5.28	5.40	2.2%	4.37	4.55	3.9%	4.02	4.25	5.4%
	$\frac{S_A + S_B}{2}$	5.27	5.38	1.9%	4.39	4.53	3.0%	4.11	4.23	3.0%
4	S_A	6.05	6.16	1.7%	4.86	4.98	2.2%	4.70	4.72	0.4%
	S_B	6.11	6.25	2.2%	4.82	5.00	3.6%	4.49	4.74	5.4%
	$\frac{S_A + S_B}{2}$	6.08	6.20	1.9%	4.84	4.99	2.9%	4.59	4.73	2.9%